INTRA**CON**TINENTAL **S**AGS (ICONS) FORMATION, EXHUMATION AND LANDSCAPE EVOLUTION: THE ETHIOPIAN TESTIMONY

By

TADESSE B. ALEMU

Bachelor of Science in Earth Sciences
Addis Ababa University
Addis Ababa, Ethiopia
2009

Master of Science in Earth Sciences (Fossil Fuel Exploration)
Addis Ababa University
Addis Ababa, Ethiopia
2012

Submitted to the Faculty of the
Graduate College of the
Oklahoma State University
in partial fulfillment of
the requirements for
the Degree of
DOCTOR OF PHILOSOPHY
July, 2019

INTRA**CON**TINENTAL **S**AGS (ICONS) FORMATION, EXHUMATION AND LANDSCAPE EVOLUTION: THE ETHIOPIAN TESTIMONY

Dissertation Approved:

Dr. Mohamed Abdelsalam, Chair

Dissertation Adviser

Dr. Estella Atekwana

Dr. Jack Pashin

Dr. Runar Nygaard

ACKNOWLEDGEMENTS

My greatest gratitude goes to my advisor, Dr. Mohamed Abdelsalam, whose work and enthusiasm for advancing the geology of Africa was an important motivation that ultimately led me to join Oklahoma State University. His mentorship and patience has been an invaluable asset that helped me navigate the most difficult times. Thank you for giving me the latitude to explore, and for helping me acquire the versatility needed to grow. I am grateful for the opportunities and exposures that my Committee member Dr. Estella Atekwana provided. Thank you to Committee members Dr. Jack Pashin, and Dr. Nygaard Runar for their time and valuable suggestions. Special thanks to Dr. Kevin Mickus for his help with potential data and methods. I am grateful to Statoil whose funding to my advisor made possible most of my work in the Mekele Basin. I thank the Boone Pickens School of Geology for the fellowships, and assistantships. I immensely benefited from the discussion at the Tectonics Research Group meetings. I also greatly enjoyed the company of so many graduate students and friends at the PhD room. Dr. Liang Xue has been a collaborator and a great colleague. Thank you to UNAVCO for the internship opportunity. Some of my field trips to Ethiopia were funded through the "Blue Nile Project", thank you to project PI's: Dr. Mark Goodwin, Dr. Randal Irmis, and Dr. Greg Wilson for the support. I am grateful to my MS advisors Dr. Balemwal Atnafu, and Dr. Dawit Lebenie, whose involvement continued into this work. Thank you to Addis Ababa University and Mekele University for providing support during the fieldwork. Thank you to all friends and families of the Ethiopian community in Stillwater and OKC. Shout out to 'Ambesoch Group', I greatly appreciate the support and encouragement. Finally, to my wife Tsi, thank you so much for all your help and love. You were always there, and for that, I am eternally grateful. Thank you to my lovely kids, Meba and Abel.

Acknowledgements reflect the views of the author and are not endorsed by committee members or Oklahoma State University.

Name: TADESSE BERHANU ALEMU

Date of Degree: JULY, 2019

Title of Study: INTRACONTINENTAL SAGS (ICONS) FORMATION, EXHUMATION AND LANDSCAPE EVOLUTION: THE ETHIOPIAN TESTIMONY

Major Field: GEOLOGY

Abstract: The study of the Mekele Sedimentary Basin (MSB) in Ethiopia revealed geological and geophysical features that can be interpreted as resembling an ICONS (IntraCONtinental Sag). ICONS are groups of sedimentary basins that develop within the interior of continental plates. The MSB is filled with ~2 km thick mixed clastic-carbonate sediments ranging in age from Ordovician/Silurian (440 to 460 Ma) to middle Cretaceous (100 to 120 Ma). This study used field, remote sensing and satellite gravity data. Gravity data is used to conduct spectral analysis, forward and inverse modelling to outline the geometry of the basin and lithospheric-scale-structures across the region. Owing to its location over the juvenile Neoproterozoic accretionary Pan-African terranes, cooling and thickening of the basement beneath the basin is proposed as an alternative basin-forming mechanism. The MSB is unique in that the sedimentary formations and geological structures associated with ICONS are almost completely exposed on the surface due to a combination of tectono-magmatic and surface fluvial incision processes. Accordingly, the combined analysis of morphometric parameters and geophysical data to evaluate the regional geodynamic link between tectono-magmatic processes and landscape evolution during Cenozoic was carried out. Broad patterns of topographic variation along the strike of the western escarpment of the Afar Depression bordering the MSB reflect general properties of lithospheric heterogeneity. In the north and central region, the escarpment is underlain by a highly extended and almost tapered crust whereas in the south the highest escarpments overlie a thickened possibly underplated crust. These features partially correspond with the along-strike variation in geomorphic features. However, it appears that the first-order landscape development is primarily controlled by a regional process. Further, the incision history of the northwestern plateau drainage system was examined based on a case study from the Blue Nile Gorge, where ~1500 m Mesozoic section is exposed along the Blue Nile River. Unlike the MSB, the Blue Nile Basin is covered with Oligocene volcanic rocks, and hence, provides a good constraint on the incision history. Here, using geomorphic proxies from field, remote sensing, and published rate of incision through time curve stratigraphic control is evaluated. Despite vast variability, the study found limited influence of lithology.

PUBLICATION DISSERTATION OPTION

This dissertation is organized in two separate sections. The first section provides a brief outline of the dissertation, including the scope and significance. The second section presents three separate manuscripts; one is published, the second is accepted with minor revision, and the third under preparation.

Paper 1 (Chapter II): Alemu, T., Abdelsalam, M. G., Dawit, E. L., Atnafu, B., and Mickus, K. L., 2018, The Paleozoic–Mesozoic Mekele Sedimentary Basin in Ethiopia: An example of an exhumed IntraCONtinental Sag (ICONS) basin: Journal of African Earth Sciences, v. 143, p. 40-58.doi: 10.1016/j.jafrearsci.2018.03.010.

Paper 2 (Chapter III): Alemu, T., Abdelsalam, M. G., and Mickus, K. L., 2019, Along-strike topographic characteristics of the western escarpments of the Afar Depression: Under preparation.

Paper 3 (Chapter IV): Alemu, T., Page, D.J., Abdelsalam, M. G., and Atnafu, B., 2019, Stratigraphic Controls on the Morpho-tectonic Evolution of the Gorge of the Nile, Ethiopia. Submitted to Arabian Journal of Geosciences, and accepted with minor revision.

TABLE OF CONTENTS

LIST OF TABLES

Table Page

LIST OF FIGURES

Figure Page

Figure Page

Figure Page

Figure Page

Figure Page

Figure Page

Figure Page

Figure Page

Figure Page

Figure Page

Figure Page

Figure Page

CHAPTER I
INTRODUCTION

1.1. SCOPE AND ORGANISATION

This dissertation presents three distinct but interrelated projects. The first project examines the formation and evolution of the Mekele Sedimentary Basin as an IntraCONtinental Sag (ICONS) in contrast to previous interpretation as a failed rift. The latest geodynamic event that unifies all Phanerozoic basins in Ethiopia is mantle plume impingement on the lithosphere, uplift and exhumation of the Ethiopian plateau. Accordingly, the second and third projects feature works that deal with exhumation history and landscape evolution of the Ethiopian plateau, particularly that of the northwestern plateau where the Mekele Basin is located. The second project presents crustal scale and geomorphological variation along the escarpment of the Afar Depression flanking the northwestern Ethiopian plateau. This uplifted flanks resulted (along with pre-rift doming due to plume impingement of the plateau) an almost complete exhumation of the Mekele Sedimentary Basin. As a result, regional analysis of the plateau and the possible scenarios of geodynamic link between surface and subsurface processes is discussed in this paper. Lastly, the third project examines the influence of stratigraphic variation on the incision history of the plateau in the Gorge of the Nile, an area where ~1500 m Mesozoic section is exposed along the Blue Nile River. The Blue Nile Basin (unlike the Mekele) is covered with Oligocene flood basalt, which provides a good constraint on incision history. In the following section, an introduction to the concept of ICONS, their placement in the scheme of sedimentary basin classification along with dominant subsidence mechanisms, is briefly discussed. In addition, the major salient geological and geophysical characteristics of ICONS that contrast them from rift, foreland and pull apart basins are presented, with examples form basins around the world.

1.2. INTRACONTINENTAL SAGS (ICONS)

Sedimentary basins are regions of prolonged subsidence of the Earth's surface whereby both the processes originating within the lithosphere and the mantle are considered to be the driving mechanisms. A number of sedimentary classification schemes proposed require horizontal forces as a primary mechanism for the formation of negative topography needed for sediments accommodation (eg. Dickinson, 1974; Kingston et al., 1983a; 1983b; Busby et al., 1995; Allen and Allen, 2005; Armitage and Allen, 2010). Accordingly, these mechanisms are divided into those causing rift basins through lithospheric stretching followed by thermal subsidence, pull-apart basins related to strike-slip faulting or those producing foreland basins through lithospheric flexure caused by tectonic loading (Busby et al., 1995; Ingersoll, 2012). Such classification scheme doesn't fully explain many enigmatic features observed in basins referred to as cratonic or IntraCONtinental basinS (ICONS) (Sloss and Speed, 1974; Leighton, 1990; Heine et al., 2008). In this dissertation, the term ICONS is used as an abbreviation for Intra-CONtinental Sags. Their origin and subsidence mechanism is still largely debatable. Proposed models include those that favor slow crustal extension (Sloss, 1988; Allen and Allen, 2005; Armitage and Allen, 2010), and those that advocate purely thermal origin (Ahern, and Dikeou, 1989, Holt et al., 2010; McKenzie, and Priestley, 2016).

Despite being associated with cratons, ICONS form over all types of terranes, and are unified by having all or most of the following geological and geophysical features (Fig. 1.1). They are generally located within the interiors of continent on a stable lithosphere and relatively flat Moho (Fig. 1.1A) (Sloss and Speed, 1974; Sloss, 1988; Heine and Müller, 2008). They characteristically exhibit long subsidence history (Fig. 1.1B, Xie and Heller, 2009) considered to be due to a low extensional strain rate (Fig. 1.1C, Allen and Allen, 2005; Armitage and Allen, 2010). They are circular to elliptical in map view (Fig. 1.1D) and saucer shaped in cross section (Fig. 1.1E) (Leighton and Kolata, 1990; Hartley and Allen, 1994; Klein, 1995). They are filled with continental and shallow water sediments (E.g. Congo, Michigan basins) with concentric gravity minima most likely due to the presence of thicker sedimentary

sections towards the center of the basin (Fig. 1.1F, Craig et al., 2011). They are found in all types of lithosphere, in all continents and spanning all geologic time (Armitage and Allen, 2010). Those found over craton, are underlain by a thick lithosphere (Artemieva, 2006; Priestley and McKenzie, 2006; Armitage and Allen, 2010).

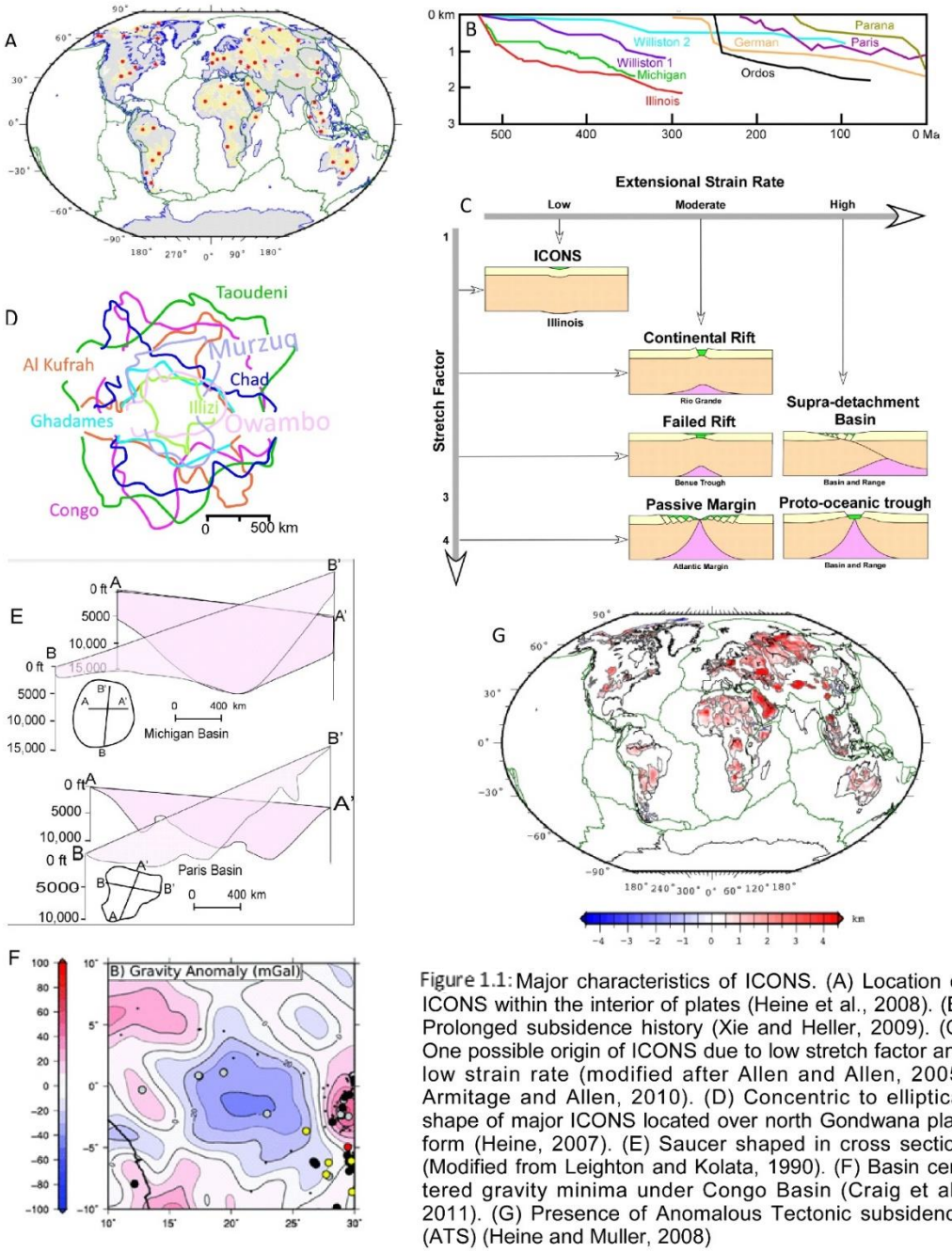

Figure 1.1: Major characteristics of ICONS. (A) Location of ICONS within the interior of plates (Heine et al., 2008). (B) Prolonged subsidence history (Xie and Heller, 2009). (C) One possible origin of ICONS due to low stretch factor and low strain rate (modified after Allen and Allen, 2005; Armitage and Allen, 2010). (D) Concentric to elliptical shape of major ICONS located over north Gondwana platform (Heine, 2007). (E) Saucer shaped in cross section (Modified from Leighton and Kolata, 1990). (F) Basin centered gravity minima under Congo Basin (Craig et al., 2011). (G) Presence of Anomalous Tectonic subsidence (ATS) (Heine and Muller, 2008)

Examples of basins with characteristically thick lithosphere include the Congo basin in Africa (Hartley and Allen, 1994; Downey and Gurnis, 2009; Craig et al., 2011) and the Michigan, Williston, Illinois and Hudson Bay basins in North America (Priestley and McKenzie, 2006). Others are located over orogenic belts (Arabian Basin and Paraná Basin in South America: Holt et al., 2015). ICONS also are believed to show 'Anomalous Tectonic Subsidence (ATS)' (Fig. 1.1G: Heine and Müller, 2008) which is a reference to the subsidence that remains an accounted for after backstripping. These authors attributed this ATS to dynamic topography processes and identified more than 228 sedimentary basins with ATS worldwide.

Disagreement still exists regarding the scale and source of thermal anomalies. For instance, some of the largest sedimentary basins in North America, the Michigan, Illinois, Williston and Hudson Bay are considered to be formed on a thick lithosphere of similar ages (Sloss, 1988; Leighton and Kolata, 1990; Allen and Armitage, 2012) but show different subsidence history. Local conventional tectonic processes such as magmatism, orogeny and rifting is often invoked to explain such local variations (e.g. Stel et al., 1993; Kaminski and Jaupart, 2000). Such processes, however, have failed to explain the many other enigmatic features of ICONS. As a result, proposed models advocate the concept of vertical tectonics to explain formation of ICONS. This is in contrast to models that attempted to explain the evolution of ICONS through horizontal tectonic forces by linking their development to within-plate low-rate extension of a thick continental lithosphere (E.g. Allen and Allen, 2005; Allen and Armitage, 2012). One major reason why we have limited understanding about ICONS is that they are formed in a stable part of the lithosphere characterized by subdued topography with little to no deformation and therefore, have remained buried since the time of their formation. Consequently, studying them requires the acquisition of expensive geophysical and borehole data, which only gives us a sparse picture about the stratigraphic and structure architecture of ICONS.

1.3. SIGNIFICANCE

1.3.1. BASIN FILL HISTORY

IntraCONtinental Sags (ICONS) lie within plate interiors, subsiding for a long period. There is substantial value in constraining their geologic history both as the sedimentary rocks within them preserve long-term record of earth history and are host to natural resources including water and hydrocarbons. Major limitation to the study of ICONS comes from the fact that they are almost completely buried, and our understanding about their geometry mostly comes from geophysical and numerical models rather than direct observations. The Paleozoic-Mesozoic Mekele Sedimentary Basin in northern Ethiopia, unlike others, is almost completely exhumed due to its location at the western flank of the Afar Depression, providing an opportunity to get an insight into internal architecture of the basin. The basin contains ~2 km thick Paleozoic-Mesozoic mixed clastic-carbonate sediments deposited on top of a metamorphic and plutonic basement complex of Neoproterozoic age.

The Mekele ICONS also has similarities with many intracontinental basins especially with those formed over an accretionary orogenic belt, which have shown to host large amount of hydrocarbon resources (Fig. 1.2). Particularly, accretionary crust such as the Neoproterozoic Pan African belt contains a disproportionate amount of reserve and hence, future basin modelling approaches need to account this unique lithospheric feature. Documentation of the Mekele Basin as ICONS will provide an outcrop analog to study internal stratigraphic and structural setting of similar basins. This will have a transformative effect on the understanding of sedimentary basins in the region. Present basin formation and subsidence models for the Mekele and neighboring basins advocate sedimentation within NW-trending rift systems. This is despite regional geophysical studies showing a relatively thicker crust, and lack of well-defined basin bounding faults in many of these basins.

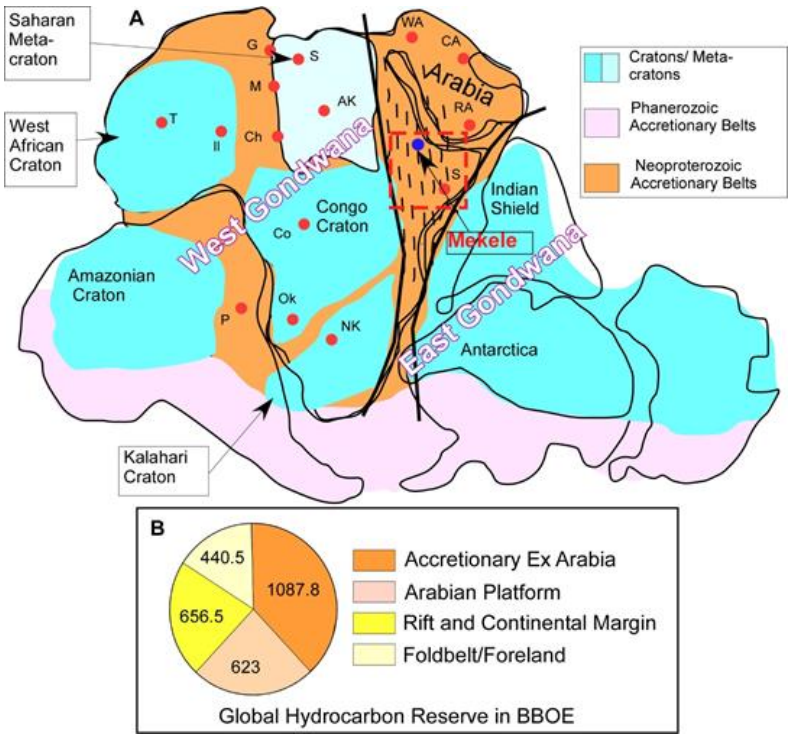

Figure 1.2: Lithosphere type, basin distribution, and hydrocarbon potential in the greater Gondwana (map modified after Doucoure et al., 1998 and Norton and Johnson, 2001; Reserve data from Klett et al., 1997; Data compiled by Ian Norton and Chris Johnson, ExxonMobil)

1.3.2. LANDSCAPE EVOLUTION

Stratigraphic and thermochronologic data indicate a period of tectonic quiescence and peneplanation during the Paleozoic and early Mesozoic (Mock et al., 1999; Pik et al., 2003). Major deformation responsible for the observed near complete three-dimensional exposure of the Mekele Basin, and extensive incision in the neighboring Blue Nile Sedimentary Basin happened during the Cenozoic (Beyth, 1972; Bosellini et al., 1989; 1997; Bosworth, 1992; Russo et al., 1994; Hunegnaw et al., 1998). Although much of the plateau itself is mostly covered with flood basalt that reaches in places up to 2 km, millions of years of erosional and tectonic processes have resulted in the exposure of deeply buried Paleozoic and Mesozoic sedimentary rocks. A complex interaction of regional mantle plume related

uplift, later extensional processes within the Afar Depression, the Main Ethiopia Rift and South Ethiopian Rift and widespread but episodic shield volcanism contributed towards accelerated uplift, which in turn resulted in widespread erosion and deep incision of the plateau. These processes thus, gave rise to the present day geomorphologic setup of Ethiopia andform the basis for classification of the landscape into the Northwestern and SE Ethiopian Plateau separated by the different segment of the Ethiopian Rift. Hence, the plateau provides an exceptional opportunity to examine uplift history of an extensional setting, as it relates to plateau growth and incision, which are discussed in paper II and III in detail.

In summary, the overarching objective of the dissertation are as follows. (i) to document the geological and geophysical features of the Mekele Sedimentary Basin, and test the hypothesis that the basin is an ICONS formed due to the cooling and thickening of an initially thin and juvenile Sub Continental Lithospheric Mantle (SCLM) of the Arabian-Nubian Shield. (ii) to characterize the topographic and tectono-magmatic features of the escarpment bordering the Mekele Sedimentary Basin, and evaluate the geodynamic link between tectono-magmatic processes and topography. (iii) to examine the role of stratigraphy (lithostratigraphy) in controlling river incision using the spectacular Southwest-flowing segment of the Blue Nile River at the Gorge of the Nile.

1.4. REFERENCES

Ahern, J. L., and Dikeou, P. J., 1989, Evolution of the lithosphere beneath the Michigan Basin: Earth and planetary science letters, v. 95, no. 1-2, p. 73-84.

Allen, P. A., and Armitage, J. J., 2012, Cratonic basins: Tectonics of Sedimentary Basins: Recent Advances, p. 602-620.

Allen, P., and Allen, J., 2005, Principles of Basin Analysis, Blackwell Scientific.

Armitage, J. J., and Allen, P. A., 2010, Cratonic basins and the long-term subsidence history of continental interiors: Journal of the Geological Society, v. 167, no. 1, p. 61-70.

Artemieva, I. M., 2006, Global 1× 1 thermal model TC1 for the continental lithosphere: implications for lithosphere secular evolution: Tectonophysics, v. 416, no. 1, p. 245-277.

Artyushkov, E., 2005, The formation mechanism of the Barents basin: Russian Geology and Geophysics, v. 46, no. 7, p. 683-696.

Avigad, D., and Gvirtzman, Z., 2009, Late Neoproterozoic rise and fall of the northern Arabian–Nubian Shield: the role of lithospheric mantle delamination and subsequent thermal subsidence: Tectonophysics, v. 477, no. 3, p. 217-228.

Baird, D., Knapp, J., Steer, D., Brown, L., and Nelson, K., 1995, Upper-mantle reflectivity beneath the Williston basin, phase-change Moho, and the origin of intracratonic basins: Geology, v. 23, no. 5, p. 431-434.

Beyth, M., 1972, Paleozoic-Mesozoic sedimentary basin of Mekele outlier, northern Ethiopia: AAPG Bulletin, v. 56, no. 12, p. 2426-2439.

Bosellini, A., 1989, The continental margins of Somalia: their structural evolution and sequence stratigraphy. Memorie di Science Geologiche, Universita di Padova 41, 373–458.

Bosellini, A., Russo, A., Fantozzi, P., Assefa, G., and Solomon, T., 1997, The Mesozoic succession of the Mekele outlier (Tigre province, Ethiopia): Memorie di Scienze Geologiche, v. 49, p. 95-116.

Bosworth, W., 1992, Mesozoic and early Tertiary rift tectonics in East Africa: Tectonophysics, v. 209, no. 1-4, p. 115-137.

Busby, C. J., Ingersoll, R. V., and Burbank, D., 1995, Tectonics of sedimentary basins, Blackwell Science Oxford.

Craig, T., Jackson, J., Priestley, K., and McKenzie, D., 2011, Earthquake distribution patterns in Africa: their relationship to variations in lithospheric and geological structure, and their rheological implications: Geophysical Journal International, v. 185, no. 1, p. 403-434.

Dickinson, W. R., 1974, Plate tectonics and sedimentation: SEPM, p. 27.

Doucoure, C. M., Wit, M. D., and Reeves, C., 1998, Towards a gravity map of Gondwana: Journal of African Earth Sciences, v. 27, no. 1, p. 195-204.

Downey, N. J., and Gurnis, M., 2009, Instantaneous dynamics of the cratonic Congo basin: Journal of Geophysical Research: Solid Earth, v. 114, no. B6.

Gurnis, M., 1993, Phanerozoic marine inundation of continents driven by dynamic topography above subducting slabs: Nature, v. 364, no. 6438, p. 589.

Hartley, R. W., and Allen, P. A., 1994, Interior cratonic basins of Africa: relation to continental break-up and role of mantle convection: Basin Research, v. 6, no. 2-3, p. 95-113.

Heine, C., 2007, Formation and Evolution of intracontinental basins, PhD Thesis, School of Geosciences, The University of Sydney, Australia, unpublished.

Heine, C., and Müller, R., 2008, The IntraCONtinental basinS (ICONS) atlas—Applications in eastern Australia.

Heine, C., Müller, R. D., Steinberger, B., and Torsvik, T. H., 2008, Subsidence in intracontinental basins due to dynamic topography: Physics of the Earth and Planetary Interiors, v. 171, no. 1, p. 252-264.

Holt, P. J., Allen, M. B., Van Hunen, J., and Bjørnseth, H. M., 2010, Lithospheric cooling and thickening as a basin forming mechanism: Tectonophysics, v. 495, no. 3, p. 184-194.

Holt, P., Allen, M., and Van Hunen, J., 2015, Basin formation by thermal subsidence of accretionary orogens: Tectonophysics, v. 639, p. 132-143.

Hunegnaw, A., Sage, L., and Gonnard, R., 1998, Hydrocarbon potential of the intracratonic Ogaden Basin, SE Ethiopia: Journal of Petroleum Geology, v. 21, no. 4, p. 401-425.

Ingersoll, R. V., 2012, Tectonics of sedimentary basins, with revised nomenclature: Tectonics of Sedimentary Basins: Recent Advances, p. 1-43.

Kaminski, E., and Jaupart, C., 2000, Lithosphere structure beneath the Phanerozoic intracratonic basins of North America: Earth and Planetary Science Letters, v. 178, no. 1, p. 139-149.

Kingston, D., Dishroon, C., and Williams, P., 1983a, Global basin classification system: AAPG bulletin, v. 67, no. 12, p. 2175-2193.

Kingston., D., 1983b, Hydrocarbon plays and global basin classification: AAPG Bulletin, v. 67, no. 12, p. 2194-2198.

Klein, G. D., 1995, Intracratonic basins: Tectonics of Sedimentary Basins, p. 459-478.

Klein, G. d., deV. and Hsui, AT (1987). Origin of cratonic basins: Geology, v. 15, no. 12, p. 1094-1098.

Klett, T. R., Ahlbrandt, T. S., Schmoker, J. W., and Dolton, G. L., 1997, Ranking of the world's oil and gas provinces by known petroleum volumes: USGS Open-File Report, p. 97-463.

Leighton, M. W., 1990, Introduction to interior cratonic basins: American Association of Petroleum Geologists Memoir, v. 51, p. 1-24.

Leighton, M., and Kolata, D., 1990, Selected interior cratonic basins and their place in the scheme of global tectonics: a synthesis: Interior cratonic basins: American Association of Petroleum Geologists Memoir, v. 51, p. 729-797.

McKenzie, D., and Priestley, K., 2016, Speculations on the formation of cratons and cratonic basins: Earth and Planetary Science Letters, v. 435, p. 94-104.

Mock, C., Arnaud, N. O., Cantagrel, J.-M., and Yirgu, G., 1999, 40 Ar/39 Ar thermochronology of the Ethiopian and Yemeni basements: reheating related to the Afar plume?: Tectonophysics, v. 314, no. 4, p. 351-372.

Norton, I. O., and Johnson, C. A., 2001, Sedimentary basin development on accretionary crust: exploration significance, in Conference Volume: AGU Chapman Conference on Exploration Geodynamics, Perth, v. 137.

Pik, R., Marty, B., Carignan, J., and Lavé, J., 2003, Stability of the Upper Nile drainage network (Ethiopia) deduced from (U–Th)/He thermochronometry: implications for uplift and erosion of the Afar plume dome: Earth and Planetary Science Letters, v. 215, no. 1, p. 73-88.

Priestley, K., and McKenzie, D., 2006, The thermal structure of the lithosphere from shear wave velocities: Earth and Planetary Science Letters, v. 244, no. 1, p. 285-301.

Ritzmann, O., and Faleide, J. I., 2009, The crust and mantle lithosphere in the Barents Sea/Kara Sea region: Tectonophysics, v. 470, no. 1, p. 89-104.

Russo, A., Assefa, G., and Atnafu, B., 1994, Sedimentary evolution of the Abay River (Blue Nile) Basin, Ethiopia. With 4 figures in the text: Neues Jahrbuch Fur Geologie Und Palaontologie-Monatshefte, no. 5, p. 291-308.

Saunders, A. D., England, R. W., Reichow, M. K., and White, R. V., 2005, A mantle plume origin for the Siberian traps: uplift and extension in the West Siberian Basin, Russia: Lithos, v. 79, no. 3, p. 407-424.

Sleep, N. H., and Snell, N. S., 1976, Thermal contraction and flexure of mid-continent and Atlantic marginal basins: Geophysical Journal International, v. 45, no. 1, p. 125-154.

Sloss, L.L., 1988, Tectonic evolution of the craton in Phanerozoic time: The Geology of North America, v. 2, p. 25-51.

Sloss. L.L, and Speed, R.C., 1974, Relationships of cratonic and continental margin tectonic episodes, in Dickinson, W.R., eds, Tectonics and Sedimentation: Society of Economic Paleontologists and Mineralogists Special Publication, v. 22, p. 98-119.

Stel, H., Cloetingh, S., Heeremans, M., and Van der Beek, P., 1993, Anorogenic granites, magmatic underplating and the origin of intracratonic basins in a non-extensional setting: Tectonophysics, v. 226, no. 1-4, p. 285-299.

Xie, X., and Heller, P. L., 2009, Plate tectonics and basin subsidence history: Geological Society of America Bulletin, v. 121, no. 1-2, p. 55-64.

CHAPTER II

THE PALEOZOIC – MESOZOIC MEKELE SEDIMENTARY BASIN IN ETHIOPIA: AN EXAMPLE OF AN EXHUMED INTRACONTINENTAL SAG (ICONS) BASIN

2.1. ABSTRACT

We investigated the evolution of the Mekele Sedimentary Basin (MSB) in northern Ethiopia using geologic field and gravity data. The depth to Moho and lithospheric structure beneath the basin was imaged using two-dimensional (2D) radially-averaged power spectral analysis, Lithoflex threedimensional (3D) forward and inverse modeling, and 2D forward modeling of the Bouguer gravity anomalies. Previous studies proposed that the basin was formed as part of a multi-branched rift system related to the breakup of Gondwana. Our results show that the MSB: (1) is circular to elliptical in map view and saucer shaped in cross sectional view, (2) is filled with terrestrial and shallow marine sedimentary rocks, (3) is not significantly structurally controlled, and the major faults are post-depositional, (4) is characterized by a concentric gravity minima, (5) is underlain by an unstretched crust (~40 km thick) and thicker lithosphere (~120 km thick). These features compare positively with a group of basins known as IntraCONtinental Sags (ICONS), especially those ICONS formed over accretionary orogenic terranes. Since the MSB is located above the Neoproterozoic accretionary orogenic terranes of the Arabian-Nubian Shield (ANS), we propose that the formation of the MSB to be related to cooling and thickening of a juvenile sub-continental lithospheric mantle beneath the ANS, which most probably provided negative buoyancy, and hence subsidence in the MSB, leading to its formation as an ICONS. The MSB could be used as an

outcrop analog for information about the internal facies architecture of ICONS because it is completely exhumed due to tectonic uplift on the western flank of the Afar Depression.

2.2. INTRODUCTION

Sedimentary basins are regions of a prolonged subsidence history of the Earth's surface. Present basin formation mechanisms are predominantly linked to plate tectonics processes in which horizontal forces are thought to be the primary cause for the formation of negative topography needed for sediment accommodation (e.g., Kingston et al., 1983a; b; Busby et al., 1995; Allen and Allen, 2005). Mechanisms for the formation of sedimentary basins are broadly divided into those causing rift basins through lithospheric stretching followed by thermal subsidence, pull-apart basins related to transtensional faulting or those producing foreland basins through lithospheric flexure caused by tectonic loading (e.g., Busby et al., 1995). This linkage of a sedimentary basin's development with plate tectonics explains the formation of many of them except a group of basins that are referred to as ‘cratonic basins’, ‘intracratonic basins’,or ‘interior sag basin’ (Sloss, 1963, 1988; Burke, 1976; Klein and Hsui, 1987; Allen and Armitage, 2012) and later abbreviated by Heine and Müller (2008) as ICONS in reference to Intra-CONtinental basinS. Here, ICONS is used as an abbreviation for Intra-CONtinental Sags.

The Paleozoic – Mesozoic Mekele Sedimentary Basin (MSB) in the northern part of the Northwestern Ethiopian Plateau at the western flank of the Afar Depression is filled with ~2 km thick mixed clastic and carbonate sedimentary rocks overlying the Neoproterozoic accretionary terranes of the Arabian-Nubian Shield represented by the crystalline basement (Figs. 2.1-3). It presents a unique setting in which sedimentary formations and geological structures that are potentially associated with an ICONS are completely exposed. Other ICONS have remained buried due to their formation within the stable part of the continent, away from active plate boundaries.

The basin covers ~8000 km^2 and is bounded to the north, west and south by Neoproterozoic crystalline basement rocks and to the east by the Afar Depression, which extends southward into the Main Ethiopian Rift (Figs. 2.1 and 2.2). It is thought to have been part of a multi-branched rift system related to the breakup of Gondwana (Bosellini et al., 1997). However, field observations, remote sensing and geophysical analysis suggest that the geological and geophysical features of the MSB are not consistent with its evolution as a rift basin.

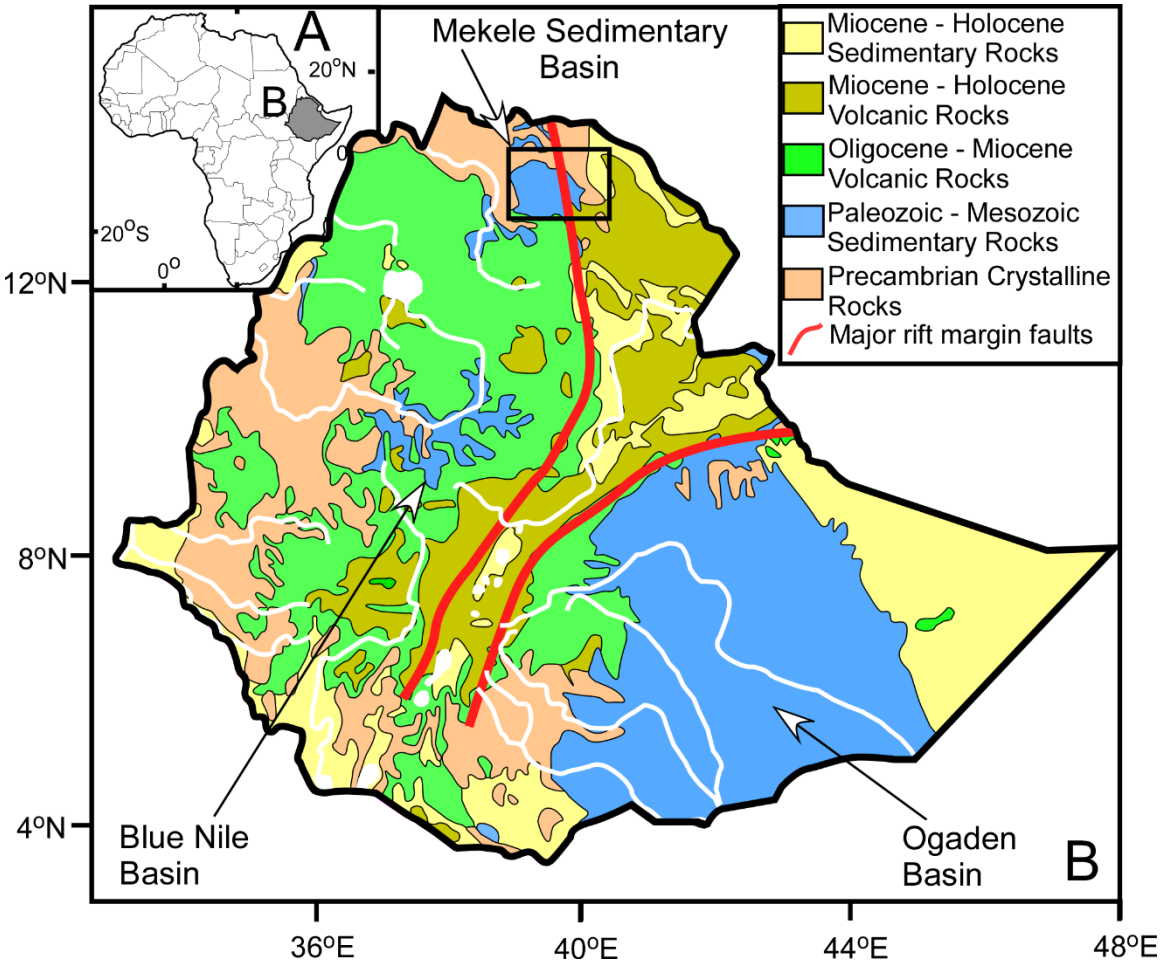

Figure 2.1: (A) Location of Ethiopia in Eastern Africa. (B) Geological map of Ethiopia showing the major stratigraphic features including the three major Paleozoic-Mesozoic sedimentary basins

(Mekele, Blue Nile, Ogaden) overlying the Precambrian crystalline basement of the Arabian-Nubian Shield and the Mozambique Belt. Modified after Tefera et al. (1996).

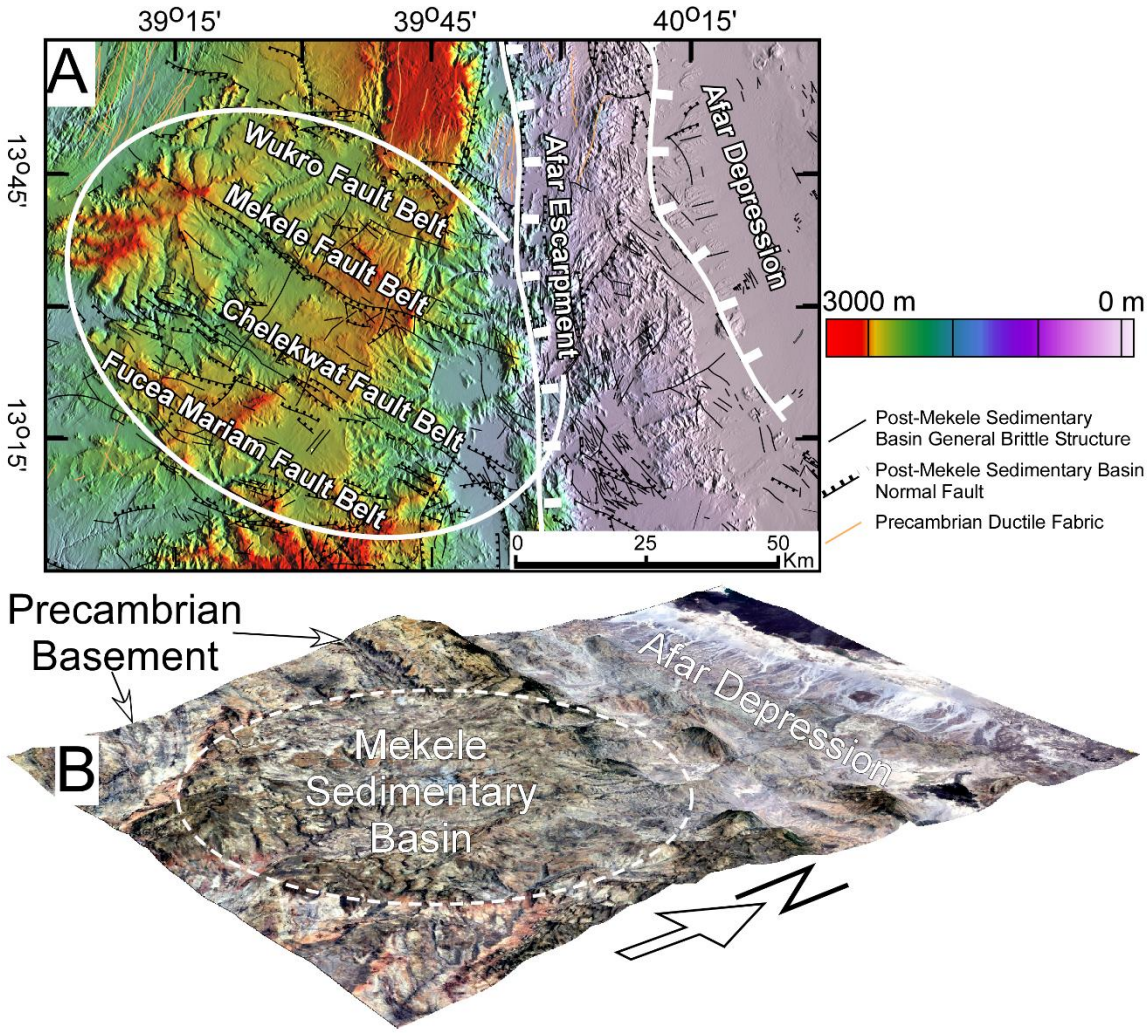

Figure 2.2: (A) Shuttle Radar Topography Mission (SRTM) Digital Elevation Model (DEM) of the Mekele Sedimentary Basin (MSB) with major NW-trending fault belts shown.(B) Threedimensional (3D) perspective view of the basin created by draping 3-2-1 Landsat Thematic Mapper (TM) image obtained from Google Earth onto the SRTM DEM.

Following studies by Sloss (1988), Leighton and Kolata (1990), Hartley and Allen (1994), Heine et al. (2008), and Xie and Heller (2009) the major geological and geophysical characteristics of ICONS can be summarized as follows: (1) they are circular to elliptical in map view and they are saucer-shaped in cross-sectional view, (2) they are filled with continental and shallow marine sediment, (3) they are located in the interior of lithospheric plates isolated from deformation along plate boundaries, (4) they were formed above cratons or Proterozoic or older accretionary orogenic terranes, hence the name "cratonic basins" only refers to their formation within the interior of stable continents, (5) they have a long and slow subsidence history, (6) they show 'Anomalous Tectonic Subsidence (ATS)' in reference to the subsidence that remains unaccounted for after back-stripping, (7) they are characterized by circular to elliptical and concentric gravity minima due to the presence of thicker sedimentary sections towards the center of the basins, and (8) they are underlain by largely un-stretched crust and sub-continental lithospheric mantle (SCLM).

Various models have been proposed for the formation of ICONS that advocated for subsidence due to vertical forces that could be due to: (1) subsidence following erosion of thermally uplifted terrains as suggested for the Michigan Basin (Sleep and Snell, 1976), (2) breakup of a supercontinent followed by emplacement of anorogenic granitic bodies as has been suggested for the Illinois, Michigan, and Williston basins (Klein and Hsui, 1987), (3) crustal and mantle phase changes from mafic composition to eclogite causing it to become denser as proposed for the Michigan and Williston basins (Ahern and Dikeou,1989; Baird et al., 1995) and for the Barents Basin in Russia (Artyushkov, 2005), (4) basaltic underplating and subsequent cooling causing negative buoyancy and long subsidence without extending the lithosphere (Stel et al., 1993), (5) subsidence associated with dynamic topography related to movement of lithospheric plates from upwelling to downwelling zones (Gurnis, 1993; Heine et al., 2008) or due to the presence ofan unstable convective mantle as proposed for ICONS in general (Hartley and Allen, 1994; Vyssotski et al., 2006; Downey and Gurnis, 2009), (6) thermal contraction of a mantle plume as proposed for

the West Siberian Basin (Saunders et al., 2005; Ritzmann and Faleide, 2009), (7) cooling and thickening following lithospheric rejuvenation as suggested for the Williston basin (Ahern and Ditmars, 1985) or of an initially thin and juvenile accretionary lithosphere as suggested for the Ghadames and Al Kufrah basins in northern Africa (Holt et al., 2010) and for the Parana basin in Brazil, the Karoo basin in South Africa, the Arabian Platform, the Scythian and Turan platforms in Central Asia, and eastern Australia (Holt et al., 2015), and (8) erosion following lithospheric thickening as proposed for ICONS in general (McKenzie and Priestley, 2016).

In this study, we examine the spatial and temporal evolution of the MSB as to whether it was formed as a rift basin or as ICONS basin. First, we outline the general geological characteristics of the MSB based on previously published geological data, remote sensing observations, and field study. Field study comprises stratigraphic analysis, such as measurement of thickness and orientation of sedimentary units, especially along the margins of the basin. These data helped to constrain part of the geological cross sections shown in Fig. 2.4. Bouguer gravity anomalies from the satellite-derived World Gravity Model 2012 (WGM, 2012; Bonvalot et al., 2012) are used to image the Moho beneath the MSB using a two-dimensional (2D) radially-averaged power spectral analysis (will refer to hereafter as the "spectral analysis"), and the Lithoflex 3D forward and inverse modeling. In addition, the Bouguer gravity anomaly was used to examine the geometry and the lithospheric structure of the basin through 2D forward gravity modeling. Using the above analyzes as constraints, the possibility that the MSB was formed as due to cooling and thickening of an initially thin and juvenile SCLM of the Arabian-Nubian Shield is examined.

2.3. THE MEKELE SEDIMENTARY BASIN (MSB)

The common theme underlying the limited number of studies conducted in the MSB and surroundings was a consistent attempt to explain the evolution of the basin in terms of a sea transgression and regression event that filled NW-trending rift system (Levitte, 1970; Beyth, 1972;

Bosellini et al., 1997). The NW-trending rift system was considered to be part of the multi-branched Paleozoic e Mesozoic rift system developed as the product of the breakup of Gondwana (Bosellini, 1989; Bosworth, 1992). The MSB is filled with ~2 km Paleozoic – Mesozoic mixed clastic-carbonate sedimentary rocks covering an area of ~8000 km2. It is underlain and surrounded to the north, west and south by peneplained Neoproterozoic crystalline basement rocks (Figs. 2.3-2.5). Early work by Levitte (1970) established the basic stratigraphy of the basin as constituting Mesozoic sedimentary formations resting on Neoproterozoic crystalline basement rocks. Beyth (1972) published the first complete map of the basin (Fig. 2.3) and divided its sedimentary rocks into six lithostratigraphic units, which have been subsequently refined by other authors (Bosselini et al., 1997; Bussert and Schrank, 2007; Dawit, 2010). The stratigraphy of the MSB includes the Neoproterozoic crystalline basement rocks of the Arabian-Nubian Shield at the bottom unconformably overlain by Paleozoic and Mesozoic sediment which in-turn are overlain and intruded by scattered Tertiary volcanic rocks (Fig. 2.3).

2.3.1. THE NEOPROTEROZOIC CRYSTALLINE BASEMENT

The Neoproterozoic crystalline basement rocks of the Arabian- Nubian Shield are predominantly low-grade volcano-sedimentary rocks intruded by syn-to post-deformation plutonic rocks. The volcano-sedimentary rocks include metabasalt, meta-greywackes and metabreccia, and other rocks such as black limestone, diamictite, conglomerate, and dolomite. Syn-to post-deformation Neoproterozoic plutons consist of granites, granodiorites, and diorites (Beyth, 1972).

2.3.2. THE PALEOZOIC AND MESOZOIC SEDIMENTS

Palaeozoic siliciclastic sediment form the oldest undeformed sedimentary succession unconformably overlying the Neoproterozoic crystalline basement rocks. In northern Ethiopia, they are subdivided in two unconformity bounded glaciogenic units, the Enticho Sandstone and the Edaga Arbi Glacials. The Mesozoic sediment comprise the bulk of the sedimentary package, and

are sub-divided into four formally and informally established formations. From the bottom, these formations are the Adigrat Sandstone, the Antalo Limestone, the Agula Shale, and the Amba Aradam Formation (Fig. 2.3).

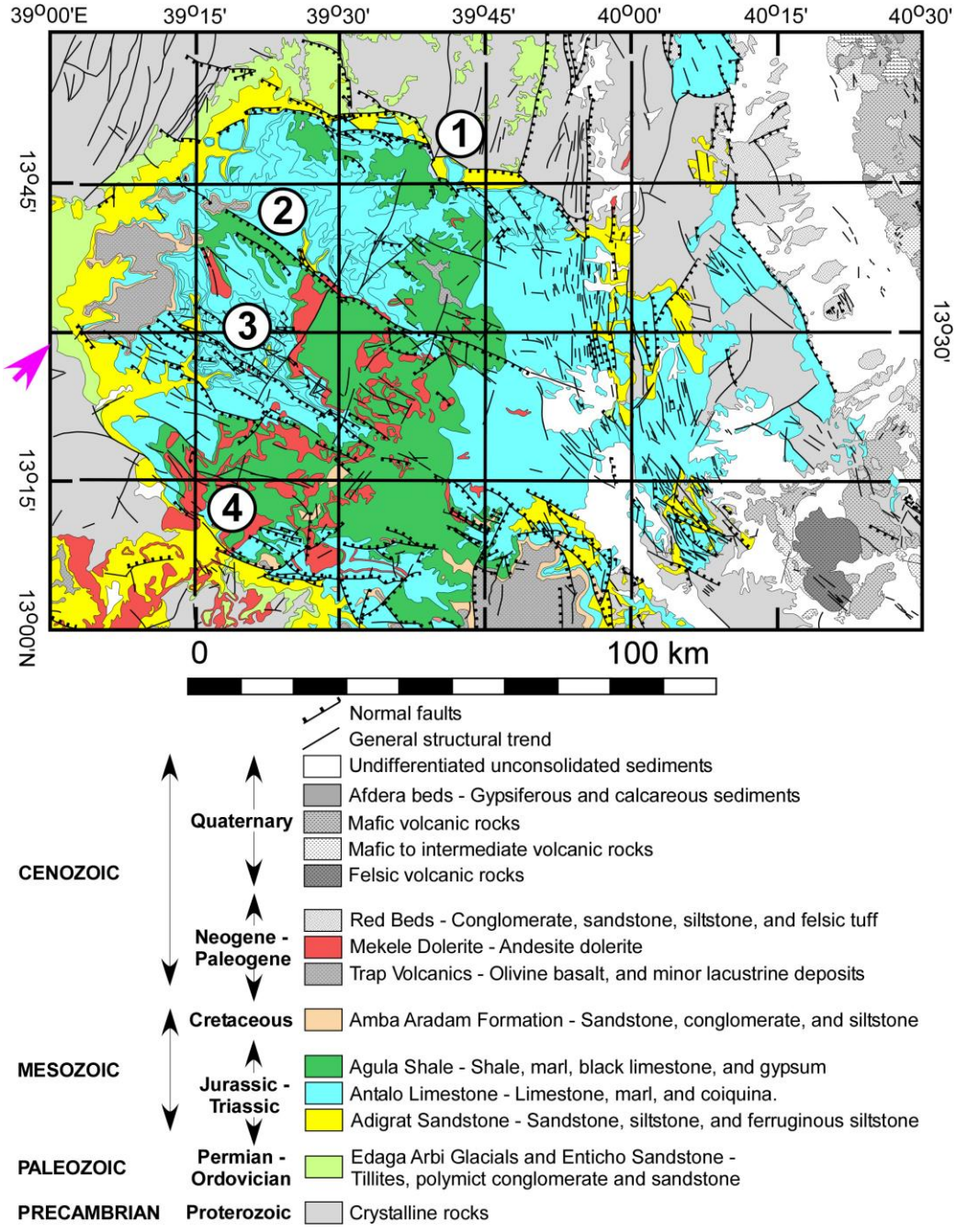

Figure 2.3: Geologic map of the Mekele Sedimentary Basin (MSB). Modified after Beyth (1972). Circled numbers denotes major NW-trending fault belts. 1 = Wukro. 2 = Mekele. 3 = Chelekwat.

4 = Fucea Mariam. Horizontal and vertical lines show the location of the cross-sections shown in Fig. 2.4. The pink arrow shows the location and direction of the field photograph in Fig. 2.5.

2.3.2.1. THE ENTICHO SANDSTONE

The Edaga Arbi Glacials unconformably overlie the Enticho Sandstone and, in places, lie directly on the Neoproterozoic crystalline basement rocks (Dow et al., 1971). Their thickness is approximately 200m in northern Ethiopia, but significant lateral thickness variations occur (Bussert, 2010). Bussert and Dawit (2009) and Bussert (2014) give detailed descriptions of the sediment facies. The Edaga Arbi Glacials consist of tillite at the base overlain by laminated clay- and siltstones, which contain scattered out-sized clasts and lenses of sandstone (Beyth, 1972; Bussert and Dawit, 2009; Bussert, 2014). The presence of abundant dropstones and other erosional features indicate deposition in a glacial setting, often in N-S oriented valleys most of which have incised into the Neoproterozoic crystalline basement rocks. The unit contains palynomorphs that provide CarboniferousePermian age (Bussert and Schrank, 2007; Bussert, 2014).

2.3.2.2. THE EDAGA ARBI GLACIALS

The Edaga Arbi Glacials unconformably overlie the Enticho Sandstone and, in places, lie directly on the Neoproterozoic crystalline basement rocks (Dow et al., 1971). Their thickness is approximately 200m in northern Ethiopia, but significant lateral thickness variations occur (Bussert, 2010). Bussert and Dawit (2009) and Bussert (2014) give detailed descriptions of the sediment facies. The Edaga Arbi Glacials consist of tillite at the base overlain by laminated clay- and siltstones, which contain scattered out-sized clasts and lenses of sandstone (Beyth, 1972; Bussert and Dawit, 2009; Bussert, 2014). The presence of abundant dropstones and other erosional

features indicate deposition in a glacial setting, often in N-S oriented valleys most of which have incised into the Neoproterozoic crystalline basement rocks. The unit contains palynomorphs that provide CarboniferousePermian age (Bussert and Schrank, 2007; Bussert, 2014).

2.3.2.3. THE ADIGRAT SANDSTONE

The Adigrat Sandstone consists of up to 430m thick continental to shallow-marine siliciclastic sediment (Blanford, 1869). Interpretation of a depositional environment for this unit is controversial as most previous studies (e.g., Assefa, 1991; Bosellini et al., 1997) consider the Adigrat Sandstone as fluviatile. However, Dainelli (1943) and more recently Dawit (2010), after a detailed investigation of the stratigraphy, sedimentary facies, depositional environments and palynology ofthe 'Adigrat Sandstone' succession in the Mekele Basin, documented a tide-dominated estuarine, storm-dominated shoreface deposits, as well as fluvio-deltaic deposits barrier-lagoon systems. Based on microflora, the Adigrat Sandstone succession in the MSBwas assigned Late Triassic-Middle Jurassic age (Dawit et al., 2009; Dawit, 2010).

2.3.2.4. THE ANTALO LIMESTONE

The Antalo Limestone is 690e740m thick and was first named by Blanford (1869). It has been considered by numerous researchers (Levitte, 1970; Beyth, 1972; Merla et al., 1979; Bosellini et al., 1997; Martire et al., 2000; Kiessling et al., 2011) as a Late Jurassic carbonate platform deposited on a homoclinal ramp subjected to marine transgression. This unit is made up of limestones interbedded with marls, shales and mudstones. It also consists of abundant fossils such as, brachiopods, gastropods, echinoderms, and small patches of corals and stromatoporoids.

2.3.2.5. THE AGULA SHALE

The Agula Shale is 60e250m thick and was first identified by Beyth (1972). It represents a predominantly shaley unit with evaporitic rocks at the top, overlying the Antalo Limestone. It is

considered to be deposited following regression of the sea during the Late Jurassic. Most of the Mekele Dolerite sills and dikes are emplaced within this unit.

2.3.2.6. THE AMBA ARADAM FORMATION

The Amba Aradam Formation is 60e200m thick and was first named by Shumburo (1968). It is considered to be upper Cretaceous and unconformably (angular in places) overlies the Agula Shale. It is predominantly sandstone with siltstone and mudstone intercalations. It is intensively lateralized in most places (Beyth, 1972) and is interpreted as being deposited in a fluviatile setting based on multiple point bar cycles (Bosellini et al., 1997).

2.3.3. THE TERTIARY IGNEOUS ROCKS

In places, the sedimentary sequences within the MSB are overlain and intruded by Tertiary igneous rocks and intercalated intertrappean sediment (Fig. 2.3). These layered volcanic units are remnant of the flood basalt magmatism that was succeeded by the domal uplift of the Ethiopian Plateau which gave rise to exhumation of the MSB and surrounding region combined with rift flank uplift in the western escarpment the Afar Depression. Abundant sills and dikes commonly referred to as the 'Mekele Dolorites' were emplaced predominantly within the Agula Shale (Arkin et al., 1971).

2.3.4. BASIN EVOLUTION

From the Paleozoic to the Late Mesozoic, the zone of sediment accumulation or the depocenter of the MSB appears to have changed and consequently three sub-basins were identified by Beyth (1972). These are: (1) The Enticho Sandstone sub-basin in the northern and eastern part of the MSB. (2) A N-S trending sub-basin filled with the Edaga Arbi Glacials. These depocenters were formed by N-S oriented glacial incision into the Neoproterozoic crystalline basement rocks during the Ordovician and Permo-Carboniferous glaciation (Bussert, 2010). (3) The Adigrat-Antalo-

Agula-Amba Aradam sub-basin which contains Mesozoic sedimentary package mostly deposited due to sea transgression coming from the east and south.

Regional correlation with sedimentary basins in Ethiopia such as the Blue Nile Basin (Russo et al., 1994) or the Ogaden Basin (Hunegnaw et al., 1998) (Fig. 2.1) shows a similar stratigraphic framework. Other studies (e.g., Hutchinson and Engels, 1972; Bosellini et al., 1997), based on similarities in stratigraphy across the Mesozoic basins of Yemen along the Red Sea coast, proposed a possible spatial connection with the MSB. Worash and Valera (2002) from a geochemical analysis of carbonate sequences identified major and rare earth element (REE) concentrations as indicative of a more oxidized water in a shallow basin influenced by clastic input from the surrounding Neoproterozoic crystalline basement rocks, but also shows that REE concentrations could be attributed to presence of localized restricted circulation.

Major structural components of the MSB are shown in Figs. 2.2A and 2.3. In general, there are two sets of normal faults that affect the basin. Stratigraphic relationship shows that both sets were developed after the formation of the basin. The oldest set is NWtrending and cuts through all formations including the Cretaceous Amba Aradam Formation which we interpret as a post-MSB sequence. The NW-trending structures can be grouped into four fault belts which essentially sub-divided the MSB into multiple structural sub-basins. These are from northeast to southwest the Wukro, the Mekele, the Chelekwat, and the Fucea Mariam fault belts (Figs. 2.2A and 2.3). The youngest set is N-trending and this is related to the rifting in the Afar Depression (Fig. 2.3). These faults are parallel to the Neoproterozoic crystalline basement fabric (Fig. 2.3) and it could be reactivation of this structure.

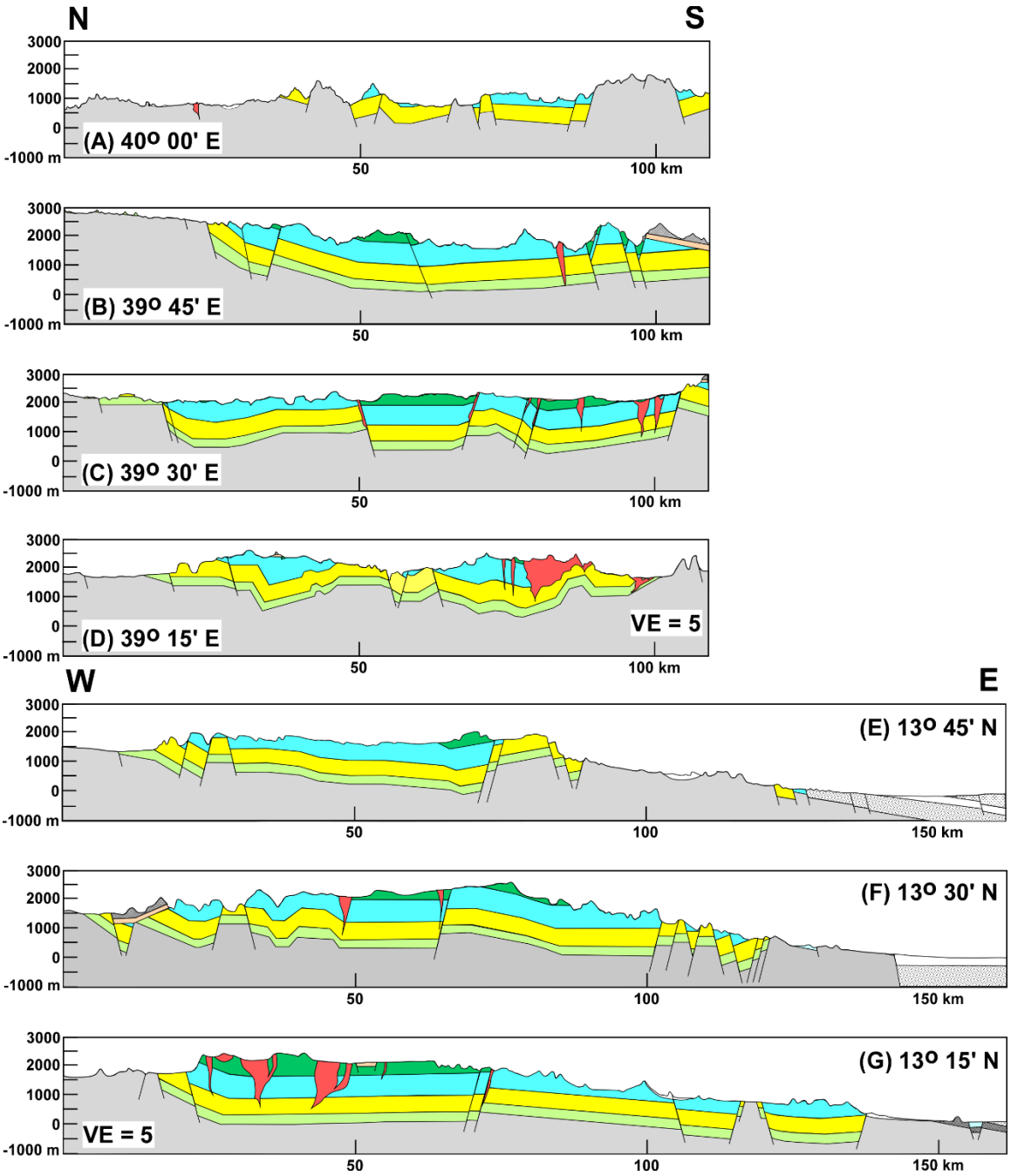

Figure 2.4: Idealized N-S (A-D) and E-W (E-G) geologic sections across the Mekele Sedimentary Basin (MSB). The longitudes of the baseline of the N-S cross-sections are shown in the lower left corners of the frames whereas the latitudes of the E-W cross-sections are shown on the upper right corners of the frames. See Fig. 2.3 for the location of the cross-sections.

Figure 2.5: Field photograph (looking northeast) of the western part of the Mekele Sedimentary Basin (MSB) showing the angular unconformity between the Paleozoic e Mesozoic sedimentary rocks and the Neoproterozoic crystalline basement rocks. See Fig. 2.3 for the location of the photograph.

2.4. DATA AND METHODS

2.4.1. SATELLITE GRAVITY DATA

The only available land gravity and magnetic data collected in the MSB are E-W and N-S profiles (Gebreyesus et al., 2000). Since the landscape is characterized by a steep and rugged topography with few roads, collecting gravity data in a straight profile is difficult, and hence the profile has lateral variations of up to ~10 km making 2D modeling difficult. Therefore, we relied on the

satellite gravity data for our study which includes Bouguer gravity analysis, spectral analysis, Lithoflex 3D inverse modeling, and 2D forward modelling along N-S and E-W profiles.

There have been numerous worldwide gravity models that have combined land, airborne, marine and satellite data. The Earth Gravitational Model 2008 (EGM 2008; Pavlis et al., 2012) and the WGM 2012 (Bonvalot et al., 2012) are among the most commonly used gravity models. The WGM 2012 data improves on its predecessor, the EGM 2008 model, which was developed from the integration of the Gravity Recovery And Climate Experiment (GRACE) and gravity data derived from terrestrial, airborne and marine surveys.

TheWGM2012 data are used in this study as it provides a better spatial resolution and comprises a more homogeneous global gravity dataset (Balmino et al., 2011). This dataset is suitable for mapping lithospheric-scale structure including depth to the Moho. It uses a topographic correction based on the Global Topographic 30 arc second (GTOPO30) digital elevation model (Bonvalot et al., 2012) to create Free-air, Bouguer and isostatic gravity anomaly datasets. The Bouguer gravity anomalies of the study area is shown in Fig. 2.6A.

2.4.2. SPECTRAL ANALYSIS

The spectral analysis method is commonly used to map depths to density interfaces (Spector and Grant, 1970; Tselentis et al., 1988) and is used here to determine the depth to the crust/mantle boundary. We use the Bouguer gravity anomalies in our analysis (Fig. 2.6A). The power spectrum method calculates spectra of a region by transforming the data from the space domain into the time domain via a Fourier transform. The most commonly used method is to determine a spectral curve via a 2D radially-averaged power spectral of a square region (Tselentis et al., 1988). The logarithm of these spectral values are assumed to have a linear relationship with the wavenumber (Mishra and Pedersen, 1982; Tselentis et al., 1988). Hence, plotting the natural logarithm of the power spectrum versus the wavenumber results in a spectral graph where the linear segments will have slopes

proportional to the depth to the top of the density interface. Commonly, the spectral graph will have three different slopes that can be broken into a lower, middle and upper linear segments which corresponds to the mean depths of the density interfaces (Fig. 2.7A). The lower segment represents a shallow depth, the middle segment represents a moderate depth and the upper segment represents a deeper depth (Tselentis et al., 1988; Gómez-Ortiz et al., 2005). The depths that are determined depend on the size of the area analyzed as Mickus and Hussein (2016) showed that the area must be 2 to 3 times larger than the depth to the interface.

The MSB only covers an area of about 80 km X 100 km, but we have produced a Bouguer gravity anomaly map covering a wider area in order to determine the regional structure and to be able to determine the depth to the crust/mantle boundary which could be up to 40e45 km deep in the Northwestern Ethiopian Plateau. The spectral methods are sensitive to noise and small-scale anomalies in the data, so to remove these small-scale anomalies, the Bouguer gravity anomaly data were upward continued to 2 km above the Earth's surface (Fig. 2.7B). We then extracted 1^{o} X 1^{o} (111 km X 111 km) square regions, with 50% overlap (in order to reduce the edge effects) (Tselentis et al., 1988; Leseane et al., 2015; Emishaw et al., 2017). For each of these regions, a 2D radially averaged power spectrum was calculated. From these spectra, the linear segments were determined and this is subject to error, so the Linest function present in Excel was used to calculate the linear segments and to determine the statistical error in this determination. Conventionally, the largest density contrast within the lithosphere is assumed to correspond to the crust-mantle boundary (the middle slope) if the region analyzed is large enough (Tselentis et al., 1988; Tanaka et al., 1999). For instance, Fig. 2.7A shows a marked change in slope at wave numbers of about 0.19 cycles/km and 0.3 cycles/km. For most of the curves, wave numbers ranging between 0.2 and 0.3 cycles/km were used to estimate the middle slope. The error in the Moho depth estimation was calculated from the standard deviation of the slope of the best fitting line for the middle segments and was found to be between 0.4 and 2 km.

An example of the spectral curve of a sub-region in the southwestern portion of the MSB (Fig. 2.7B) is shown in Fig. 2.7A. The curve has three distinct linear segments. However, in areas near the Afar Depression, where the geology is complex and the density significantly varies horizontally over a short distance, mostly due to extensive diking and faults, the spectral curves often show multiple sharp slope breaks (Fig. 2.7C). Hence, particular care was taken in selecting the segment of the spectral curves representing the depth to Moho in this region. The depth to Moho map of the MSB and surroundings obtained from the spectral analysis is shown in Fig. 2.8A.

2.4.3. THREE-DIMENSIONAL (3D) MODELING

Approximate depths to the Moho can be obtained via 3D modeling of Bouguer gravity anomalies (Ebbing et al., 2007). We used the Lithoflex modeling routine (Braitenberg et al., 2007) which is a multi-purpose algorithm that combines 3D forward and inverse modeling to determine the depths to density interfaces and investigates the isostatic state of a region. From the Bouguer gravity anomalies of the WGM 2012, we determined the Moho topography beneath the MSB. Lithoflex uses the Parker inverse method (Parker, 1972) to determine the depth to a single density interface. First, the algorithm determines the gravity anomalies due to a starting model through forward and then iteratively finds the best fitting interface through an inverse calculation (Braitenberg et al., 2007).

The Bouguer gravity anomaly data are inputted in a grid format and the input parameters include: First, as a starting depth, we used 35km since we are interested in the depth to the Moho. The 35km starting model was based on seismic studies that were primarily focused on the Afar Depression as there are few studies in the Northwestern Ethiopian Plateau (Dugda et al., 2005; Hammond et al., 2011), and none of which are specifically focused on the MSB. These studies, and additional gravity based inverse models (Tiberi et al., 2005; Mammo, 2013) estimated a ~40 km to 45 km deep Moho in the plateau region that tends to decrease to ~30 km to 20 km towards the Afar Depression. We also extracted a crustal thickness map from the global crustal thickness compilation

of Laske et al. (2013), and got an average 35km deep Moho beneath the plateau. Thus, the 35km compensation depth preferred in this model represents a mean depth of the Moho in this region. Second, an approximate density contrast between the mantle and the crust of 0.5 g/cm3 was assigned. The 2D seismic refraction modelling across the Main Ethiopian Rift, which partly included the Northwestern Ethiopian Plateau, found P-wave velocities between 6.0 km/s - 6.8 km/s and 8.1 km/s, respectively, for the crust and upper mantle (Maguire et al., 2003; Mackenzie et al., 2005). These velocities can be used to constrain the densities of the crust and upper mantle based on the velocity/density relationships. These relationships were applied to determine density contrasts of 0.4 g/ cm3 (Mammo, 2013) and 0.53 g/cm3 (Tiberi et al., 2005), with initial Moho depths of 28 km and 30 km, respectively. We tested a combination of density contrast values vs our initial compensation depth (35 km), and have chosen a density contrast of 0.5 g/cm3 as a reasonably acceptable value. Third, a 100 km cut-off wavelength, which is a low-pass filter where high frequency features are removed, was applied. As discussed above, for a depth of 35 km and density contrast of 0.5 g/cm3 various Moho models were generated using different cut-off wavelengths. The 100 km cut-off gave us a realistic representation of the Moho depth based on the above constraints.

Using the above parameters, a resultant depth to the Moho is shown in Fig. 2.8B. In general, the highest elevation areas in the Northwestern Ethiopian Plateau are underlain by a deeper Moho, while areas in the Afar Depression are underlain by a shallow Moho, showing an inverse topographic relationship. One aspect we would like to caution is that in areas with complex geology such as the study area, the use of a similar compensation depth and density contrast values may potentially introduce uncertainties in the derived Moho depths. However, we are interested in the regional variations of the Moho depth and the model shown is one acceptable model that agrees with the available seismic constraints. Fig. 2.8B shows a topography change in the Moho depth as one goes from the western MSB (the part of the basin that is in the Northwestern Ethiopian Plateau)

to the Afar Depression. These values will be used as well as the results of the spectral analysis to better constrain the Moho depth beneath the MSB in the 2D forward gravity modelling (see below).

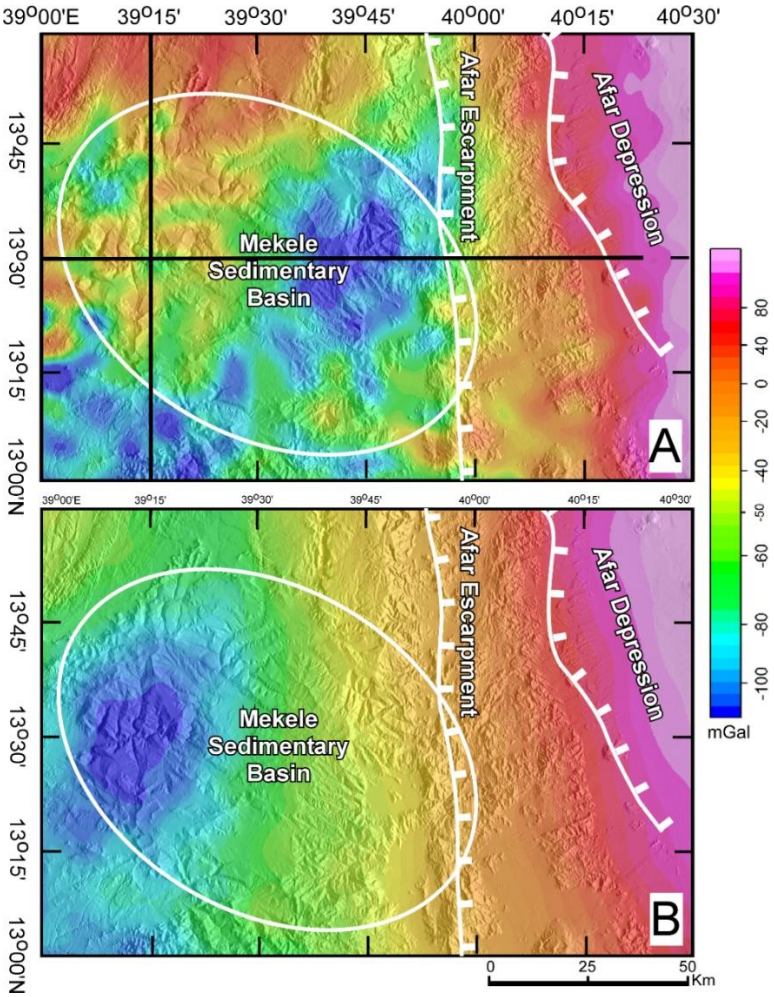

Figure 2.6: (A) Bouguer gravity anomaly map of the Mekele Sedimentary Basin (MSB) extracted from the World Gravity Model 2012 (WGM 2012). (B) Five km upward continuation of the Bouguer gravity anomalies. Horizontal and vertical black lines in Fig. 2.6A show the location of the E-W and N-S two-dimensional (2D) forward gravity models shown in Fig. 2.9A and B, respectively.

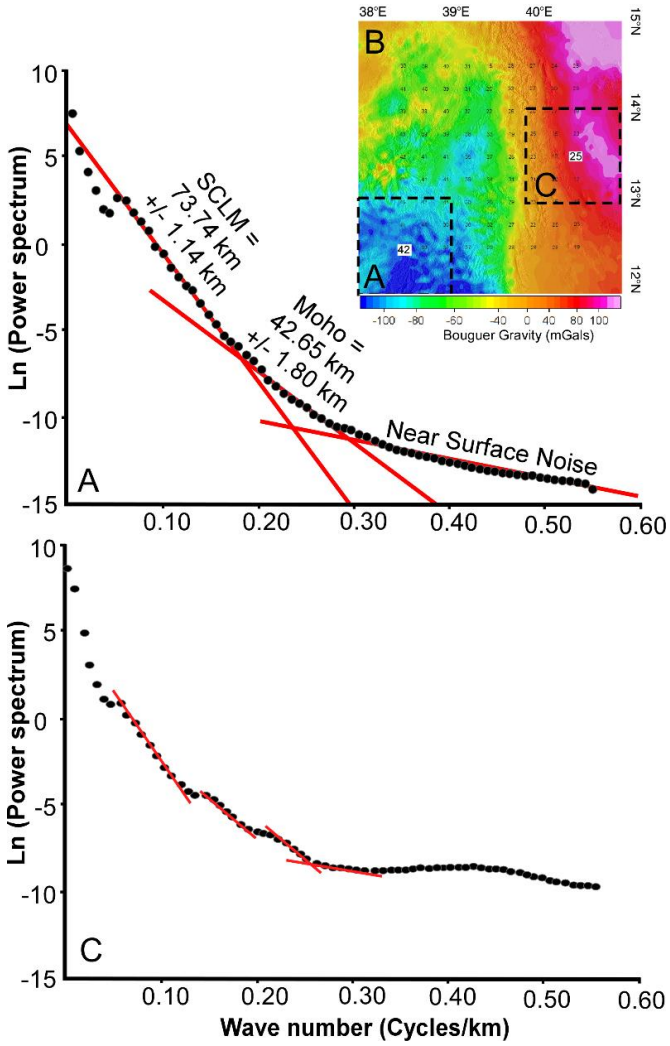

Figure 2.7: (A) An example of the two-dimensional (2D) radially-averaged power spectral curve used to estimate the depth to Moho from the Bouguer gravity anomaly map of the World Gravity Model 2012 (WGM 2012). The middle slope is taken as the approximate depth to the Moho calculated for a 1^0X1^0 (~111 X 111 km) sub-window from the southwestern part of the Mekele Sedimentary Basin (MSB) as shown in Fig. 2.7B. (B) Two km upward continuation of the Bouguer gravity anomaly map with Moho depth estimates from the 2D radially averaged power spectral analysis. (C) An example of the 2D radially-averaged power spectral curve for a 1oX1o sub-region region within the Afar Depression as shown in Fig. 2.7B. The spectral curve shows multiple sharp slope breaks.

2.4.4. TWO-DIMENSIONAL (2D) FORWARD MODELING

To determine the general crustal and upper mantle structure of the MSB region, two profiles (Fig. 2.9A and B) of the Bouguer gravity anomalies were modeled using 2D forward modeling. Since we are interested in the overall lithospheric structure, the detailed basin stratigraphy and structure was not modeled. To obtain reasonable models, constraints are needed and we used the crustal thickness estimates obtained from the above spectral analysis (Fig. 2.8A) and the 3D modeling (Fig. 2.8B) along with constraints from receiver function studies (Hammond et al., 2011). Density values of the sedimentary sequences were not available and there are no seismic refraction models in the MSB where the P-wave velocities could be used to estimate densities, so we used commonly accepted densities for sedimentary rocks (e.g., Telford et al.,1990), and values from nearby seismic refraction experiments (e.g., Mackenzie et al., 2005) for crustal and mantle lithologies. The P-wave velocities were converted to densities using velocity-density empirical relationships (Nafe and Drake, 1957). We used a density of 2.5 gm/cm3 for the sedimentary rocks within the MSB, 2.4 g/cm3 for the recent sediment in the Afar Depression, 2.7 g/cm3 for the upper crust, 2.95 g/cm3 for the lower crust, 3.33 g/cm3 for the normal SCLM, and 3.1 g/cm3 for the metasomatised SCLM. Due to its location bordering the highly extended and volcanically active Afar Depression, mafic bodies intruding the MSB were incorporated in the modeling using a density of 3.0 g/cm3. The above values were used as starting values in the modeling. These density values were varied iteratively in order to obtain a reasonable fit between the observed and calculated gravity anomalies (Fig. 2.10). The final model is shown in Fig. 2.9.

2.5. RESULTS

2.5.1. BOUGUER GRAVITY ANOMALY ANALYSIS

The Bouguer gravity anomalies range between ~130 and ~110 mGal with the highest values occurring over the Afar Depression (Fig. 2.6A) due to the thinner crust (Mickus et al., 2007).

However, despite the effect of the Afar Depression on the Bouguer gravity anomalies, the MSB is characterized by a gravity minimum that reaches in places ~ -110 mGal (Fig. 2.6A). The lowest amplitude Bouguer gravity anomalies are generally confined to where the MSB crops out (Fig. 2.6A). However, similar amplitude gravity minima are observed outside the southwestern margin of the basin (Fig. 2.6A). These might be due to the presence of outcrops of the Adigrat Sandstone that are found to the southwest of the MSB (Fig. 2.3).

The upward continued Bouguer gravity anomaly map shows the western part of the MSB to be characterized by a gravity minimum reaching ~ -110 mGal (Fig. 2.6B). According to Jacobson (1987), the source of the gravity signature obtained by upward continuing 5 km would be at or close to 2.5 km. This suggests that the upward continued gravity signature, which shows a concentric pattern (especially in the western part of the MSB away from the effect of the Afar Depression) represent sources at ~2.5 km. Stratigraphic studies have shown that the MSB is filled with ~2 km of sedimentary rocks.

2.5.2. GRAVITY-DERIVED MOHO DEPTHS

Both Moho depth maps produced from the spectral analysis and the 3D forward and inverse modeling of the Bouguer gravity anomalies capture, in general terms, the thinning of the crust from the west within the Northwestern Ethiopian Plateau towards the Afar Depression in the east (Fig. 2.8A and B). Both maps show the region to the southwest of the MSB with the thickest crust reaching ~40 km (Fig. 2.8A and B). Also, both maps show that the thinnest crust is beneath the Afar Depression reaching ~20 km on average (Fig. 2.8A and B). Additionally, the 3D forward and inverse modeling results show that the MSB is underlain by a relatively thicker crust approaching ~40km and that this thicker crust extends to the north of the MSB (Fig. 2.8B).

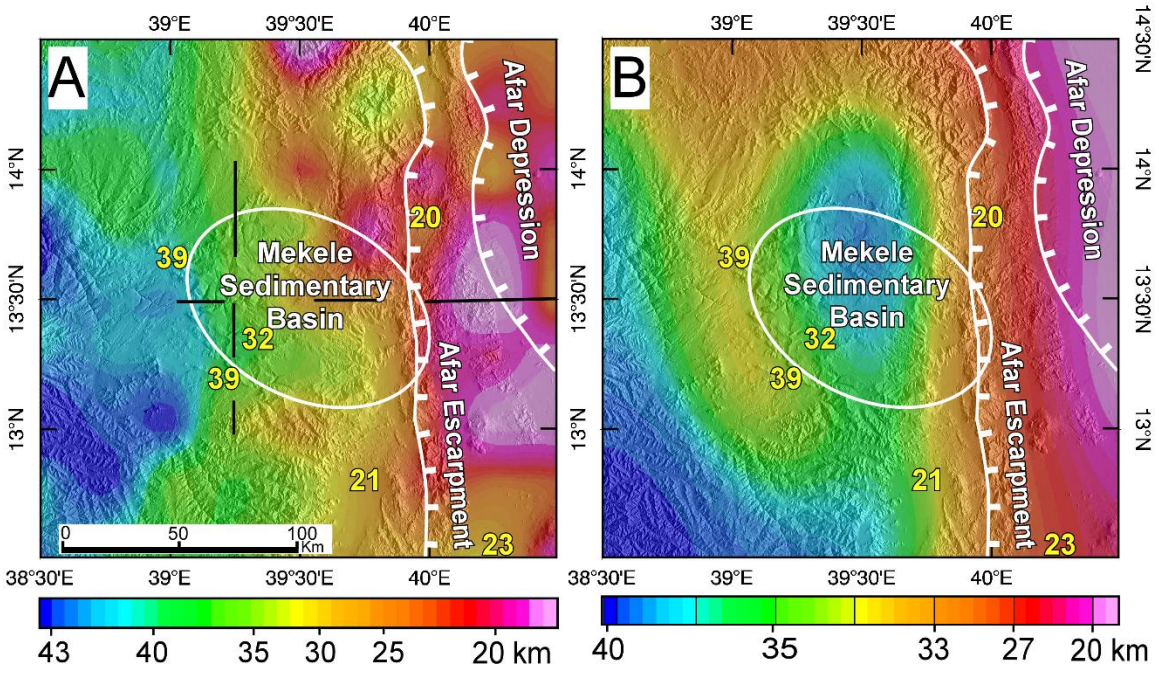

Figure 2.8: Crustal thickness estimates beneath the Mekele Sedimentary basin (MSB) and surroundings from the Bouguer gravity anomaly map of World Gravity Map 2012 (WGM 2012) using: (A) two-dimensional (2D) radially-averaged power spectral analysis. (B) Lithoflex modeling. Numbers in yellow indicate depth obtained from broadband passive seismic receiver function analysis (Hammond et al., 2011). Horizontal and vertical black lines in Fig. 2.8A show the location of the E-W and N-S 2D forward gravity models shown in Fig. 2.9A and B, respectively.

Seismic receiver function studies have imaged an abrupt decrease of the depth to Moho beneath the Northwestern Ethiopian Plateau where the MSB is located, from ~40 to ~20km beneath the Afar Depression (Hammond et al., 2011, 2013; Gallacher et al., 2016). Using the spectral analysis, an average crustal thickness of 39 km was found at the western and southern margins of the MSB (Fig. 2.8A). However, closer to the Afar Depression, the spectral curves for some sub-regions did not indicate a clear linear slope for the deeper layers possibly due to the crust being anomalously thin and the crust of the Afar being petrologically complex containing a number of recently active

magmatic segments (e.g., Keir et al., 2009). Therefore, we have systematically shifted the upper limit of the middle slope towards a higher wavenumber in order to capture these higher frequency features near areas where we have a significant lateral variation. This gave us a reasonable Moho depth estimates expected from a highly extended region.

2.5.3. RESULTS OF THE TWO-DIMENSIONAL FORWARD GRAVITY MODELING

The geologic cross sections constructed primarily from the surface geology illustrate a geometry for the MSB that resembles a saucer-shaped sedimentary basin (Fig. 2.4). However, the geometry of the eastern boundary along the border with the Afar Depression is complicated due to interaction with structures related to the rifting event. In addition, multiple sills and dikes associated with this rift are also widespread in the southern portion of the basin creating a complex stratigraphic architecture as shown in the E-W cross sections (Fig. 2.4).

The gravity model along the N-S profile follows longitude 39^0 15' E away from the Afar Depression (see Fig. 2.6A for location of the profile). At the southwestern edge of the MSB, the model has a crustal thickness estimate of ~39 km determined from seismic receiver functions (Fig. 2.8A; Hammond et al., 2011). Fig. 2.9A was modeled with a relatively flat Moho with no significant thinning beneath the center of the MSB. The E-W trending model (Figs. 2.6A and 2.8B) is constrained by a crustal thickness determined by a receiver function along its eastern edge (Hammond et al., 2011). The model shows significant crustal thinning from the Northwestern Ethiopian Plateau where it reaches a thickness of~40km towards the Afar Depression where it is ~20 km thick (Fig. 2.9B). The model also required a less dense (3.1 gm/cm^3) SCLM in its eastern part (Fig. 2.9B) that is attributed to possible hydrothermal alteration of the SCLM through metasomatic processes due to rifting in the Afar Depression or higher temperatures related to the rifting that is seen in high Vp/Vs ratios in parts of the Afar Depression (Stab et al., 2016).

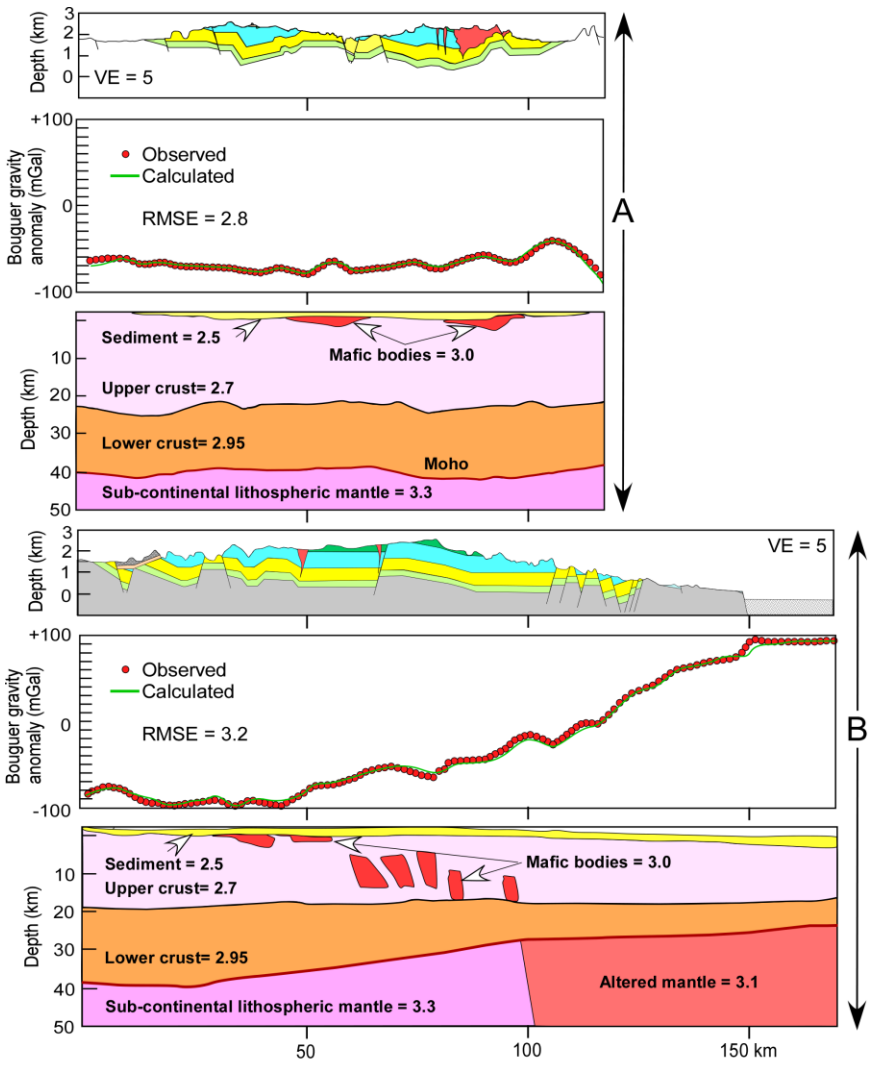

Figure 2.9: Two-dimensional (2D) forward gravity models showing the lithospheric structure beneath the Mekele Sedimentary Basin (MSB) along longitude 390 15'E (A) and latitude 130 15' N (B). See Fig. 2.6 for location of the models. In both (A) and (B) the upper panel is an idealized geological cross-section from the surface geology. The middle panel is the observed Bouguer gravity anomaly from the World Gravity Map 2012 (WGM 2012) and the calculated one. The lower panel is the 2D lithospheric model with the best fit between the observed and calculated Bouguer gravity anomaly.

The RMS error values for the N-S and E-W profile is 2.8 and 3.2 mGal, respectively. We provided one example of our sensitivity analysis on the E-W profile (Fig. 2.9B), using density values of 2.3e2.6 g/cm3 for the sediment, 2.65e2.75 g/cm3 for the upper crust, 2.9 to 3.0 for the lower crust, 3.05e3.15 g/cm3 for the altered SCLM, and 3.25e3.4 g/cm3 for the SCLM (Fig. 2.10). The model has high sensitivity to density variation for all units, except the lower density limit and upper density limit of the sediment and SCLM, respectively. A slight density change in other blocks, however, introduces large errors. We found the smallest error (3.27) to be associated with densities of 2.5 gm/cm3 for the sediment, 2.7 g/ cm3 for the upper crust, 2.95 g/cm3 for the lower crust, 3.33 g/cm3 for the normal SCLM, and 3.1 g/cm3 for the altered SCLM (Fig. 2.10).

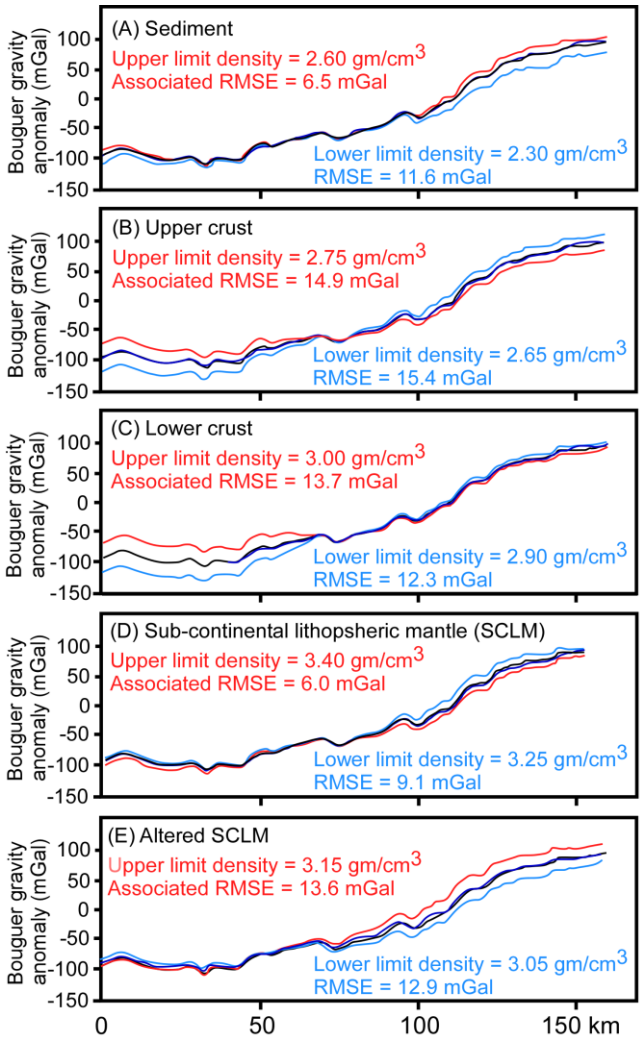

Figure 2.10: Density sensitivity analysis on the E-W two-dimensional (2D) forward gravity model shown in Fig. 9B by using different density values and calculating the associated Root Mean Square Error (RMSE) for sediment (A), upper crust (B), lower crust (C), sub-continental lithospheric mantle (SCLM) (D), and altered SCLM (E).

2.6. DISCUSSION

The interpretation of the MSB as an ICONS has important implications for the formation and evolution of sedimentary basins formed over similar settings. Below, we explore those implications to the stratigraphic and structural evolution of the MSB, the nature of lithospheric architecture, and possible subsidence mechanisms.

2.6.1. THE MEKELE SEDIMENTARY BASIN (MSB) AS AN INTRA-CONTINENTAL SAG BASIN (ICONS)

Regardless of its smaller size compared to other ICONS worldwide (Heine et al., 2008), the MSB possesses the diagnostic characteristics of an ICONS as outlined above. There are no detailed studies of the basin formation, as the MSB seems to have had a slow subsidence history based on the long history of sedimentary deposition. The oldest sedimentary rocks are Ordovician in age and the youngest sedimentary rocks are Jurassic in age. Recent seismic tomographic imaging using broadband seismic stations (Hammond et al., 2013; Gallacher et al., 2016) have shown that the MSB occurs close to a broad region (~200 km radius) of high shear wave velocities between 40 km and 132 km in depth that is distinctive from the slower shear wave velocities within the Afar Depression. Also, these faster shear wave velocities are distinctively faster than the relative faster shear wave velocities beneath the Northwestern Ethiopian Plateau (Fig. 2.11). These faster shear wave velocities are particularly prominent in the southwestern half of the MSM and the region to its southwest where it reaches 4.3 km/s within a ~100 km circular region (Fig. 2.11).

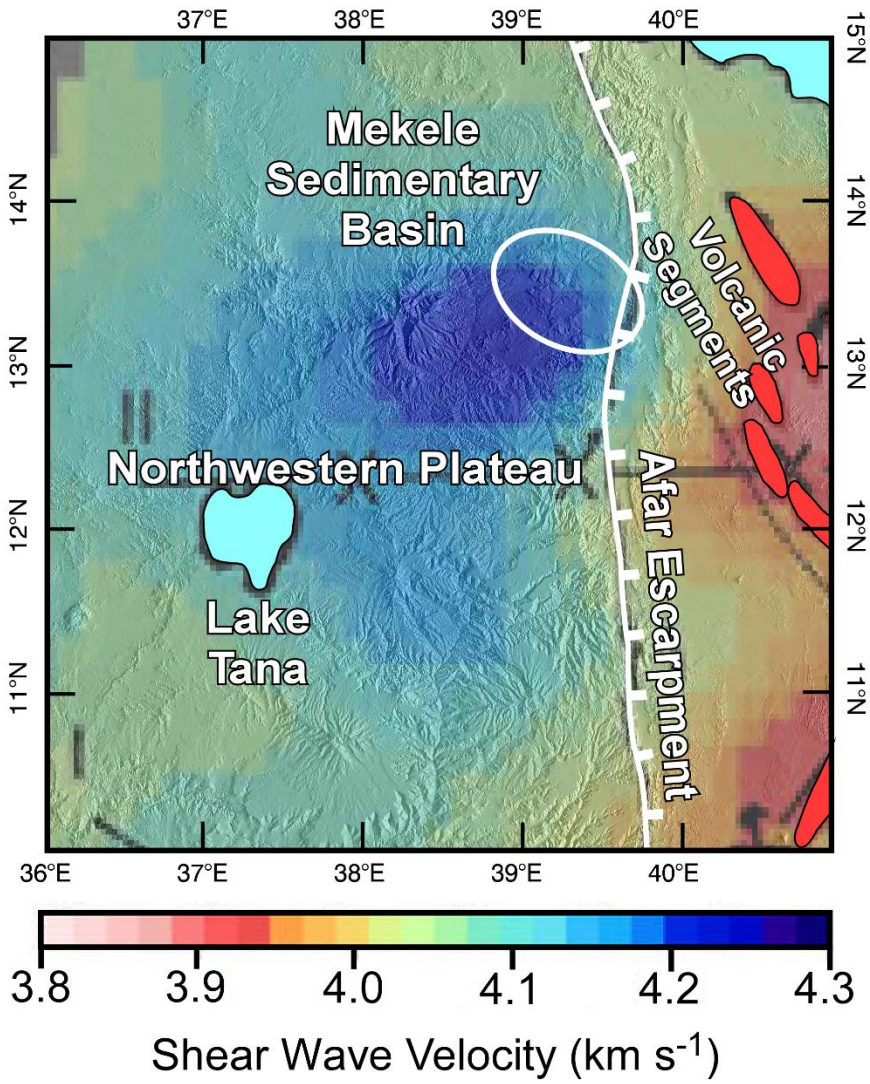

Figure 2.11: Shear wave velocity distribution beneath the Mekele Sedimentary Basin (MSB) and surroundings at 40e132 km depth showing the MSB is underlain by a broad zone of faster shear wave velocity. From Gallacher et al. (2016).

The MSB has been considered part of a multi-branched rift system related to the breakup of Gondwana (Bosellini et al., 1997). It is argued that it might be a NW-trending rift based on the presence of NW-trending faults within the basin (Fig. 2.2A), especially, the Wukro and the Fucea Mariam fault zones in the northeastern and southwestern parts of the MSB, respectively. The fault zones appear to represent what could be considered the border faults of a "Mekele rift" (Fig. 2.2A).

These structures seem to be extensional with a minor strike-slip component. Intraplate stresses are thought to be responsible for the development of widespread rifting in eastern and central Africa (Bosworth, 1992). It was mentioned above that the NW-trending faults cut through all formations including the Cretaceous Amba Aradam Formation (Figs. 2.3 and 2.4) which we interpret as a post-MSB sequence. Hence, these NW-trending faults do not appear to control sedimentation and they were developed after the formation of the MSB. Moreover, detailed examination of the boundary between the Neoproterozoic crystalline basement and the overlying Paleozoic Edaga Arbi Glacial sediment and the Enticho Sandstone (the preserved formation within the MSB) shows an angular unconformity relationship, especially in the western part of the basin where there is less structural complexities or faulting (Fig. 2.5). Thus, the contact between the Paleozoic sediment and the Neoproterozoic crystalline basement shows no apparent significant structural disturbance or faulting. Rather, in most part of the basin and specifically along the western margins, these sedimentary successions overlie the Neoproterozoic crystalline basement and gently dip eastward towards the center of the basin. Additionally, the Antalo Limestone gradually thins towards the western margin of the MSB before it completely disappears being replaced by the older Adigrat Sandstone (Figs. 2.3 and 2.4). These relationships show that the distribution of the clastic sedimentary rocks is not entirely limited to the present day MSB, and hence the Wukro and Fucea Mariam fault zones being the basin's border faults might not be accurate. Furthermore, the N-S gravity model also supports a concept of an ICONS underlain by a relatively flat Moho (Fig. 2.9A). Thus the extensive brittle deformation, which was interpreted as a reactivation of a rift system as inferred from surface geologic mapping, is not supported by crustal scale geometry. Rather, the MSB might have been part of a broader slowly subsiding platform that may have been compartmentalized due to the development of younger NW-trending fault belts.

2.6.2. NATURE OF THE LITHOSPHERE BENEATH THE MSB

The MSB is located above the Neoproterozoic accreted terranes of northern Ethiopia which represent part of the Arabian-Nubian Shield of northeastern Africa and western Saudi Arabia. The shield is dominated by island arc/back arc basins, terranes and micro-continents accreted together along sutures containing ophiolites (Kröner et al., 1987; Stern, 1994; Abdelsalam and Stern, 1996; Fritz et al., 2013). These terrane accretions accompanied the closure of the Mozambique Ocean, which was formed due to the break-up of the supercontinent Rodinia.

The main feature of these accretionary orogens that are important to our discussion is their lithospheric thickness. Many studies have indicated that accretionary orogens had an initially thin SCLM (e.g., Stern, 2002; Hyndman et al., 2005; Avigad and Gvirtzman, 2009). There are a number of mechanisms that are responsible for the creation of such a condition. One such mechanism involves the thickening of the SCLM and subsequent delamination due to gravitational instability (Avigad and Gvirtzman, 2009). The other and more plausible mechanism especially for the MSB region assumes a thinner lithosphere to be part of the nature of the accretionary orogens. The processes that are responsible for the formation of the terranes in this setting favor crustal growth but not the formation of a SCLM (Hyndman et al., 2005). Following the termination of orogenesis, the SCLM will start to cool and thicken to a 'normal' thickness, in a similar fashion as a newly formed oceanic crust would cool and thicken. Cooling and thickening of the SCLM is a major cause of post rift subsidence in extensional basins (McKenzie, 1978) except that in accretionary orogens where the thinner SCLM is not due to rifting. Various numerical modelling and geochronologic studies suggest that it takes about 250e300 Ma for an initially thin accretionary SCLM to reach its normal thickness of 125 km (e.g. Holt et al., 2010). During this period, the previously hot and light SCLM will become thicker and denser hence, creating negative buoyancy and subsequent subsidence. This mechanism has been attributed to account for the regional long-term subsidence patterns of basins located over the Neoproterozoic orogenic belt in North Africa and Arabia (Holt

et al., 2010, 2015). It is worth mentioning that almost all the 40Ar/39Ar ages obtained from different minerals extracted from rocks of the crystalline basement of Ethiopia cluster around ~540 Ma and this is taken to indicate the beginning of cooling of the Arabian-Nubian Shield juvenile SCLM (Stern et al., 2012).

2.6.3. BASIN EVOLUTION AND SUBSIDENCE MECHANISM

Based on the above gravity models and the sedimentary sequences, a thickening and cooling of a juvenile SCLM beneath the Arabian-Nubian Shield is a plausible mechanism for the formation of the MSB similar to the model of Holt et al. (2010, 2015) for sedimentary basins within accretionary terranes in North Africa and Arabia. Such a mechanism would have likely created a thick SCLM, and the subsidence would have been caused by the negative buoyancy created due to the SCLM's cooling and thickening. Seismic tomography images a circular to elliptical high velocity P and S-wave anomaly beneath the MSB (Hammond et al., 2013) and this may correspond to a SCLM layer beneath the basin and the immediate region under the basin that is thicker and colder than the surrounding region (Fig. 2.11). It is clear that this seismic anomaly mimics the surface and shallow subsurface geologic features that we interpret as indicative of geologic and geophysical characteristics of ICONS. However, there are still questions regarding how long this mechanism could sustain subsidence, which may be as long as 300Ma for thinner lithospheres of approximately 50 km to reach to a ‘normal thickness’ of 125 km (Holt et al., 2010). In addition, given the size of the MSB, which is small compared to other ICONS, how broad and large lithospheric scale processes would affect such a small area requires further analysis.

To try to answer why such a small area could form an ICONS, the subsidence model of Holt et al. (2010) was modified to accommodate the stratigraphic and structural features of the MSB. Accordingly, we classified the developmental history of the MSB into three phases (Fig. 2.12).

(1) Pre sag phase: This phase represents the time just after the formation of the Arabian-Nubian Shield in which most of the process was dominated by simultaneous peneplanation and exhumation of a just assembled continental lithosphere. Geomorphologic data show extensive erosion and peneplanation of the region (Coltorti et al., 2007) creating a smooth flat topography still preserved between the Paleozoic sedimentary rocks and the Precambrian crystalline basement rocks.

(2) Sag phase: this phase represents the major subsidence and sediment accumulation that shaped the MSB. Sedimentological evidence shows marine deposition indicates that the region, including the MSB may have been near sea level during the Ordovician time (Bussert and Dawit, 2009). Initially, deposition was extensive and occurred within N-S oriented linear valleys possibly between basement highs. Subsidence was facilitated by the cooling and thickening of the SCLM that may have continued until the Jurassic during the Gondwana breakup. Thermochronology and structural data also show that the area remained undisturbed until the end of Jurassic (Mock et al., 1999). The Paleozoic and early Mesozoic units (Enticho, Edaga Arbi and Adigrat Sandstone) are not localized to the MSB and have been reported throughout the region, forming a widespread basal blanket of clastic sedimentary rocks. A significant regional and possibly local tectonic disturbance in the region happened during the Jurassic that is related to the breakup of Gondwana. During this time, far field stresses associated with extensive rifting and continental breakup across the continent may have created a marked, perhaps localized tectonic disturbance within the MSB, which in turn, may have compartmentalized sedimentation. This is followed by deposition of the Antalo Limestone a

(3) Post-sag phase: This period represents the time following the deposition of the Agula Shale, which represents the withdrawal of the Jurassic sea (Bosellini et al., 1997) and this was followed by the deposition of the Amba Aradam Formation.

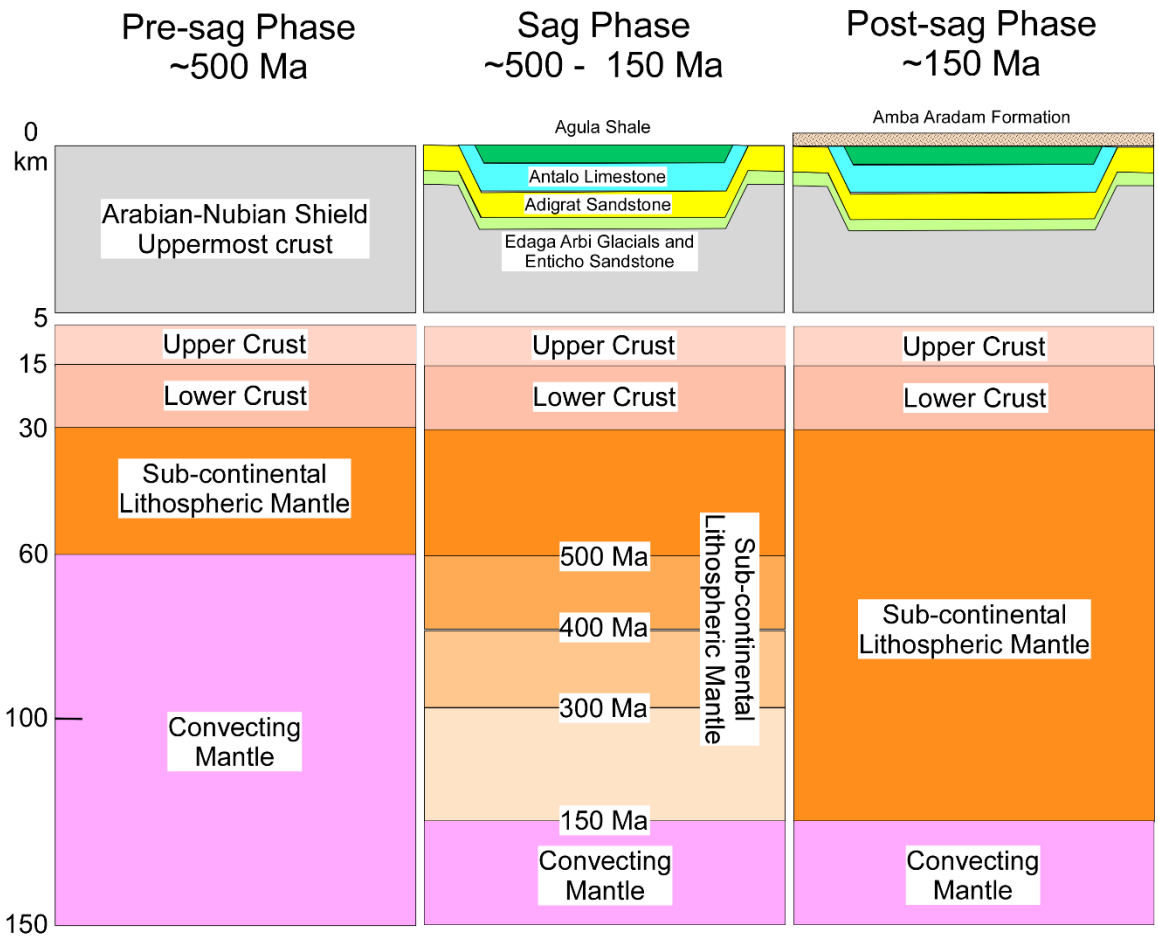

Figure 2.12: Lithospheric cooling model for the Mekele Sedimentary Basin (MSB) showing pre-sag phase, sag phase and post-sag phase. The concept is adapted from Holt et al. (2010).

2.7. CONCLUSIONS

The Mekele Sedimentary Basin in northern Ethiopia was previously interpreted as a fossil rift that developed in relation to the disintegration of Gondwana. Instead, our study revealed, in contrast to rifts, the MSB shows circular to elliptical shape in map view, terrestrial-shallow sedimentary saucer shaped cross section, angular unconformity between Paleozoic e Mesozoic unit and Precambrian

crystalline rocks whereby most sedimentary units are shown gently dipping to the center of the basin. In addition our combined analysis shows a gravity minima at the center of the basin accompanied by a 'normal crustal thickness' in parts of the basin away from the influence of the Afar tectonics. The basin is also partly underlain by a lithospheric fabric that shows a relatively faster seismic velocity signature which we interpreted to be a cold and thicker SCLM. These geological and geophysical features of the MSB are unique features of ICONS, especially those formed over an accretionary terrane. Such basins are abundantly found in the North African and the Arabian platform and are characterized by a very subdued topographic expression due to their formation far away from the active deformation regions. Hence, our understanding about their formation and evolution comes from indirect methods such as numerical and geophysical modelling.

The MSB is completely exhumed and exposed on the surface, not because it is Paleozoic – Mesozoic history is related to extensional tectonics, we shall argue, but due to Cenozoic uplift of the Ethiopian plateau and its present location at the western flank of the Afar Depression. The Cenozoic tectono-magmatic processes also resulted in structural modification especially in the eastern portion of the basin. Despite these complexities, we have considerable observational evidence that architecture of the Paleozoic e Mesozoic features of the MSB are vastly preserved. Based on these ICONS features, we suggest a new subsidence mechanism predominantly responsible for the formation of the MSB. Accordingly, given the fact that the MSB is located over the Neoproterozoic terrane of the Arabian Nubian Shield, we propose, origin of its subsidence could be related to cooling and thickening of this juvenile sub-continental lithospheric mantle, not rifting as previously stated.

2.8. ACKNOWLEDGEMENT

This work was partially supported by Statoil award number 4501505097l. We thank Addis Ababa University, Ethiopia for logistical support. We thank two anonymous reviewers for detailed and constructive comments. This is Oklahoma State University, Boone Pickens School of Geology contribution number 2018-84.

2.9. REFERENCES

Abdelsalam, M. G., and Stern, R. J., 1996, Sutures and shear zones in the Arabian-Nubian Shield: Journal of African Earth Sciences, v. 23, p. 289-310.

Ahern, J. L., and Dikeou, P. J., 1989, Evolution of the lithosphere beneath the Michigan Basin: Earth and Planetary Science Letters, v. 95, p. 73-84.

Ahern, J. L., and Ditmars, R. C., 1985, Rejuvenation of continental lithosphere beneath an intracratonic basin: Tectonophysics, v. 120, p. 21-35.

Allen, P., and Allen, J., 2005, Principles of Basin Analysis, Blackwell Scientific.

Allen, P. A., and Armitage, J. J., 2012, Cratonic basins: Tectonics of Sedimentary Basins: Recent Advances, p. 602-620.

Arkin, Y., Beyth, M., Dow, D.B., Levitte, D., Temesgen, H., Tsegaye, H., 1971. Geological Map of Mekele Sheet Area ND 37-11 Tigre Province. Ministry of Mines, Geological Survey of Ethiopia, Addis Ababa.

Artyushkov, E., 2005, The formation mechanism of the Barents basin: Russian Geology and Geophysics, v. 46, p. 683-696.

Assefa, G., 1991, Lithostratigraphy and environment of deposition of the Late Jurassic–Early Cretaceous sequence of the central part of Northwestern Plateau, Ethiopia: Neues Jahrbuch fur Geologie und Paläontologie Abhandlungen, v. 182, p. 255-284.

Avigad, D., and Gvirtzman, Z., 2009, Late Neoproterozoic rise and fall of the northern Arabian–Nubian Shield: the role of lithospheric mantle delamination and subsequent thermal subsidence: Tectonophysics, v. 477, p. 217-228.

Baird, D., Knapp, J., Steer, D., Brown, L., and Nelson, K., 1995, Upper-mantle reflectivity beneath the Williston basin, phase-change Moho, and the origin of intracratonic basins: Geology, v. 23, p. 431-434.

Balmino, G., Vales, N., Bonvalot, S., and Briais, A., 2012, Spherical harmonic modelling to ultra-high degree of Bouguer and isostatic anomalies: Journal of Geodesy, v. 86, p. 499-520.

Beyth, M., 1972, Paleozoic-Mesozoic sedimentary basin of Mekele outlier, northern Ethiopia: American Association of Petroleum Geologists Bulletin, v. 56, p. 2426-2439.

Blanford, W., 1869, On the geology of a portion of Abyssinia: Quarterly Journal of the Geological Society, v. 25, p. 401-406.

Bonvalot, S., Balmino, G., Briais, A., Kuhn, M., Peyrefitte, A., Vales, N., Biancale, R., and Gabalda, G., 2012, World gravity map, 1:50000000 map: Bureau Gravimetrique International (BGI), Map, CGMW-BGI-CNES728, IRD, Paris.

Bosellini, A., 1989, The continental margins of Somalia: their structural evolution and sequence stratigraphy: Mem. Sci. Geol. v. 41, p. 373–458.

Bosellini, A., Russo, A., Fantozzi, P., Assefa, G., and Solomon, T., 1997, The Mesozoic succession of the Mekele outlier (Tigre province, Ethiopia): Memorie di Scienze Geologiche, v. 49, p. 95-116.

Bosworth, W., 1992, Mesozoic and early Tertiary rift tectonics in East Africa: Tectonophysics, v. 209, p. 115-137.

Braitenberg, C., Wienecke, S., Ebbing, J., Born, W. and Redfield, T., 2007, Joint gravity and isostatic analysis for basement studies–a novel tool: In EGM 2007 International Workshop, Extendended Abstracts, Villa Orlandi, Capri - Italy.

Burke, K., 1976, The Chad Basin: an active intra-continental basin: Tectonophysics, v. 36, p. 197-206.

Busby, C. J., Ingersoll, R. V., and Burbank, D., 1995, Tectonics of sedimentary basins, Blackwell Science Oxford.

Bussert, R., and Schrank, E., 2007, Palynological evidence for a latest Carboniferous-Early Permian glaciation in Northern Ethiopia: Journal of African Earth Sciences, v. 49, p. 201-210.

Bussert, R., and Dawit, E., 2009, Unexpected diversity: new results on the stratigraphy and sedimentology of Palaeozoic and Mesozoic siliciclastic sediments in Northern Ethiopia: Zentralblatt für Geologie und Paläontologie Teil, v. 1, p. 181-198.

Bussert, R., 2010, Exhumed erosional landforms of the Late Palaeozoic glaciation in northern Ethiopia: Indicators of ice-flow direction, palaeolandscape and regional ice dynamics: Gondwana Research, v. 18, p. 356-369.

Bussert, R., 2014. Depositional environments during the Late Palaeozoic ice age (LPIA) in northern Ethiopia, NE Africa: Journal of African Earth Sciences, v. 99, p. 386–407.

Coltorti, M., Dramis, F., and Ollier, C., 2007, Planation surfaces in northern Ethiopia: Geomorphology, v. 89, p. 287-296.

Dainelli, G., 1943, Geologia dell'Africa Orientale (3 vols. text, 1 vol. maps). R: Accad. Ital., Roma.

Dawit, L.E., Bussert, R., and Schrank, E., 2009, Palynomorphs from Jurassic Siliciclastic Sequences of the Mekelle Basin, Northern Ethiopia: Stratigraphic and Palaeoecologic Implications: Zentralblatt für Geologie und Paläontologie Teil I (1/2), p. 1–19.

Dawit, L.E., 2010, Adigrat Sandstone in Northern and Central Ethiopia: Stratigraphy,

Facies, Depositional Environments and Palynology, Ph.D. Thesis: Technische Universität, Berlin, p. 166.

Dow, D., Beyth, M., and Hailu, T., 1971, Palaeozoic glacial rocks recently discovered in northern Ethiopia: Geological Magazine, v. 108, p. 53-60.

Downey, N. J., and Gurnis, M., 2009, Instantaneous dynamics of the cratonic Congo basin: Journal of Geophysical Research v. 114, p. 1-29.

Dugda, M. T., Nyblade, A. A., Julia, J., Langston, C. A., Ammon, C. J., and Simiyu, S., 2005, Crustal structure in Ethiopia and Kenya from receiver function analysis: Implications for rift development in eastern Africa: Journal of Geophysical Research: Solid Earth, v. 110, p. 1-15.

Ebbing, J., Braitenberg, C., and Wienecke, S., 2007, Insights into the lithosphere structure and tectonic setting of the Barents Sea region from isostatic considerations: Geophysical Journal International, v. 171, p. 1390-1403.

Emishaw, L., Laó-Dávila, D.A., Abdelsalam, M.G., Atekwana, E.A. and Gao, S.S., 2017. Evolution of the broadly rifted zone in southern Ethiopia through gravitational collapse and extension of dynamic topography: Tectonophysics, v. 699, p. 213-226.

Fritz, H., Abdelsalam, M., Ali, K.A., Bingen, B., Collins, A.S., Fowler, A.R., Ghebreab, W., Hauzenberger, C.A., Johnson, P.R., Kusky, T.M., and Macey, P., 2013, Orogen styles in the East African Orogen: a review of the Neoproterozoic to Cambrian tectonic evolution: Journal of African Earth Sciences, v. 86, p. 65-106.

Gallacher, R. J., Keir, D., Harmon, N., Stuart, G., Leroy, S., Hammond, J. O., Kendall, J.-M., Ayele, A., Goitom, B., and Ogubazghi, G., 2016, The initiation of segmented buoyancy-driven melting during continental breakup: Nature Communications, v. 7, p. 1-9.

Gebreyesus, G., Aregay, S., and Nigusse, E., 2000, A report on the gravity and magnetic survey of the Mekele Basin: Geological Survey of Ethiopia, Addis Ababa, Ethiopia, p. 52.

Gómez-Ortiz, D., Tejero-López, R., Babín-Vich, R., and Rivas-Ponce, A., 2005, Crustal density structure in the Spanish Central System derived from gravity data analysis (Central Spain): Tectonophysics, v. 403, p. 131-149.

Gurnis, M., 1993, Phanerozoic marine inundation of continents driven by dynamic topography above subducting slabs: Nature, v. 364, p. 589-593.

Hammond, J., Kendall, J.-M., Stuart, G., Ebinger, C., Bastow, I., Keir, D., Ayele, A., Belachew, M., Goitom, B., and Ogubazghi, G., 2013, Mantle upwelling and initiation of rift segmentation beneath the Afar Depression: Geology, v. 41, p. 635-638.

Hammond, J., Kendall, J. M., Stuart, G., Keir, D., Ebinger, C., Ayele, A., and Belachew, M., 2011, The nature of the crust beneath the Afar triple junction: Evidence from receiver functions: Geochemistry, Geophysics, Geosystems, v. 12, p.1-24.

Hartley, R. W., and Allen, P. A., 1994, Interior cratonic basins of Africa: relation to continental break-up and role of mantle convection: Basin Research, v. 6, p. 95-113.

Heine, C., 2007, Formation and Evolution of intracontinental basins, PhD Thesis, School of Geosciences, The University of Sydney, Australia, unpublished.

Heine, C., and Müller, R.D., 2008, The IntraCONtinental basinS (ICONS) atlas—Applications in eastern Australia: in Blevin J.E. et al., eds., Eastern Australasian Basins Symposium III: Sydney, Petroleum Exploration Society of Australia Special Publication, p. 275–290.

Heine, C., Müller, R. D., Steinberger, B., and Torsvik, T. H., 2008, Subsidence in intracontinental basins due to dynamic topography: Physics of the Earth and Planetary Interiors, v. 171, p. 252-264.

Holt, P. J., Allen, M. B., Van Hunen, J., and Bjørnseth, H. M., 2010, Lithospheric cooling and thickening as a basin forming mechanism: Tectonophysics, v. 495, p. 184-194.

Holt, P., Allen, M., and Van Hunen, J., 2015, Basin formation by thermal subsidence of accretionary orogens: Tectonophysics, v. 639, p. 132-143.

Hunegnaw, A., Sage, L., and Gonnard, R., 1998, Hydrocarbon potential of the intracratonic Ogaden Basin, SE Ethiopia: Journal of Petroleum Geology, v. 21, p. 401-425.

Hutchinson, R. W., and G. G. Engels, 1972, Tectonic evolution in the southern Red Sea and its possible significance to older rifted continental margins: Geological Society of America Bulletin, v. 83, p. 2989-3002.

Hyndman, R.D., Currie, C.A., and Mazzotti, S.P., 2005, Subduction zone backarcs, mobile belts, and orogenic heat: GSA Today, v. 15, p. 4-10.

Jacobsen, B. H., 1987, A case for upward continuation as a standard separation filter for potential-field maps: Geophysics, v. 52, p. 1138-1148.

Keir, D., Hamling, I. J., Ayele, A., Calais, E., Ebinger, C., Wright, T. J., and Baker, E., 2009, Evidence for focused magmatic accretion at segment centers from lateral dike injections captured beneath the Red Sea rift in Afar: Geology, v. 37, p. 59-62.

Kiessling, W., Pandey, D. K., Schemm-Gregory, M., Mewis, H., and Aberhan, M., 2011, Marine benthic invertebrates from the Upper Jurassic of northern Ethiopia and their biogeographic affinities: Journal of African Earth Sciences, v. 59, p. 195-214.

Kingston, D., Dishroon, C., and Williams, P., 1983a, Global basin classification system: American Association of Petroleum Geologists Bulletin, v. 67, p. 2175-2193.

-, 1983b, Hydrocarbon plays and global basin classification: American Association of Petroleum Geologists Bulletin, v. 67, p. 2194-2198.

Klein, G. D., and Hsui, A.T., 1987, Origin of cratonic basins: Geology, v. 15, p. 1094-1098.

Kröner, A., Greiling, R., Reischmann, T., Hussein, I.M., Stern, R.J., Durr, S., Kruger, J., and Zimmer, M., 1987, Pan-African crustal evolution in the Nubian segment of NE Africa, in Kröner, A., eds., Proterozoic Lithospheric Evolution, American Geophysical Union Geodynamics Series, v. 17, p. 235–257.

Laske, G., Masters, G., Ma, Z., and Pasyanos, M., 2013, Update on CRUST1. 0—A 1-degree global model of Earth's crust: Geophysical Research Abstracts, v. 15, p. 20132658abstrEGU.

Leighton, M., and Kolata, D., 1990, Selected interior cratonic basins and their place in the scheme of global tectonics: a synthesis: in Leighton, M. W., Kolata, D. R., Oltz, D. F., and Eidel, J. J., eds., Interior cratonic basins: American Association of Petroleum Geologists Memoir 51, p. 729-797.

Leseane, K., Atekwana, E.A., Mickus, K.L., Abdelsalam, M.G., Shemang, E.M., and Atekwana, E.A., 2015, Thermal perturbations beneath the incipient Okavango Rift Zone, northwest Botswana: Journal of Geophysical Research: Solid Earth, v. 120, p. 1210-1228.

Levitte, D. 1970, The Geology of Mekelle: Report on the Geology of the Central Part of Sheet ND 37-11: Ethiopian Institute of Geological Survey, Addis Ababa.

Mackenzie, G. D., Thybo, H., and Maguire, P. K. H., 2005, Crustal velocity structure across the Main Ethiopian Rift: results from two-dimensional wide-angle seismic modelling: Geophysical Journal International, v. 162, p. 994-1006.

Maguire, P. K. H., Ebinger, C. J., Stuart, G. W., Mackenzie, G. D., Whaler, K. A., Kendall, J. M., and Harder, S., 2003, Geophysical project in Ethiopia studies continental breakup: EOS, Transactions American Geophysical Union, v. 84, p. 337-343.

Mammo, T., 2013, Crustal Structure of the Flood Basalt Province of Ethiopia from Constrained 3-D Gravity Inversion: Pure and Applied Geophysics, v. 170, p. 2185-2206.

Martire, L., Clari, P., and Pavia, G., 2000, Discontinuities and sequence stratigraphy of the Antalo Limestone (Upper Jurassic, North Ethiopia): GeoResearch Forum, v. 6, p. 333-344.

McKenzie, D., 1978, Some remarks on the development of sedimentary basins: Earth and Planetary Science Letters, v. 40, p. 25-32.

McKenzie, D., and Priestley, K., 2016, Speculations on the formation of cratons and cratonic basins: Earth and Planetary Science Letters, v. 435, p. 94-104.

Merla, G., Abbate, E., Azzaroli, A., Bruni, P., Canuti, P., Fazzuoli, M., Sagri, M., and Tacconi, P., 1979, A Geological Map of Ethiopia and Somalia: 1973; 1: 2.000. 000 and Comment with a Map of Major Landforms, University of Florence.

Mickus, K., Tadesse, K., Keller, G. R., and Oluma, B., 2007, Gravity analysis of the main Ethiopian rift: Journal of African Earth Sciences, v. 48, p. 59-69.

Mickus, K., and Hussein, M., 2016, Curie Depth Analysis of the Salton Sea Region, Southern California. Pure and Applied Geophysics, v. 173, p. 537-554.

Mishra, D.C., and Pedersen, L.B., 1982, Statistical analysis of potential fields from subsurface reliefs: Geoexploration, v. 19, p. 247-265.

Mock, C., Arnaud, N. O., Cantagrel, J.-M., and Yirgu, G., 1999, 40 Ar/39 Ar thermochronology of the Ethiopian and Yemeni basements: reheating related to the Afar plume?: Tectonophysics, v. 314, p. 351-372.

Nafe, J., and Drake, C. L., 1957, Variation with depth in shallow and deep water marine sediments of porosity, density and the velocities of compressional and shear waves: Geophysics, v. 22, p. 523-552.

Parker, R. L., 1972, The rapid calculation of potential anomalies: Geophys. J. R. Astr. Soc., v. 31, p. 447-455.

Pavlis, N. K., Holmes, S. A., Kenyon, S. C., and Factor, J. K., 2012, The development and evaluation of the Earth Gravitational Model 2008 (EGM2008): Journal of Geophysical Research: Solid Earth, v. 117, p. 1-38.

Ritzmann, O., and Faleide, J. I., 2009, The crust and mantle lithosphere in the Barents Sea/Kara Sea region: Tectonophysics, v. 470, p. 89-104.

Russo, A., Assefa, G., and Atnafu, B., 1994, Sedimentary evolution of the Abay River (Blue Nile) Basin, Ethiopia. With 4 figures in the text: Neues Jahrbuch für Geologie und Paläontologie-Monatshefte, p. 291-308.

Saunders, A. D., England, R. W., Reichow, M. K., and White, R. V., 2005, A mantle plume origin for the Siberian traps: uplift and extension in the West Siberian Basin, Russia: Lithos, v. 79, p. 407-424.

Saxena, G.N., and Assefa, G. 1983, New evidence on the age of the glacial rocks of northern Ethiopia: Geol. Mag., v. 120, p. 549–554.

Shumburo, M., 1968, The Amba Aradam Formation (formerly the Upper Sandstone): Mobil Petroleum Ethiopia Inc., unpublished.

Sleep, N. H., and Snell, N. S., 1976, Thermal contraction and flexure of mid-continent and Atlantic marginal basins: Geophysical Journal International, v. 45, p. 125-154.

Sloss, L., 1963, Sequences in the cratonic interior of North America: Geological Society of America Bulletin, v. 74, p. 93-114.

-, 1988, Tectonic evolution of the craton in Phanerozoic time: The Geology of North America, v. 2, p. 25-51.

Spector, A., and Grant, F.S., 1970, Statistical models for interpreting aeromagnetic data: Geophysics, v. 35, p. 293-302.

Stab, M., Bellahsen, N., Pik, R., Quidelleur, X., Ayalew, D., and Leroy, S., 2016, Modes of rifting in magma-rich settings: tectono-magmatic evolution of Central Afar: Tectonics, v. 35, p. 2-38.

Stel, H., Cloetingh, S., Heeremans, M., and Van der Beek, P., 1993, Anorogenic granites, magmatic underplating and the origin of intracratonic basins in a non-extensional setting: Tectonophysics, v. 226, p. 285-299.

Stern, R. J., 1994, Arc-assembly and continental collision in the Neoproterozoic African orogen: implications for the consolidation of Gondwanaland: Annual Review of Earth and Planetary Sciences, v. 22, p. 319-351.

-, 2002, Subduction zones: Reviews of Geophysics, v. 40, p. 1-42.

Stern, R. J., Ali, K. A., Abdelsalam, M. G., Wilde, S. A., and Zhou, Q., 2012, U–Pb zircon geochronology of the eastern part of the Southern Ethiopian Shield: Precambrian Research, v. 206, p. 159-167.

Tanaka, A., Okubo, Y. and Matsubayashi, O., 1999, Curie point depth based on spectrum analysis of the magnetic anomaly data in East and Southeast Asia: Tectonophysics, v. 306, p. 461-470.

Telford, W. M., Telford, W. M., Geldart, L. P., and Sheriff, R. E., 1990, Applied geophysics, v.1: Cambridge University Press.

Tiberi, C., Ebinger, C., Ballu, V., Stuart, G., and Oluma, B., 2005, Inverse models of gravity data from the Red Sea-Aden-East African rifts triple junction zone: Geophysical Journal International, v. 163, p. 775-787.

Tselentis, G.-A., Drakopoulos, J., and Dimitriadis, K., 1988, A spectral approach to moho depths estimation from gravity measurements in Epirus (NW Greece): Journal of Physics of the Earth, v. 36, p. 255-266.

Vyssotski, A., Vyssotski, V., and Nezhdanov, A., 2006, Evolution of the West Siberian basin: Marine and Petroleum Geology, v. 23, p. 93-126.

Worash, G., and Valera, R., 2002, Rare earth element geochemistry of the Antalo Supersequence in the Mekele Outlier (Tigray region, northern Ethiopia): Chemical Geology, v. 182, p. 395-407.

Xie, X., and Heller, P. L., 2009, Plate tectonics and basin subsidence history: Geological Society of America Bulletin, v. 121, p. 55-64.

CHAPTER III

ALONG-STRIKE TOPOGRAPHIC CHARACTERISTICS OF THE WESTERN ESCARPMENTS OF THE AFAR DEPRESSION

3.1. ABSTRACT

We used the analysis of a combination of digital elevation model (DEM), geophysical data, and the nature of the bedrock geology to characterize the along-strike topographic, tectono-magmatic, and crustal thickness variation in the escarpment system of the western Afar Depression. With the exception of the northern segment (which is covered with Precambrian basement and Paleozoic - Mesozoic sediments), much of the study area is covered with Cenozoic volcanics. Structurally, interaction among the system of NS trending grabens, NW oriented faults and magmatic segments, and EW oriented transverse zones and dikes play considerable role, possibly representing reactivation of the pre-existing heterogeneity. Geomorphologicaly, the escarpment system forms a north-trending topographically distinct boundary between the elevated and deeply incised plateau, and the magmatically and tectonically active low-lying rift floor of the Afar Depression. As a site of competing surface geomorphic and sub-surface tectono-magmatic processes, it provides a key insight into scenarios of tectonic and surface-process interactions along a classic continental rift margin. Thus far, studies aimed at establishing a link between tectono-magmatic processes and topography tended to restrict their focus on either the regional topographic development or strike-perpendicular segments of topography — with little emphasis on along strike geodynamic link.

Analysis of swath profile patterns and maps of elevation, local relief, slope, Hypsometric Index (HI), steepness index (ksn), and surface roughness generated using the 30m DEM data reveals second-order topographic differences along the strike of the escarpment system. The escarpment is characterized by a relatively narrow region of extreme relief, steep slopes, and series of small graben controlled by large marginal bounding faults. The adjoining plateau has a relatively flat topography with an average elevation of 2500 m above sea level (asl) dotted with shield volcanoes and deep gorges carved by rivers, while the elevation within the floor of the escarpment ranges between 500 and 0 m asl.

Crustal thickness from the Crust 1.0 model and receiver function studies shows considerable relief both across and along the escarpment. The highest and lowest thickness of 46 and 15 km, were recorded in the north within the Danakil Depression and in the south at the edge of the plateau, respectively. Analysis of gravity and magnetic data reveals tectono-magmatic segmentation along the rift floor transect of the escarpment. Both the Bouguer gravity and isostatic anomaly are negative over the plateau and positive over the rift floor. The tilt-derivative of the gravity delineated the distinct tectono-magmatic segments along the rift and drainage and geomorphic features along the edge of the plateau. The reduced to equator magnetic and tilt maps also show correspondence with tectonic and magmatic features with three distinct regions, and predominant trends identified on the basis of magnetic anomaly patterns.

In summary, broad patterns of topographic variation along the strike of the escarpment reflect general properties of lithospheric heterogeneity. In the north and central region, the escarpment is inboard of a highly extended, and in the former almost tapered crust where as in the south the highest escarpments overlie a thickened possibly underplated crust. These tectonic features partially correspond with the along-strike variation in geomorphic features such as the local relief, HI and slope. However, it appears that the first-order topographic development is primarily

controlled by a regional process, possibly due to the pre-rift dynamic topography generated by the plume impingement or later lithospheric foundering.

3.2. INTRODUCTION

The Ethiopian Plateau represents an anomalously uplifted non-orogenic mountain region that, as part of the greater East African Rift System, experienced plume originated Cenozoic doming and continental flood basalt volcanism, widespread subsequent continental rifting, and Late-Cenozoic focused magmatism (Schilling, 1973; Mohr and Zanettin, 1988; Hayward and Ebinger, 1996; Hofmann et al., 1997; Ebinger and Sleep, 1998; Rogers et al., 2000; Şengör, 2001; Pik et al., 2003; Keir et al., 2009). The plateau is long appreciated as a prime example of topography produced by a combination of dynamic mantle plume (Ebinger et al., 1989; Pik et al., 2008; Moucha and Forte, 2011; Nyblade, 2011; Sembroni et al., 2016a), isostatic response to erosional unloading (McDougall et al., 1975; Weissel et al., 1995; Pik et al., 2003; Gani et al., 2007; Sembroni et al., 2016a), and flexural uplift due to crustal extension and mafic underplating (Weissel et al., 1995; Ebinger and Hayward, 1996; Mackenzie et al., 2005; Tiberi et al., 2005). Even though each of these processes play a role at different times with varying intensities, the extent to which the present day topography reflects dominance of one or more of the foregoing processes remains controversial.

Three broad physiographic regions have been identified in Ethiopia; (1) the Northwestern Plateau, (2) the Southeastern Plateau, and (3) the Ethiopian Rift System separating the two uplifted regions (Fig. 3.1). Two contrasting models have been proposed to describe topographic development in the Ethiopian Plateau; a steady state, long-lived topography primarily generated during the Oligocene, and is continuously supported by plume-induced uplift (Şengör, 2001; Pik et al., 2003; Sembroni et al., 2016b) or episodic and accelerated plateau growth due to later tectono-magmatic processes, particularly in the last 10 Ma (Gani et al., 2007; Ismail and Abdelsalam, 2012). Overall, both

glaciation (due to its location near the equator) and tectonic exhumation (due to its non-orogenic nature), play insignificant role in building topography in this region (Molnar and England, 1990; Gani et al., 2007). Thus, a greater coupling and feedback effects between surface denudation and tectono-isostatic uplift has been suggested (Gani et al., 2007). Each of these plateaus are bounded by escarpments marking the boundary with the rift region. Escarpments, as a site of competing surficial and tectono-magmatic processes, are known to provide a key insight into the large-scale geomorphic development of continental rift margins (Tucker and Slingerland, 1994; Beek et al., 1995; Seidl et al., 1996; Burov and Cloetingh, 1997; Matmon et al., 2002; Gunnell and Harbor, 2008). In addition, these escarpments are shown to persist and exert greater control over the landscape evolution including sedimentation even after development into passive margin (Weissel and Karner, 1989; Gilchrist and Summerfield, 1990; Gilchrist and Summerfield, 1991).

The escarpment of the Northwestern Ethiopian Plateau bordering the western margin of the Afar Depression forms a north-trending topographically distinct boundary between the elevated and deeply incised plateau, and the magmatically and tectonically active low lying rift floor of the Afar Depression (Fig. 3.1). Embedded into the geodynamics of this escarpment system is complex process of rifting, magmatism, river incision and sedimentation (Bareberi et al., 1974; Collet et al., 2000; WoldeGabriel et al., 2000; Wolfenden et al., 2005; Beyene and Abdelsalam, 2005; Rooney et al., 2013; Korostelev et al, 2015). These observations provide important insights into what many consider to be a classical example of a continental rift margin preceding and/or at the nascent stage of oceanisation i.e. in some places, rifting may have already transitioned to passive margin drifting (E.g. Makris and Ginzburg, 1987; Bridge et al., 2012; Varet, 2018). Though studies aimed at establishing a link between this tectono-magmatic processes and topography were conducted (Pik et al., 2003; Gani et al, 2007; Ismail et al., 2012; Sembroni et al, 2016a and b; Xue et al., 2018), they tended to restrict their focus on either the regional topographic development or strike-perpendicular segments of topography — with little emphasis on along strike geodynamic link.

Thus, research aimed at improving our understanding of the degree to which the topographic features along the strike of the escarpment reflect interaction among surface and subsurface processes is needed.

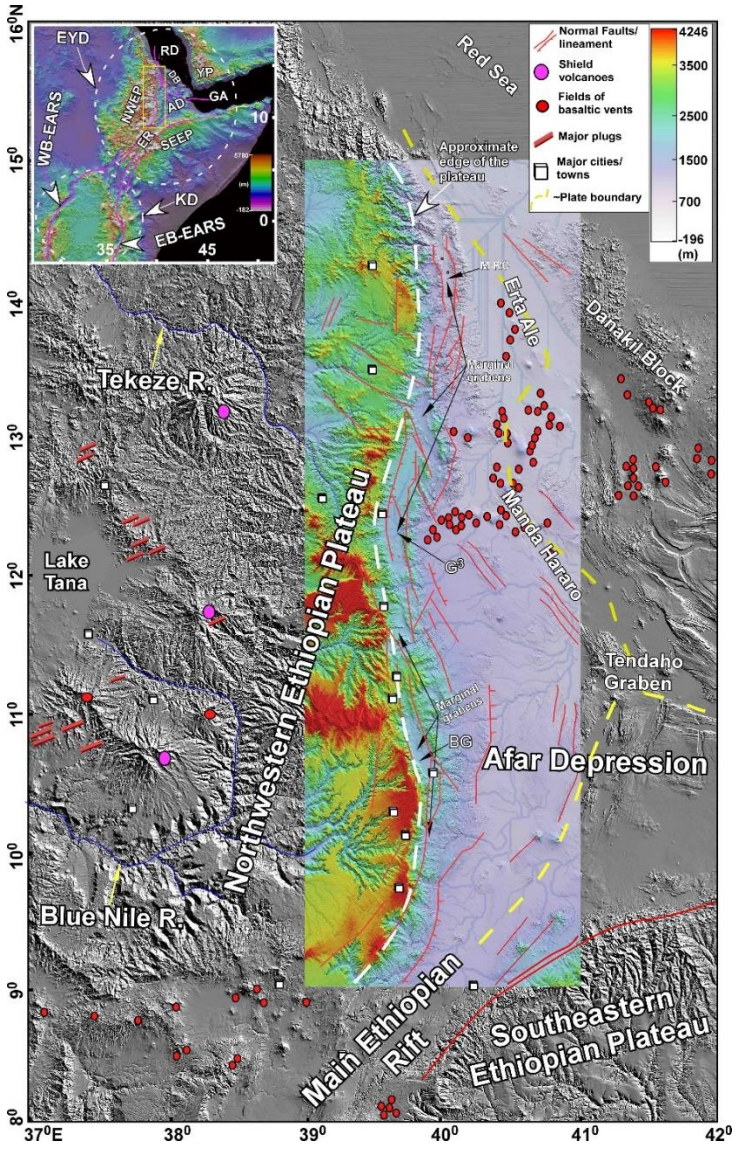

Figure 3.1: Color-coded hillshade 30m x-y resolution Advanced Spaceborne Thermal Emission and Reflection Radiometer (ASTER) digital elevation model (DEM) of the study area showing major tectonic elements including major faults, marginal grabens, magmatic centers and shield volcanoes. Inset figure shows the location of the Ethiopian Plateau (or EYD: Ethio-Yemen Plateau,

the circular domal region) with respect to simplified tectonic framework of the surrounding plates. The yellow solid box in the inset shows the location of the study area. Abbreviations: WB-EARS – Western Branch of the East African Rift System, EB-EARS – Eastern Branch of the East African Rift System, KD – Kenyan Dome, NWEP – Northwestern Ethiopian Plateau, SEEP – Southeastern Ethiopian Plateau, ER – Ethiopian Rift, AD – Afar Depression, DB – Danakil Block, RD – Red Sea, GA – Gulf of Aden, YP – Yemen Plateau, BG – Borkena Graben, G3 – Guf-Guf Graben, M-RC – Maglala-Renda Coma Graben.

The main objective of this study is therefore to investigate the along-strike topographic and tectonic variation including crustal thickness along the strike of the western escarpment of the Afar Depression. The study area encompasses an elevated and deeply incised plateau that is underlain by a normal continental crust, a narrow rift margin within the escarpment characterized by extreme relief, steep slopes, and series of small grabens controlled by large marginal bounding faults, and a magmatically active region (with in the Afar Depression) underlain by a highly thinned crust. An improved understanding of coupling scenarios of tectonic and surface-process interaction along the margin requires an integrated approach that applies geologic, geomorphic and geophysical data. Here, we used the analysis of a combination of digital elevation model (DEM), satellite gravity and magnetic data, and the bedrock geology data from previous studies. Furthermore, we generated a map of the steepness index, the slope, and the relief from geomorphic proxies in-order to characterize the near surface geomorphic features. These scales of characterizations are then discussed in order to establish scenarios of an along-strike topographic differences and possible segmentation including its coupling to crustal thickness variation.

3.3. GEOLOGICAL SETTING

The two elevated geomorphic regions in Ethiopia, namely the Northwestern and Southeastern Plateaus, are of roughly similar origin and evolution (E.g. Xue et al., 2018). These plateaus are separated by the variably oriented Ethiopian Rift, which is further subdivided into three segments of variable volcano-tectonic history and geomorphic features: the Southern Ethiopian Rift (SER), the Main Ethiopian Rift (MER: also further subdivided into south, central, and north), and the Afar Depression (AD). The study area includes the edge of the Northwestern Plateau and the western flank of the Afar Depression. Much of this region is covered with Cenozoic age, thick pile of volcanic material, and hence, the subsurface basement geology hasn't been mapped in detail. However, the Precambrian crystalline basement to recent geology is exceptionally exposed on the surface, and relatively well studied in the northern segment of the study area (E.g. Levitte, 1970; Beyth, 1972; Kazmin, 1978; Garland, 1980; Tefera et al., 1996; Bosellini et al., 1997). This includes our own study which recently reclassified the Paleozoic-Mesozoic sedimentary basin over this area as an IntraCONtinetal Sag (ICONS) based on field, remote sensing and geophysical data (Alemu et al., 2018).

In the central and northern segments of the study area (south of 13 degree), the pre-rift geology is covered by flood-basalts extruded in during the Cenozoic, and reaching up to 2 km thickness in places (Mohr and Zanettin, 1988; Hofmann et al., 1997; Pik et al., 1998). Near the margins, the volcanic cover is not deeply incised enough to expose the geology under it at-least within ~ 100 km of the edge of the plateau. In addition, despite the documented cases of hydrocarbon seeps and presence of possible sedimentary basin under the central segment of the study area (Wolela, 2007; Mammo, 2010), there has not been any meaningful exploration including seismic which would have provided valuable data on the subsurface geology of the plateau due to the volcanic cover. Thus, much of our understating about the structure of these segments comes from indirect geophysical observations and few outcrops analysis from the faulted blocks within the escarpment

system. Overall, the under-basalt subsurface lithostratigraphy across the edge of the plateau is assumed to be similar to those exposed in the northern segment. Nevertheless, the detailed nature of the basement and sedimentary basin in the central and southern region remains unknown.

Basement rocks of the Ethiopian Plateau belongs to the Pan-African Orogenic network, which in Ethiopia, encompasses two Precambrian mobile belts of similar age but distinct metamorphic grade; the Mozambique belt in the south and the Arabian-Nubian Shield in the north. These two Pan-African structures formed during the collusion of East and West Gondwana during the Meso-Neoproterozoic (Kroner, 1985; Vail, 1985; Shackleton, 1986; Stern, 1994; Abdelsalam and Stern, 1996). Though this two structures inter-finger in central Ethiopia, the study area is solely underlain by the Neoproterozoic accretionary Arabian-Nubian Shield (ANS) basement rocks (Asrat et al., 2001). The ANS basement in the study area is dominated by low-grade metavolcanics and metasedimentary suites, and syn-late orogenic granitoid that outcrop in a general north-south orientation in the northern and as faulted blocks in the central segment of the study area (Fig. 3.2). Structurally, the basement fabric indicates an E-W closure and development of well recognizable metamorphic features and foliations trending N/NNE within an overall greenschist facies suite (Levitte, 1970; Kazmin, 1971; Beyth, 1972; Tadesse, 1996; Asrat et al., 2001).

The crystalline basement is unconformably overlain by a Paleozoic-Mesozoic sedimentary cover of variable thickness (Fig. 3.2). Paleozoic rocks are generally considered of glacial origin deposited within N-S oriented glacial valleys (Dow et al., 1971; Bussert, 2010). They are well exposed in the northern segment of the study area. During the Mesozoic, ~2km thick mixed clastic-carbonate continental and marine sediments were deposited, mainly confined to the two large basins located on the Northwestern Plateau; the Mekele Sedimentary Basin in the north and the Blue Nile Basin in the south (Jepsen and Athearn, 1962; Dainelli, 1943; Levitte, 1970; Beyth, 1972; Merla et al., 1979; Bosellini et al., 1997; Alemu et al., 2018). The relationship between these two adjoining basins remains enigmatic due to the extensive flood basalt cover. The formation of the main

depocenters or main subsidence phases in both of these basins, however, was thought to coincide with break-up of Gondwanaland during the Early-Middle Mesozoic (Beyth, 1972; Bosellini, 1986; Bosworth, 1992; Russo et al., 1994). The Cenozoic geology of the study area (and the region) is one of regional uplift, extensive magmatism and rifting, and severe denudation as discussed separately below.

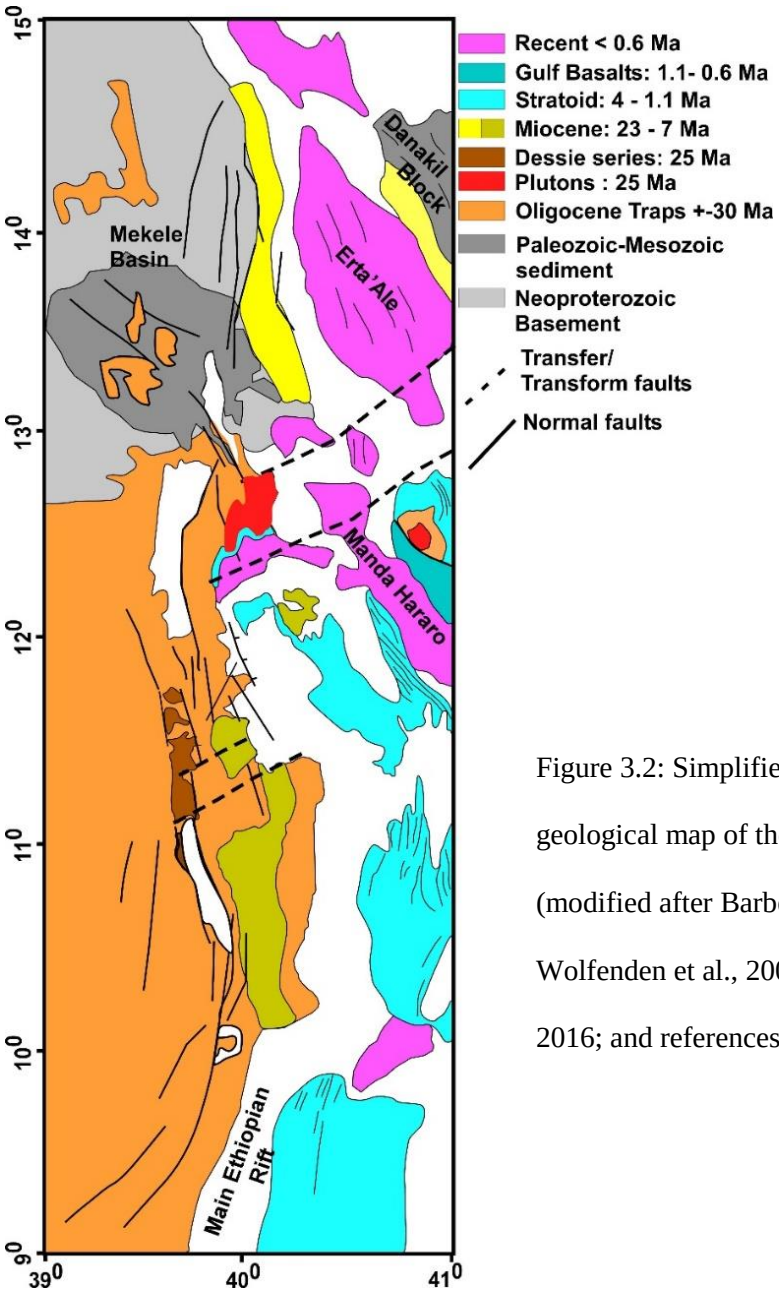

Figure 3.2: Simplified regional geological map of the study area (modified after Barberi et al., 1975; Wolfenden et al., 2005; Stab et al., 2016; and references there in).

3.4. CENOZOIC GEODYNAMICS

The present-day topography setting of the study area reflects the complex tectonic, magmatic, and surface processes that is undergoing in the Ethiopian Plateau region. In general, the Ethiopian Plateau (including the inter-plateau rift region) exhibits a ~ 1300 km wide domical topographic feature which is covered with ~ 500,000 km^2 volcanic material that presumably erupted in a short time span—representing one of the youngest flood basalt provinces in the world (Mohr and Zanettin, 1988; Hofmann et al., 1997; Rochette et al., 1998; Şengör, 2001; Ayalew et al., 2002; Coulié et al., 2003). The plateau and the rift region have been a subject of multiple studies including its mantle plume origin, dynamic topographic support and pulsed plateau growth, and crustal extension and magmatism along-axis of the rift. Specifically, the plateau is underlain by both large negative Bouguer gravity (particularly in the topographically elevated region), and low shear-wave velocity anomalies in the rift regions. Based on the foregoing topographic, geophysical and additional geochemical evidence (E.g. Pik et al., 1999), a mantle plume (Afar Plume) origin that likely impinged the lithosphere in the southern Ethiopia region during the Eocene and, presumably migrated northeast into the Afar Depression has been proposed. This episode is considered as the major process that exerts a primary control on the tectono-magmatic and subsequent morphotectonic evolution of the plateau. Owing to the presence of similar but distinct topographic dome in Kenya, a two mantle plume origin has also been proposed (George et al., 1998; Rogers et al., 2000; Rogers, 2006). In addition, even though the bulk of volcanism happened during the Oligocene, the age of volcanics in the southern Ethiopia is older (generally Eocene) compared to central Ethiopia (Davidson and Rex, 1980; Ebinger et al., 1993; George et al., 1998).

The topography, to first order, is considered as a relic of the mantle plume doming episode prior to flood basalt volcanism (Şengör et al., 2001; Pik et al, 2003; Sembroni et al., 2016a). Next, two tectono-magmatic events i.e. relatively older phase of shield volcanism in the interior of the plateau and a most recent lithospheric foundering and rift-flank uplift, are suggested to have exerted

considerable influence on landscape evolution (Gani et al., 2007; Ismail and Abdelsalam, 2012). Rifting and crustal thinning in the Afar Depression is believed to have started around 24 Ma following the gravitational collapse of the plume generated dynamic topography (Kursten, 1975; Barberi et al., 1975; Ukstins et al., 2002; Beyene and Abdelsalam, 2005) and possible erosion of the base of the lithosphere due to plume impact (Ayalew and Gibson, 2009). The Collapsing of the then Ethiopian-Yemen dome may have been influenced by both the reactivation of the Precambrian basement structure which happens to be parallel to the present-day escarpment and regional kinematics associated with the drift of the Arabian plate (Barberi et al., 1975; Ukstins et al., 2002; Gashawbeza et al., 2004; Cornwell et al., 2010). Subsequently, the northwestern escarpment began to form as widespread and localized magmatism, and extension associated with the rifting and rotation of the Danakil block away from the Nubian plate around 20 Ma (Manighetti et al., 2001; Beyene and Abdelsalam, 2005; Wolfenden et al., 2005).

The separation and subsequent rotation of the Danakil block from the Nubian plate was triggered by the onset of westward propagation of the Gulf of Aden ridge (Courtillot et al., 1984; Lahitte et al., 2003). Though the detailed timing, kinematics and dynamics of how each of these marginal grabens are formed has not been established, a few models were proposed within the scheme of the broader tectonics between the Nubian and Danakil block. These includes; multi-stage development involving southward and then eastward migration of extension (Zanettin and Justin-Visentin, 1975), eastward migrating normal-faulting (Asrat et al., 1990), and in contrast to the foregoing models, Chorowicz et al. (1999) proposed a sinistral transtensional origin for the development of these en echelon arrays of isolated grabens. Such interpretation, according to Wolfenden et al., (2005), only works for a limited segment of the margin, and doesn't characterize the whole northwestern escarpment. Today's escarpment region is characterized by badlands and series of marginal grabens filled with sediments and volcanics with some of the biggest one's considered to be as old as the rift margin itself (Chorowicz et al., 1999; Tesfaye et al., 2003; Wolfenden et al.,

2005; Stab et al., 2016). The major marginal grabens from south to north are Borkena, Dergaha-Sheket, Guf-Guf, and Maglala-Renda Coma (Fig. 3.1) (Mohr, 1972; 1974a; 1974b; Chorowicz et al., 2005). The margin is also shown to have past and present seismic, hydrothermal and volcanic activity.

During the early phase of plateau development, sparse post-flood basalt shield volcanism has continued within the interior of the plateau as evidenced by series of shield volcanoes ranging in age from 28 Ma to 10 Ma (Kiefer et al., 2004). These episodes have added considerable material and exerted observable control over drainage pattern and plateau incision (Gani et al., 2007; Ismail and Abdelsalam, 2012). Meanwhile, diachronous rifting within the various sectors of the Main Ethiopian Rift (MER) is believed to have started very late compared to the Afar Depression, and is generally dated around Late Miocene (11 to 6 Ma) (WoldeGabriel et al. 1990; Wolfenden et al., 2004; Bonini et al., 2005). Moreover, much of the magmatic and volcanic activity (both in the Afar and MER) has migrated towards the rift axis in the last 5 Ma or so (Zanettin et al., 1978; Ebinger et al., 1993; Keir et al., 2009). These stage of focused magmatism and rifting is shown to coincide with accelerated river incision and plateau growth both in the Northwestern (Gani et al., 2007; Ismail and Abdelsalam, 2012), and Southeastern Ethiopian plateaus (Xue et al., 2018).

3.5. DATA AND METHODS

3.5.1. TOPOGRAPHIC ANALYSIS

3.5.1.1. SWATH PROFILES

Swath profiles are used to horizontally expand cross-section line into a rectangular swath and condense that data in order to be able to show the maximum, minimum and mean of topographic features such as elevation, local relief, and HI into a single plot (Eg. Telbisz et al, 2013). For topographic analysis, we used the 30m x-y resolution Advanced Spaceborne Thermal Emission and

Reflection Radiometer (ASTER) digital elevation model (DEM) (hereafter abbreviated as ASTER-DEM) downloaded from USGS EarthExplorer. All analysis was conducted using ArcGIS 10.4 software. In summary, ones the ASTER-DEM data is imported into the ArcGIS environment, the focal statistics tool found within the Spatial Analyst extension is used to generate the desirable statistics (mean, min or max) of the region of interest. The mean provides an overall trend in elevation or local relief, whereas the minimum and maximum parameters outline the extreme variations present along those transect. We used swath profiles to extract a good approximation to the general topographic trend of the landscape within the swath profile for various topographic parameters. We also generated swath profiles of geophysical data. The profiles were made both along the strike of the escarpment and along the transverse of the three 50 km wide segments that were selected to represent the northern, central and southern portions of the study area (Fig. 3.3A).

3.5.1.2. ELEVATION SWATH PROFILES

Along the strike, we subdivided the study area into three transects and took topographic swath profiles to characterize those regions (Fig. 3.3A). These are (i) The plateau edge: taken along the edge of the Northwestern Plateau repressing the elevated region (1500 m above sea level and higher), (ii) The transitional region: taken along the escarpment or margin which includes a rifted plateau and part of the rift flank of the Afar Depression (between 2000 m and 800 m above sea level), and (iii) Rift floor region: taken along the floor of the Depression (800m above sea level and below). In addition, we generated one topographic swath profile for the whole study area. All swath profiles start from south (are south to north). Three other topographic swath profiles were made perpendicular to the strike of the escarpment encompassing the three segments in the north, Central and South regions of the escarpment (Fig. 3.3A). The width of these traverse swath profiles is 50 km. For all profiles, maximum, mean and minimum elevation, local relief, and HI envelop was generated.

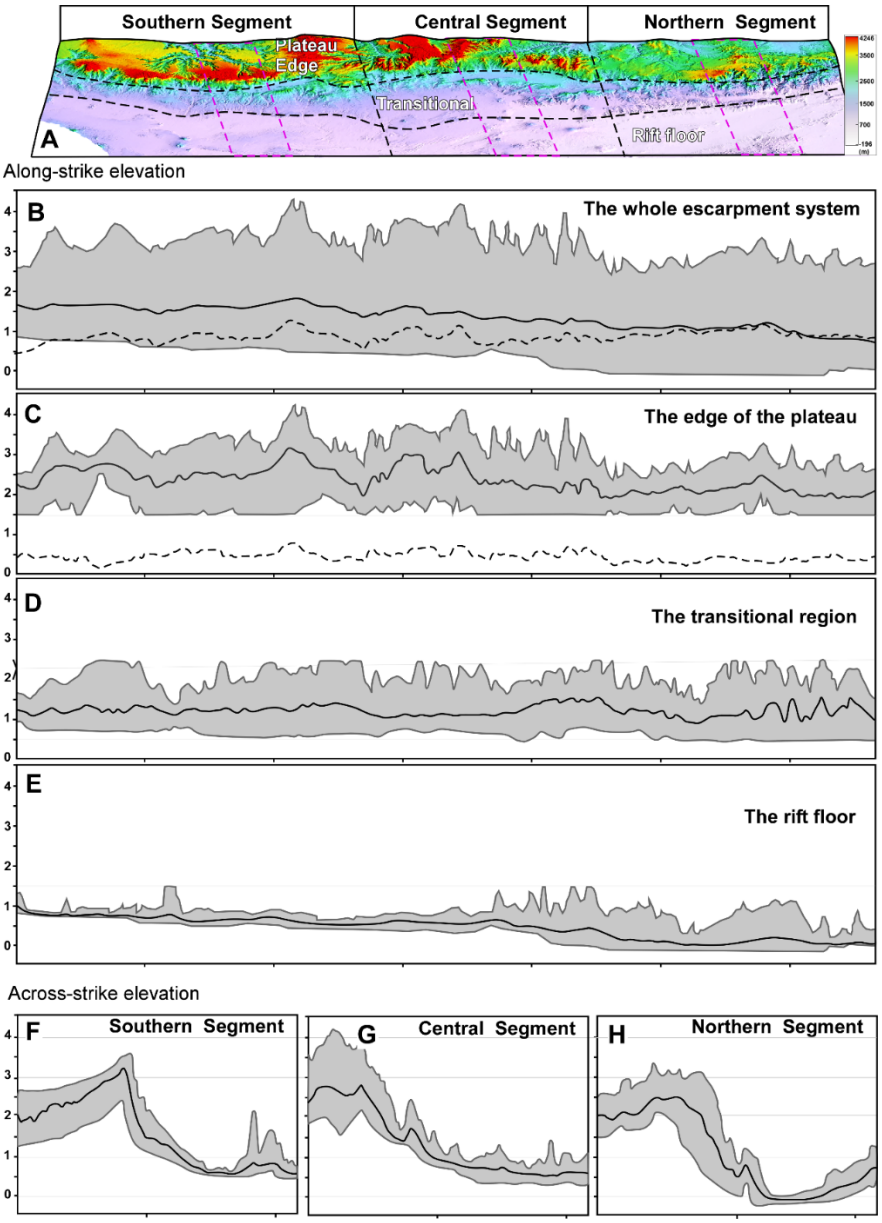

Figure 3.3: Swath profiles illustrating the maximum, mean, and minimum elevation pattern along the strike of the escarpment. (A) Color-coded hillshade Advanced Spaceborne Thermal Emission and Reflection Radiometer (ASTER) digital elevation model (DEM) showing the three transects and segments. (B) Swath profile of elevation for the whole escarpment system. (C) Swath profile of elevation for the edge of the plateau transect. (D) Swath profile of elevation for the transitional region transect. (E) Swath profile of elevation for the rift floor transect. (F) Swath profile of elevation for the southern segment along the 50 km window. (G) Swath profile of elevation for the

central segment along the 50 km window. (H) Swath profile of elevation for the northern segment along the 50 km window.

3.5.1.3. LOCAL RELIEF AND SLOPE

The local relief or relative relief of an area refers to the difference between the highest and lowest elevation within an area (window) manually designated by the user. In this study we used 3 km by 3 km revolving window. For each window, the lowest and highest elevation is determined and then interpolated using Inverse Distance Weighted (IDW) interpolation technique (Fig. 3.4A and B). In addition, slope maps for the whole study area were created (Fig. 3.4C).

3.5.1.4. HYPSOMETRIC INTEGRAL (HI) AND TOPOGRAPHIC ROUGHNESS

We generated gridded hypsometric integral (HI) map and topographic roughness maps using the ASTER-DEM data (Fig. 3.4D). Using HI technique, the relative distribution of a certain elevation within a landscape can be quantified. This is then used to assess the various maturity stages of topography, maturity. We used a 10 km moving window to and sampled the minimum, maximum, mean and range values for each window. Then, HI was calculated using the following formula:

(Mean elevation – Minimum elevation)/ (Range)

Even though HI is often calculated for separate basin or watershed, we believe we have enough information to make reasonable assumptions using the gridded regional HI map shown in Fig. 3.4D. The map is used to further highlight the topographic variation and any anomalous feature that may exist along the strike of the escarpment. Our calculated HI values range between 0.02 and 0.87. These values are considered to encapsulate the overall relief within the selected window, with higher HI values (greater than 0.3) indicating a matured region or basin whilst low HI values generally indicate tectonically sable or matured areas.

The local elevation index method (Jennes, 2006) was used to create topographic roughness map of the study area. We used 300 by 300 m window to first calculate the minimum, maximum and mean elevation within each window. Then, the following formula is used to generate the topographic roughness map shown in Fig. 3.5A.

(Mean-Minimum) / (Maximum-Minimum)

The index has been shown to be useful for landscape classification (Tagil and Jenness, 2008; Mora-Vallejo et al., 2008). Here, we used the map to identify geomorphic features that may correspond with predominant geological and structural elements along the escarpment. The values range between 0 and 1, with higher values representing ridges which might be structural or lithological boundaries.

3.5.1.5. STEEPNESS INDEX

The normalized channel steepness index (ksn), which is derived from the slope–area regression is a morphometric parameter widely used to detect relative variation in uplift rates at various tectonic settings (Whipple and Tucker, 1999; Whipple, 2004; Kirby et al., 2003; Wobus et al., 2006; Cyr et al., 2010). We used the 30 m ASTER-DEM and the TopoToolbox MATLAB program (Schwanghart and Scherler, 2014) to generate the Ksn map (Fig. 3.5B). Then, the ksn values were interpolated using the nearest neighbor triangulation algorithm to make the gridded map shown in Figure B. In general, taking the climate and lithologic variation into account, ksn could be used to assess tectonic uplift rate (e.g. Wobus et al., 2006; Kirby and Whipple, 2012). Higher ksn values often imply presence of tectonic deformation or knickpoints in a homogenous lithologic setting.

3.5.2. GEOPHYSICAL DATA AND METHODS

3.5.2.1. GRAVITY DATA

The different gravity maps (Free Air, Bouguer and Isostatic) shown in Figure 3.6 were all extracted from the World Gravity Model (WGM 2012) map of the International Gravimetric Bureau (BGI).

The WGM 2012 gravity model provides a homogeneous global coverage at 2 min spatial resolution (Balmino et al., 2011; Bonvalot et al., 2012). The data used to generate the model was derived from the ETOPO1 Global Relief model and its predecessor the EGM2008 (Earth Gravity Model 2008), which itself was largely derived from satellite altimetry, satellite gravity, airborne and the surface gravity data. Upward Continuation (UC) filtering was carried out on the gravity data to remove the effect of near surface anomaly (Jacobsen, 1987). The tilt derivative filter was also applied to a 5 km upward continued Bouguer anomaly data in order to enhance deep seated anomalies (Fig. 3.6D). The technique, which is based on the ratio of the first vertical derivative of the potential field to the horizontal gradient of the field, has been shown to be more sensitive to both shallow and deep sources (Miller and Singh, 1994).

3.5.2.2. MAGNETIC DATA

We extracted the magnetic data (Fig. 3.7) from the 2-arc-minute resolution Earth Magnetic Anomaly Grid (EMAG2v3) provided by NOAA. The data is compiled from satellite, ship, and airborne magnetic measurements gridded at an altitude of 4 km above the geoid, and relies only on observed data (Meyer et al., 2017). Unfortunately, the data gaps in the EMAG2v3 model is very wide in the western half of the study area, and hence, we decided not to incorporate it into the final magnetic anomaly map shown in Figure 3.7A. The TMI grid data were then transformed using the reduction to the equator (RTE) filter with Oasis Montaj software. RTE is generally recommended ahead of the reduction to the pole (RTP) filter in areas located within the low magnetic latitudes such as ours due to the low geomagnetic inclination that will render the RTP filter unusable (E.g. Jain, 1986; Ndougsa-Mbarga et al., 2012; Geosoft Inc., 2015).

3.5.2.3. CRUSTAL THICKNESS DATA

Crustal thickness (also referred to as Moho depth) studies has been conducted especially in the rift and surrounding region using both receiver function and gravity approach (Tiberi et al., 2005;

Mackenzie et al., 2005; Dugda et al., 2005; Hummond et al., 2011; Mammo, 2013). The result of these and other similar studies has provided a crustal thickness pattern showing considerable thinning within the rift (30 to 15 km) and normal (~35 to 40 km) to thickened crust (~46 km) within the elevated plateau region. Although these studies were able to shed new information regarding the across-strike tectonic and topographic heterogeneity in the study area and its surrounding regions, there is limited data particularly in the plateau region to thoroughly investigate and extract important constraints for understanding the tectonic-surface processes interaction along-strike of the escarpment. Crustal thickness data from the plateau region is based on sparse receiver function studies (Hammond et al., 2011; Dugda et al., 2005) and rough gravity-based estimates (Mammo, 2013; Tiberi et al., 2005; Alemu et al., 2018). Therefore, we decided to use the CRUST1.0 global crustal thickness model (Laske et al., 2013) in conjunction with other available seismic based Moho depth estimates (Fig. 3.8). CRUST1.0 is a 1-by-1 degree global crustal model produced from active source seismic and receiver function studies.

3.6. RESULTS

3.6.1. TOPOGRAPHIC CHARACTERISTICS

We generated maps and swath profiles of elevation, local relief, slope, gridded hypsometric index (HI), topographic roughness and normalized steepness index (ksn). In general, there is a good correspondence between the various morphometric parameters along the escarpment. Overall, almost all parameters show distinct, but low anomalous values in the north, central and southern sections of the escarpment.

The escarpment spans ~ 800 km from the boundary with northern MER, with elevations > 3km, to the Red Sea, with elevations near sea level (Fig. 3.1). Within the study area, the mean elevation decreases from about 1.7 km in the south to 700 m at the northern margin (Fig. 3.3B). We

subdivided the escarpment system into three zones both along and across the escarpment system. Elevation along the edge of the plateau averages 2.5 km in the north and ~ 2 km in the south (Fig. 3.3C). Along the faulted transitional zone, elevation averages around 1.2 km throughout the escarpment (Fig. 3.3D). Elevation averages 1 km to near sea level from south to north along the rift floor (Fig. 3.3E).

Across the escarpment, mean elevation in the southern segment averages about 2.5 km, before failing to ~ 500 m on average in the rift floor (Fig. 3.3F), whereas in the north, elevation drops from about 2 km to ~ -100 m below sea level in the Danakil Depression (Fig. 3.3H). The central segment exhibits a relatively higher elevation due to the presence of the Guguftu shield volcano (Fig. 3.3G).

The local relief along the escarpment shows three distinct segments with elevations of 1 km to 1.5 km range in the north, central and southern segments (Fig. 3.4A). The rift floor contains the lowest relief throughout the escarpment, with few volcanoes showing a relatively moderate relief (Fig. 3.4A). The swath profile of the local relief (Fig. 3.4B), especially maximum relief along the escarpment shows a very rugged topographic setting characteristics of the edge of the plateau. The slope map (Fig. 3.4C), even though not as distinctive as the local relief, also shows highest (above 30 degree) slope in the north central and southern segments.

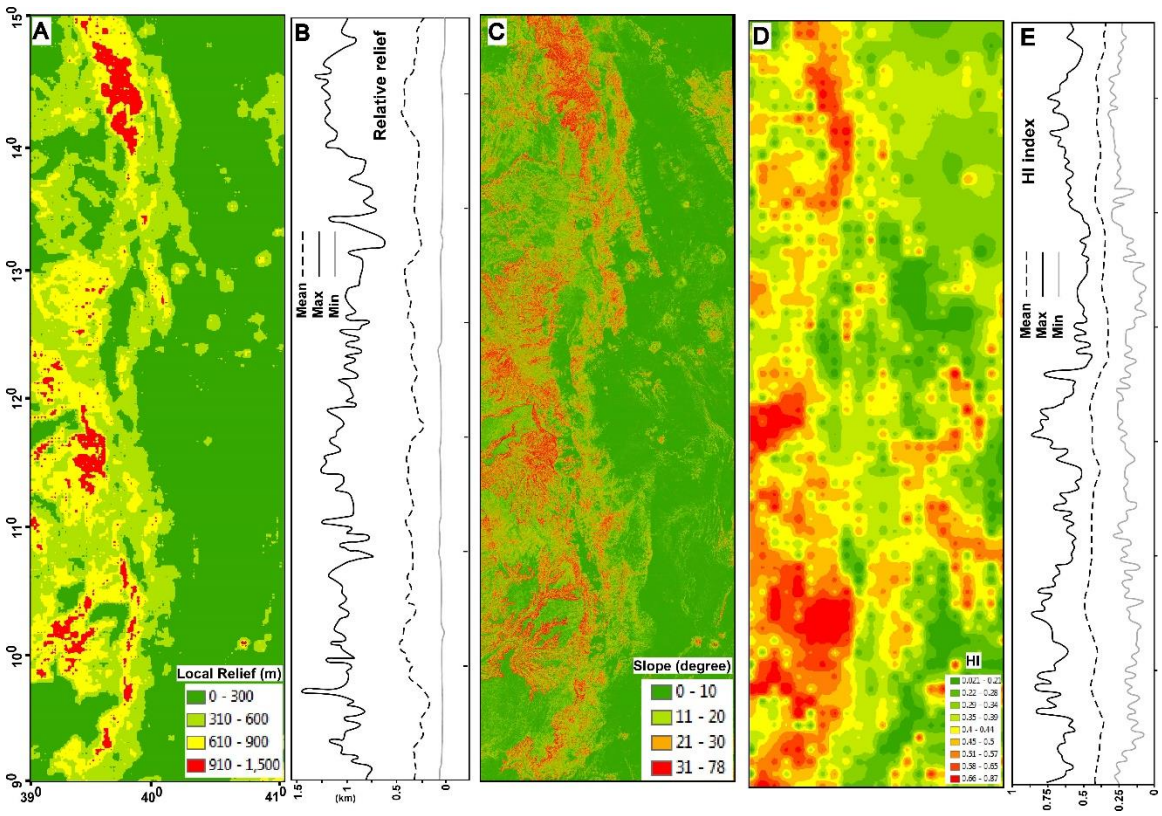

Figure 3.4: (A) Map of the local relief of the study area. (B) Swath profile of local relief showing the maximum, mean, and minimum relief pattern for the whole escarpment system. (C) Map of the slope (in degree). (D) Map of the Hypsometric Integral (HI) calculated for the whole escarpment using the grid-based method. (E) Swath profile of HI showing the maximum, mean, and minimum values for the whole escarpment system.

The hypsometric index (HI) for the entire escarpment system was generated using gridded method (Fig. 3.4D). It also shows highest values corresponding to the three segments identified in the local relief map. In addition, the swath profile of the HI values (Fig. 3.4E) was also able to show the relatively segmented maximum values along the escarpment. We used the topographic ruggedness/roughness map (Fig. 3.5A) to highlight major lithologic or structural boundaries constructed in figure 3.9. Steepness index (ksn) maps are normally a powerful means of

highlighting tectonic activity within a landscape and are much more productive when conducted for individual basins or drainage. Due to the nature of our regional analysis, the variation along the escarpment isn't that apparent except some local high values in the south and central segment (Fig. 3.5B).

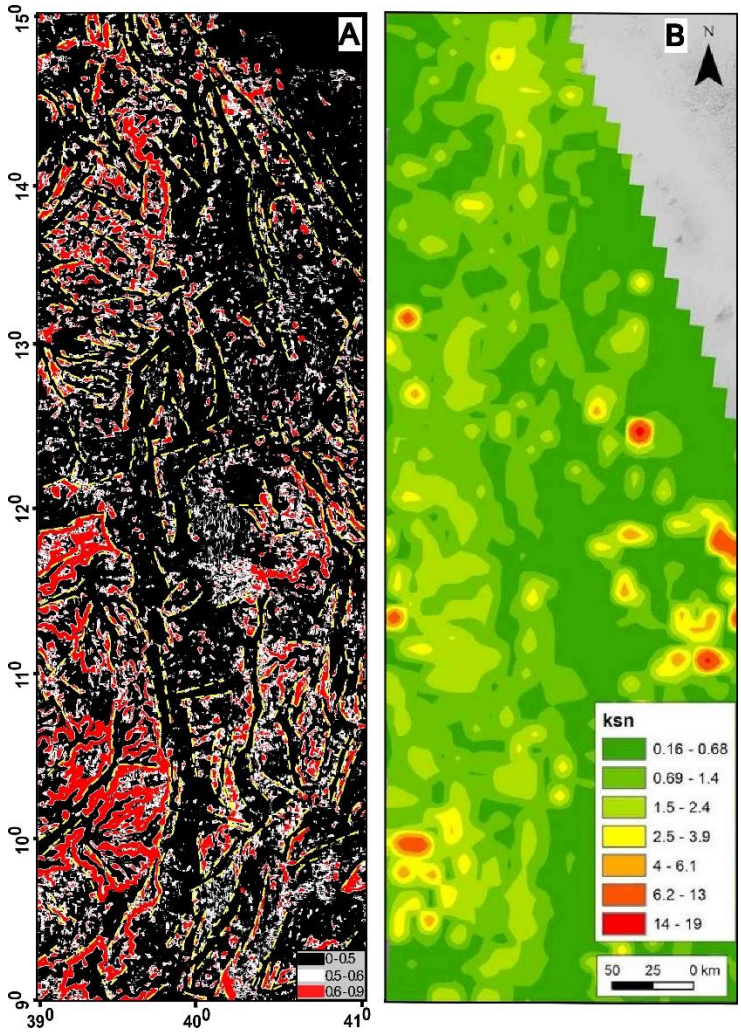

Figure 3.5: (A) Map of the topographic ruggedness/roughness index showing major structural or lithologic trends or boundaries traced as yellow broken lines. (B) Map of the steepness index calculated for the whole escarpment using the TopoToolbox matlab routines (Schwanghart and Scherler, 2014).

3.6.2. GEOPHYSICAL CHARACTERISTICS

The Bouguer gravity map mainly shows first order morphotectonic features with the plateau exhibiting low gravity minima characteristics of plume-induced uplift and incised mountainous regions, and a relatively higher anomaly within the rift region. A distinct gravity signature between the low-lying magmatic rifts showing regional gravity maximum that becomes more positive and cover larger area towards the north and of lower Bouguer gravity anomalies over the Northwestern Plateau that becomes more negative towards the south/southwest (Fig. 3.6A). Overall, the anomalies range between ~130 and – 150 mGal with the highest values occurring over the Danakil Depression. The mean Bouguer gravity values within the study area increase from north to south from about –60 mGal to 40 mGal. Within each segment (across the strike of the escarpment), mean Bouguer gravity values increase from about –130 to +50 mGal. The gravity maximum over the Afar Depression has been attributed to crustal densification due to replacement of crustal material by a dense asthenosphere magma or rocks.

The free-air (FA) gravity ranges from 280 mGal to -120 mGal and is characterized by north–south trending anomalies (Fig. 3.6B), parallel to the main topographic trends including the major marginal grabens. Though slightly segmented, the edge of the plateau shows a rather continuous relatively high FA anomaly due to the highly uplifted nature. Areas with low FA anomaly within the edge of the plateau correspond with deeply incised gorges, rivers and their tributaries. The rift floor bordering the escarpment on the other hand, exhibits relatively low FA anomaly in the northern and southern segment and an average ± 20 mgal in the central region. The isostatic anomaly ranges from 52 mGal to – 76 mGal. Major positive anomalies lie within the rift in the northern and southern segment, whereas major negative anomalies lie on the edge of the plateau, particularly in the southern segment (Fig. 3.6C). The magmatic segments in the northern and southern segment are characterized by wide and positive 20 to 50 mGal isostatic anomalies. Figure 3.6D shows the tilt derivative of 5 km upward continued Bouguer anomaly data.

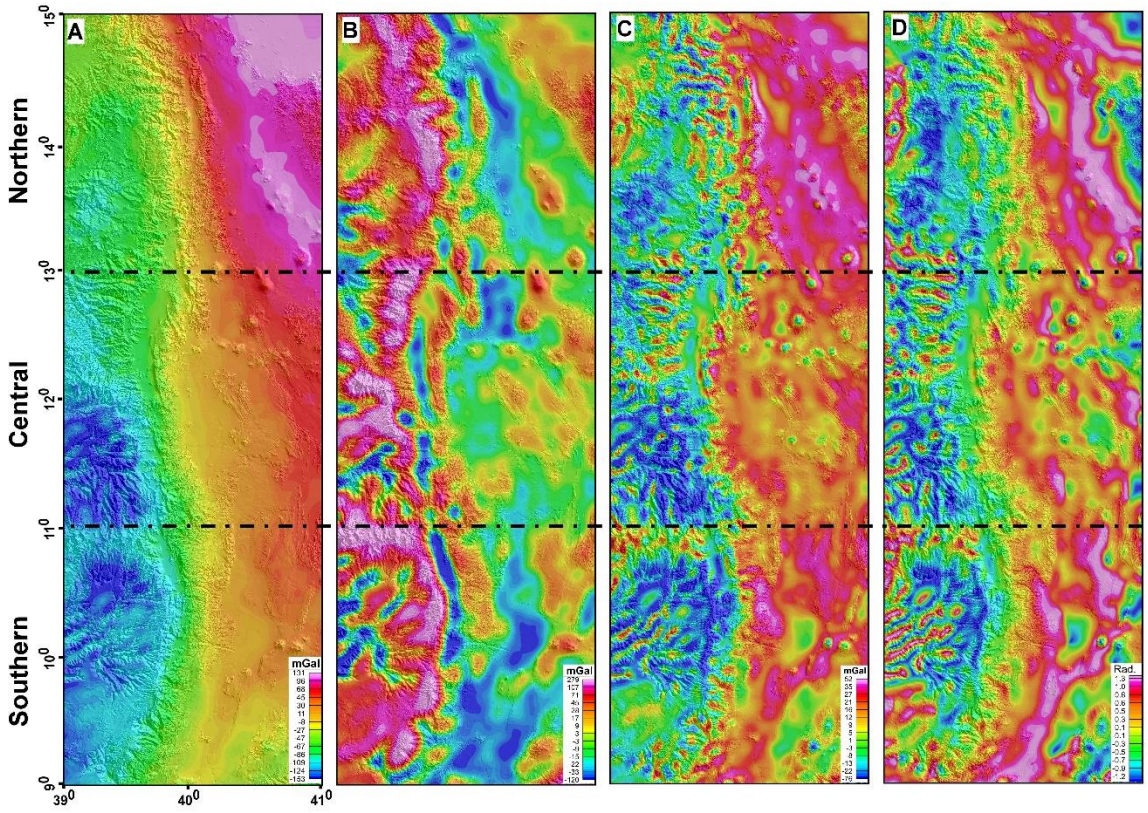

Figure 3.6: Gravity data extracted from World Gravity Model 2012 (WGM2012) (Bonvalot et al., 2012). All maps are superimposed over the hillshade DEM. (A) Bouguer gravity anomaly and upward continued to 2km to remove shallow drainage effects. Uplifted regions along the edge of the plateau show low anomaly and the rift floor region show a Bouguer gravity high. (B) Free-Air anomaly- an overall anomaly showing a NS trend with negative anomaly over marginal grabens and rift floor. The marginal grabens along the transitional transect with the escarpment system are especially well delineated. (C) Isostatic anomaly - major positive anomalies are located within the rift-floor transect in the magmatic northern and southern segment, while deeply incised drainages along the edge of the plateau transect in the southern segment show low isostatic anomaly. The central transect, across the escarpment shows possible compensated zone. (D) Tilt derivative of the upward continued (to 5km) Bouguer anomalies showing well delineated gravity lineaments corresponding to various tectono-magmatic segments.

The total magnetic anomaly anomalies in EMAG-2v in our study region range between –100 and +100 nT (Fig. 3.7A). Magnetic intensity is a function of the magnetic minerals such as magnetite within the rock. In the study area, possible source magnetic anomaly patterns are the strongly foliated basement complex in the plateau and faulted escarpment region, and tectono-magmatic processes in the rift floor. In addition to lacking good coverage, the basement of the plateau is also covered with thick sedimentary packages and basalts which influence magnetic anomalies, except at the northern edge where basement rocks are readily exposed with apparent high magnetic anomaly (Fig. 3.7B). Within the rift and escarpment region, areas with active magmatic segments show low magnetic anomalies, especially within the central segment (Fig. 3.7B). In addition, both the Erta' Ale volcanic complex and the Manda Hararo rift segment magnetic anomaly shows characteristic lows.

The tilt derivative of the total magnetic intensity map also shows three well-defined anomaly patterns mimicking tectono-magmatic boundaries oriented in the NW, NE and EW direction (Fig. 3.7C). The E-W trending magnetic anomalies, especially well delineated in the tilt map occur mainly in the central part of the escarpment system. They central segment also contains the highest magnetic minima which separates the escarpment system into regional domains, with higher positive anomalies to the north and segmented lower positive and negative anomalies to the south (Fig. 3.7A and B). The high positive anomaly in the northern segment is related to the exhumed basement structures, which is oriented parallel to the rift margin and may have controlled the present-day rifting in the Afar Depression. The large magnetic lows in the central segment are probably related to the Dabahu magmatic segment, which was very much active as recently as in 2009. It also coincides with large volcano-related seismic structures and thick sedimentary basin. To the south, the magnetic anomalies tend to be oriented NW. This area represents a region in which predominantly north trending structures from the Afar Depression interact with NE trending structures from the Northern Main Ethiopian Rift. However, unlike the gravity data, which shows

the bifurcation of the structure from NE to NS as we go from the MER to the southern Afar, the tilt derivative of the magnetic anomaly is oriented orthogonal to the MER trend and at angle to the margin (Fig. 3.7C).

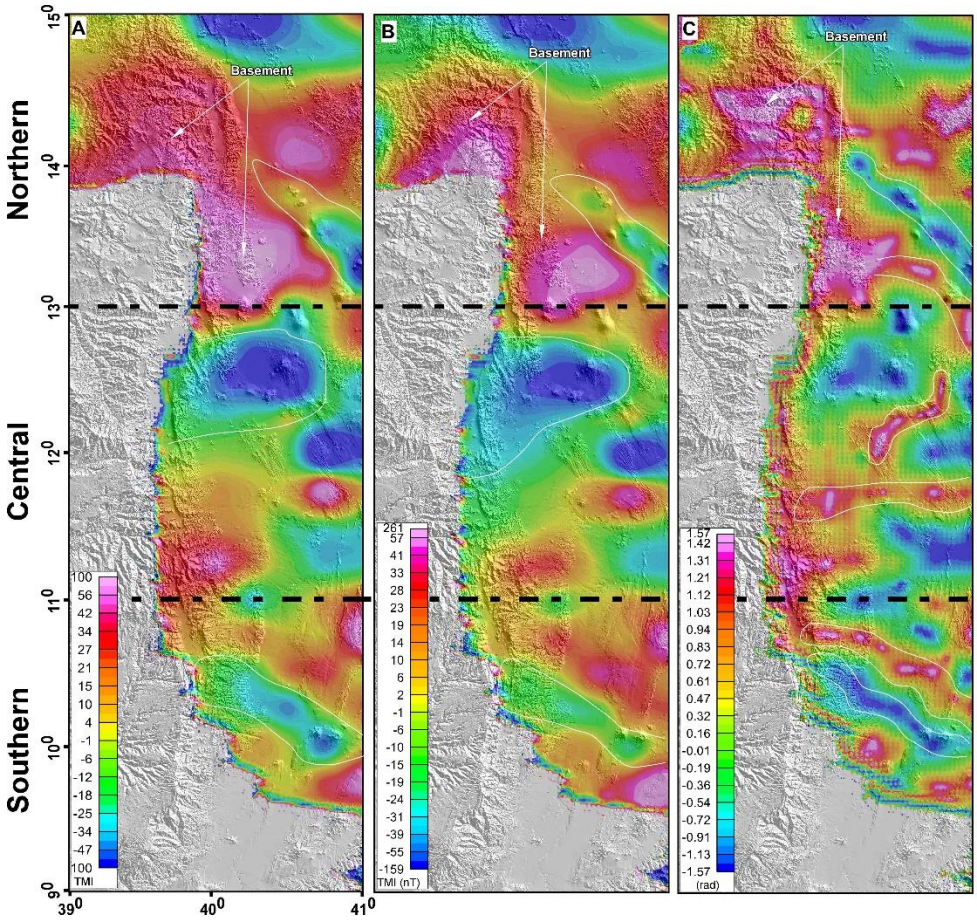

Figure 3.7: Magnetic data extracted from the 2-arc-minute resolution Earth Magnetic Anomaly Grid (EMAG2-v3) (Meyer et al., 2017). (A) Map of Total magnetic intensity (TMI), and (B) Total magnetic intensity reduced to the equator. Major orientation of volcanic segments and other geologic features such as the exposed Precambrian basement in the north (see geologic map in Fig. 3.2) are well delineated on the magnetic map. (C) The tilt-derivative map of the TMI. The tilt is positive, particularly over the basement highs in the north segment and volcanic transverse boundaries, and negative over active volcanic centers and sediment filled grabens. The tilt is assumed to be zero along magnetic contacts.

3.6.3. LITHOSPHERIC STRUCTURE

Crustal thickness values obtained from the Crust 1.0 global model and merged with those values compiled from receiver-function and refraction studies (Dugda et al., 2005; Hammond et al., 2011). Contoured over the crustal thickness map is the lithospheric rigidity (Te) of the area (Ebinger and Hayward, 1996). The map shows crustal thickness decreases northward from 46 km to 35 km in the plateau region and from ~30 km to ~16 within the rift (Fig. 3.8B and C). This northward decrease in crustal thickness has been attributed to different phases of rifting and magmatism along the various segment of the rift. Crust also thickens southwest of the study area, where it reaches thickness of 39 to 46 (Fig. 3.8), in agreement with the general thickening of the crust beneath the plateau due to possible underplating (Tiberi et al., 2005).

Strictly defined, tapered crust refers to a region in which crustal thickness thins from about 30 km average thickness to 10 km in a relatively short distance, usually less than 100 km (Osmundsen and Redfield, 2011). In such a scenario, we will end up with an extension factor of 3 (30 km divided by 10 km). In our case, most of the edge of the plateau is within the range of 40 km thickness, and the highly thinned region in the central and northern rift regions between 15 and 20 km, which is an extension corresponding to a factor of ~ 2 to 2.66. We measured distance from the tip of the plateau (the highest elevated regions along the escarpment) to the potential plate boundaries and/ magmatic segments as suggested by previous studies (Fig. 3.8D). While our designation of tapered crust contains some limitations, it is not without precedent since many of the regions are already shown to exhibit active deformation characteristics of a crust at a nascent stage of oceanisation (E.g. Makris and Ginzburg, 1987; Bastow and Keir, 2011; Hammond et al., 2011; Bridge et al., 2012).

In addition, the southern and central region show, slower shear-wave velocity, indicative of a magmatically active and warmer region (Fig. 3.12). Multiple studies have indicated lithospheric

modification due to tectono-magmatic processes including ponding of magma (e.g. Gallacher et al., 2016; Illsley-kemp et al., 2018), hence the low velocity zones. It is likely that areas (eg. in south Fig. 3.12) with a strong negative anomaly or pronounced lithospheric heating experience a more intensive thermal uplift than places such as in the north, where part of the Mekele Basin is shown to overlie, a slower, likely colder lithosphere. As a result of the development of the Mekele Basin as an ICONS due to lithospheric cooling and thickening. Elsewhere in the rift region, the slower anomaly is due to the active magmatic processes going under the Afar.

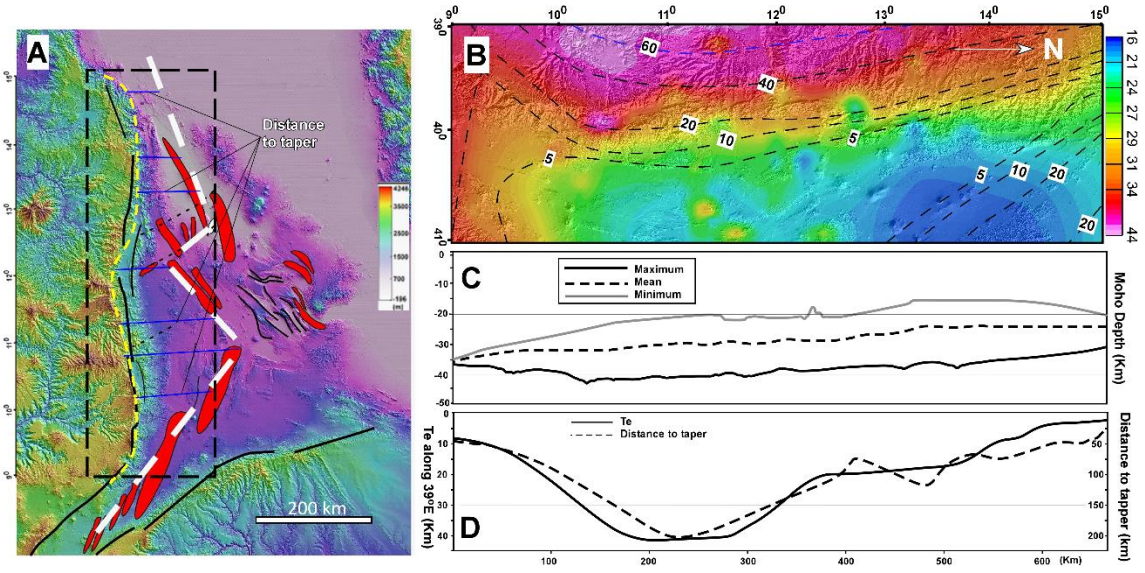

Figure 3.8: (A) Tectono-magmatic segments (red ellipses) and probable plate boundary (bold broken white lines), edge of the plateau (broken yellow lines), and distance to taper (blue lines). (B) Flexural rigidity (Te) data (from Ebinger and Hayward, 1996) plotted (dark broken lines) over the crustal thickness map extracted from Crust 1.0 global crustal thickness data (Laske et al., 2013) and receivers function studies (Dugda et al., 2005 and Hammond et al., 2011). Numbers indicate Te values I km. (C) Swath profile of crustal thickness showing the maximum, mean, and minimum values for the whole escarpment system. (D) Distance to the taper from the edge of the plateau (from the yellow line) (Osmundsen and Redfield, 2011) overlapped with Te values along the 39^0 E longitude.

3.7. DISCUSSION

We have documented the first comprehensive analysis of topographic and tectono-magmatic relationship along the strike of the escarpment of the western Afar Depression using DEM, geophysical data, and available geological information. The existing morphotectonic framework underlying the formation and evolution of the Ethiopian plateau and the escarpment system is that of a strong coupling between tectonic-magmatic processes undergoing at depth and in the neighboring rift, and surface denudation in the plateau region (e.g. Pik et al., 2003; Gani et al., 2007; Sembroni et al., 2016b). We set out to evaluate whether the crustal thickness and tectono-magmatic segmentation along the axis of the rift has any discernible control over surface processes along the strike of the escarpment. In the following section, we discuss the results and its implication in a greater detail.

While maximum values of some morphometric parameters such as local relief and HI are observed in the north, central and southern segments, our morphometric analysis indicates an overall fist-order mean escarpment similarity along the strike of the escarpment (Fig. 3.9). Such a scenario is indicative of a possibly regional, common cause mechanism. Secondly, given the significant segmentation and variation of tectono-magmatic processes along the rift axis, correspondence or spatial correlation can be reasonably made between the highly uplifted regions in the plateau, and crustal scale processes underneath or adjoining the escarpment. Though attributing which mechanism contributes to what degree is a difficult task, we have outlined the possible mechanisms for the consistently large anomalies (such as local relief, HI, crustal thickness and so on) observed within each segment.

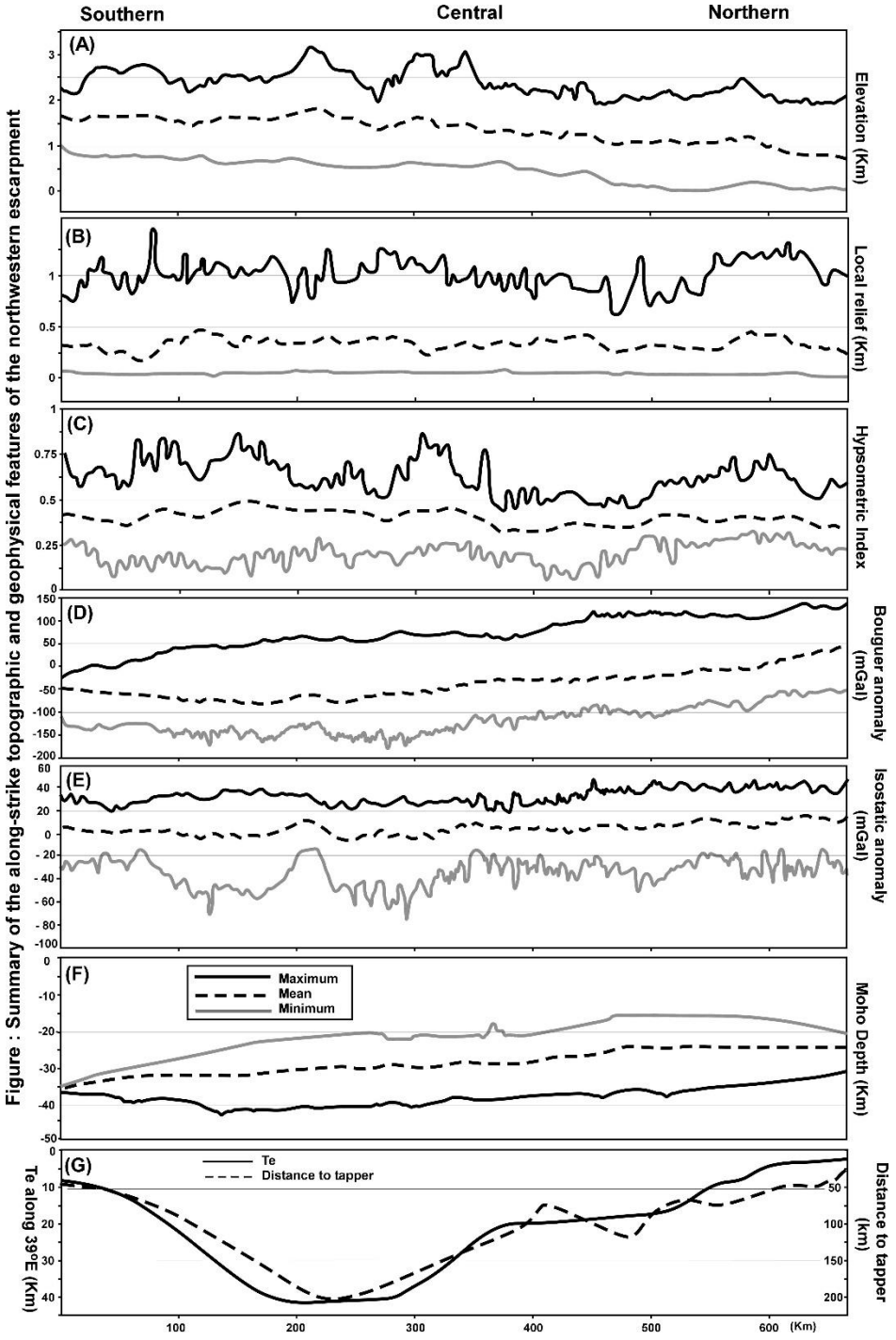

Figure 3.9: Summary of most parameters used in this study showing variation in topographic and geophysical features along the strike of the escarpment. (A) Elevation. (B) Local relief. (C) Hypsometric Index (HI). (D) Bouguer gravity. (E) Isostatic anomaly. (F) Moho depth. (G) Distance to taper and flexural rigidity (Te).

3.7.1. RELATIONSHIP BETWEEN PRESENT DAY AND PRE-EXISTING STRUCTURES

The NS trending flank forms the first-order structure along the escarpment system (Fig. 3.10A). This trend coincides with a preexisting weak structure of Precambrian origin and trend. The NS Precambrian structures are linked to an E-W closure of east and west Gondwana termed the Pan-African orogeny, and development of N-trending foliations during the Neoproterozoic (Stern, 1994). Their reactivation in many rifts and rift margins within the East African Rift System, especially those where magmatism tends to be very low or the so-called 'dry rifts' have been shown to wield significant control over both the geometry and kinematics of the rift system (e.g. Daly et al., 1989; Ring, 1994; Nyblade and Brazier, 2002; Chrowicz, 2005; Smets et al., 2016; Katumwehe et al., 2016).

Precambrian structures control rifting in this region at various scales. First, the whole East African Rift System including the Afar Depression primarily developed within the Pan-African mobile belt. For example, crustal extension within the Main Ethiopian Rift (MER) is especially controlled by relatively narrow lithospheric-scale pre-existing structure (Gashawbeza et al., 2004; Bastow et al., 2005; Keranen and Klemperer, 2008; Corti et al., 2018). In the study area, and within the transitional transect of the escarpment, conspicuous NS trending series of large grabens are parallel to Precambrian trend, and may as well been controlled by it. However, in the greater Afar Depression, where thermal anomaly is very high, and rifting is relatively distributed among various segments, the structural setting is complex with competing trends between NS-oriented Precambrian fabric, NW-oriented Mesozoic extensional structures, and Cenozoic E-W oriented transverse faults (Fig. 3.10).

The NW-oriented structures correspond to Mesozoic extensional tectonics related to break-up of Gondwanaland that has been attributed to the development of multiple NW oriented sedimentary

basins (Beyth, 1972; Bosellini, 1986; Bosworth, 1992; Russo et al., 1994). These structures are filled with thick mixed carbonate-clastic sedimentary packages unconformably overlying Paleozoic and early Mesozoic clastic sediments. In the study area, the Mekele in the north and the Blue Nile in the south constitute the largest Mesozoic sedimentary basins. Another sub-basalt sedimentary basin in the central region was also suggested from gravity analysis (E.g. Mammo, 2010). The Mekele Basin is almost completely exposed on the surface due to its location near the rift flank. Like the rest of the study area, the Mekele Basin lies within the Pan-African juvenile Arabian-Nubian Shield lithosphere (Stern, 1994). It was recently reinterpreted as an intracontinental basin due to the presence of geological and geophysical features such as its elliptical shape, saucer shaped cross-section, low gravity signature and a relatively thicker crust and lithosphere (Alemu et al., 2018). How and to what extent such large-scale lithospheric heterogeneity controls rift segmentation along-strike of the escarpment might be something of an interest in the future. Here, we can speculate that the relatively thick lithosphere under the Mekele Basin and surrounding region (i.e. northern segment), as can be observed in the shear wave tomographic model (Fig. 3.12), may have deflected the propagation of the Dabbahu-Manda Hararo segment into the Earta-Ale segment, and resulting in the convex shape of the overall escarpment in the north (Fig. 3.1). In the southern segment, the escarpment system is characterized by NS trending major border fault system, and NE trending Main Ethiopian trend, possibly connected by intersegment accommodation zones (Fig. 3.10).

A further important trend is documented by EW to ENE oriented transform fault zones that are associated with Cenozoic rift segmentation and transfer, and dyke swarms which outcrop in the central segment of the escarpment. These structures are generally parallel to transverse faults systems that serve as an accommodation zones and help transfer extension among the various segments. Geophysical data, particularly the tilt map (Fig. 3.7), provided additional evidence for this major EW to ENE striking transverse fault system. The location and interaction among these

structures appears to exert notable control over the orientation and location of the various magmatic segments within the rift system, and drainage pattern and topographic features in the uplifted plateau.

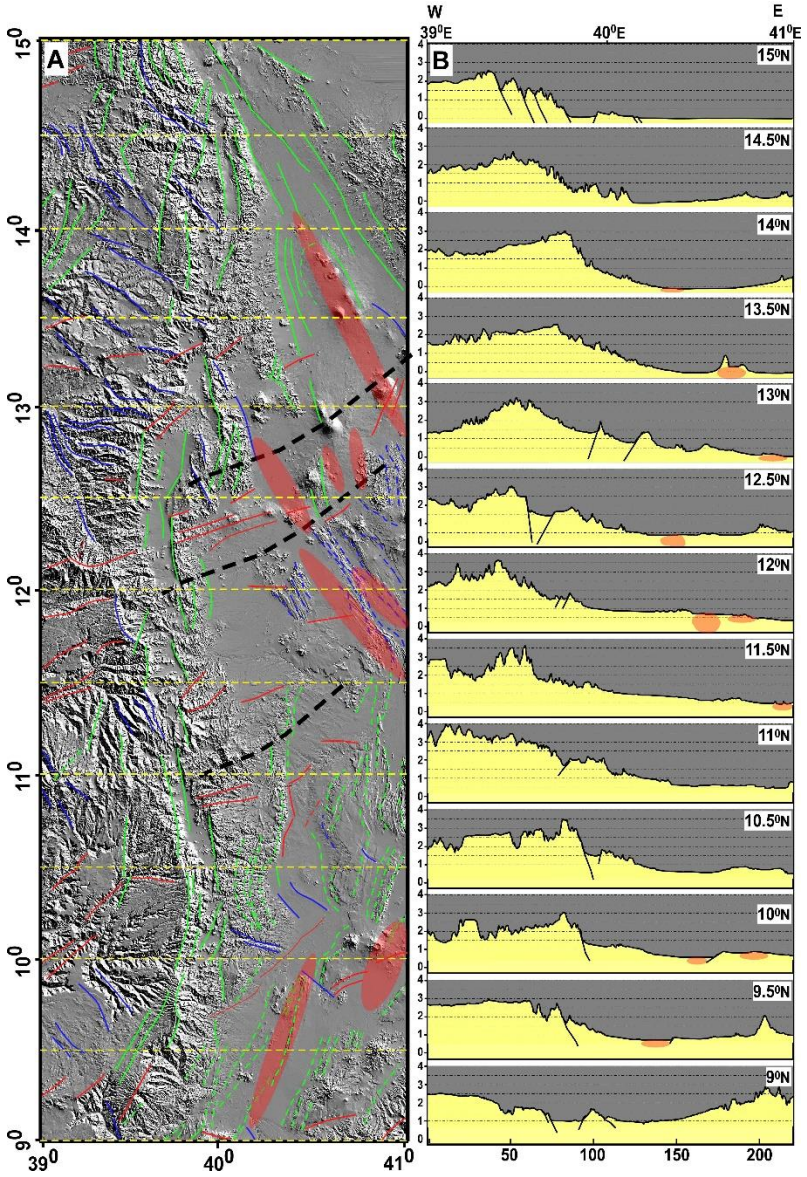

Figure 3.10: (A) Structural trends traced from the topographic ruggedness/roughness index map (shown on Fig. 3.5A) classified based on orientation and possible origin. Green lineaments generally trend NS to NWN and NEN and coincide with Precambrian structures, Blue lineaments correspond to NW Mesozoic structures, and Red lineaments coincide with EW oriented transfer

faults. Red ellipses indicate active magmatic segments. (B) Topographic cross section across the escarpment, taken every half degree (~55 km) from south to north.

3.7.2. PATTERNS OF ALONG-STRIKE TECTONO-MAGMATIC VARIATION

The escarpment system is clearly divided into topographically high plateau and low rift floor subdivided by a transitional segment (Fig. 3.1). The fact that continental rifts show significant along strike variation or segmentation in rifting and magmatism is a well-documented case that also applies for the Afar Depression and the East African Rift System in general (Hayward and Ebinger, 1996; Corti 2009; Keir et al., 2014). Particularly in the Afar Depression, the along-strike segmentation is prominent due to part of it being at a nascent stage of oceanisation (E.g. Makris and Ginzburg, 1987; Bastow and Keir, 2011; Hammond et al., 2011; Bridge et al., 2012). Within the rift floor transect of our study area (along the axis of the Afar Depression), major discontinuities in the rift segments are observed; where remarkable magmatic and seismic activities are happening within multiple segments including the Alu-Dalafill, Dabbahu-Manda-Hararo, and Erta-ale (Fig. 3.1). These segments are shown to function as a magma plumbing system and may eventually develop into segmented mantle upwelling zones following post-continental rifting (Gallacher et al., 2016; Illsley-kemp et al., 2018).

One of the major tectonic processes driving extension within the Afar Depression is the rotation of the Danakil block. The displacement vectors along the escarpment of the Northwestern Plateau relative to the Danakil block decreases toward the north (Fig. 3.1B), consistent with the counterclockwise rotation of the Danakil block. In fact, extension significantly decreases from ~30 mm in the south to near zero at the northern end of the Afar Depression; the location at which the extension is transferred to the Red Sea rift in the northeast (McClusky et al., 2010). Within the study area, extension increases from about 15 mm/yr in the north to ~ 20 mm/yr in the central segment to ~ 30 mm/yr (McClusky et al., 2010). Although variation in extension rate has been

attributed to exert notable control over escarpment morphology, there is no systematic analysis of such effect in the study area (in addition to the fact that extension in central Afar is distributed among various segments e.g. Keir et al., 2013). Therefore, it has relatively little influence on rift flank morphology. Rather, for escarpments bordering a tapered crust (Osmundsen and Redfield, 2011), we used the distance from edge of the escarpment to the tapered region (thinned crust) which coincides with active magmatic segments — with aim of evaluating its effect on escarpment morphology (Fig. 3.8A and D).

3.7.3. CORRESPONDENCE AMONG SURFACE AND SUBSURFACE PROCESSES

What is apparent is different stages of crustal thinning within the low-lying escarpment in the Afar Depression, only appears to exert a second-order control over the topographic patterns in the plateau. In accordance with previous geophysical studies (Dugda et al., 2005; Stuart et al., 2006; Dugda et al., 2007; Hammond et al., 2011), the crustal thickness map extracted from Crust1.0 and published estimates shows significant crustal thickness variation along the axis of the rift, from ~ 15 km in the north to around 30 km average thickness in the south and central part of the AD (Fig. 3.8). Significant variation along the strike of the escarpment is especially observed between the central segment and the northern segment, where crust thins from about 25 km in the central and surrounding regions to ~ 15 km beneath the Danakil depression surrounding the Erta Ale in the northern segment. The study area is also characterized by an abrupt decrease in the lithospheric strength (Te) from about 40 km along the plateau to 5 km along the rift floor (Fig. 3.8). In addition, segmented low and high magnetic zones and tilt-derivative map of the Bouguer gravity (Fig. 3.6 and 3.7), S-wave perturbation at an average depth of 40-80 km and 80 km (Fig. 3.12), all correlate with tectonic and magmatic segments. Such an obvious segmentation of tectonism, particularly crustal thickness variation along the axis of the rift is expected to produce corresponding, spatially variable topographic features. However, the segmentation only exhibits correspondence with maximum values of topographic features including elevation, local relief and HI, while for the

mean values of topographic features no such relationship was observed (Fig. 3.9). Moreover, like many other escarpments (e.g. Gilchrist and Summerfield, 1990; Gallagher et al., 1994), the northwestern plateau escarpment system is maintained by a high elevation plateau interior with an average elevation of 2500 m a.s.l. Therefore, the whole escarpment is probably formed at the same time and in which its inception was controlled by a primary regional process and structure. This regional uplift could be explained by dynamic topography associated with plume impingement prior to rifting (Pik et al., 2003) or regional lithospheric drip during rifting (Gani et al., 2007). More data is needed to quantify the uplift rate, and therefore, associate the regional uplift to particular model.

Across the strike of the escarpment, crustal thickness changes abruptly over a very short distance, particularly along the north and central segments. The result of a 50 km wide swath profile crustal thickness value (Fig. 3.11C) along the north profile shows, the Moho is 35 km deep beneath the plateau, whereas beneath the adjacent Danakil depression, it acquires the shallowest depth of 16 km recorded from the study area. Within the central segment, similar abrupt but a relatively wide zone of thinning, characterized by widespread volcanic and seismicity is observed (Fig. 3.1). In the southern segment, the highest escarpment uplift directly overlies a thickened ~ 46 km crust (Fig. 3.11C). Each of these segments also exhibit a higher than average channel steepness index values emulating elevation, HI and local relief patterns (Fig. 3.9). Accordingly, we hypothesize that mechanisms for the small albeit recognizable topographic variation could be the inboard highly extended, and almost tapered crust in the north and central region resulting in thermally induced anomalous uplift, whereas in the south uplift could be due underplating. However, the temporal evolution and relative rates of uplift and denudation a particular mechanism may result in a segment is not yet quantified, and require additional geologic and thermochronologic data to do so.

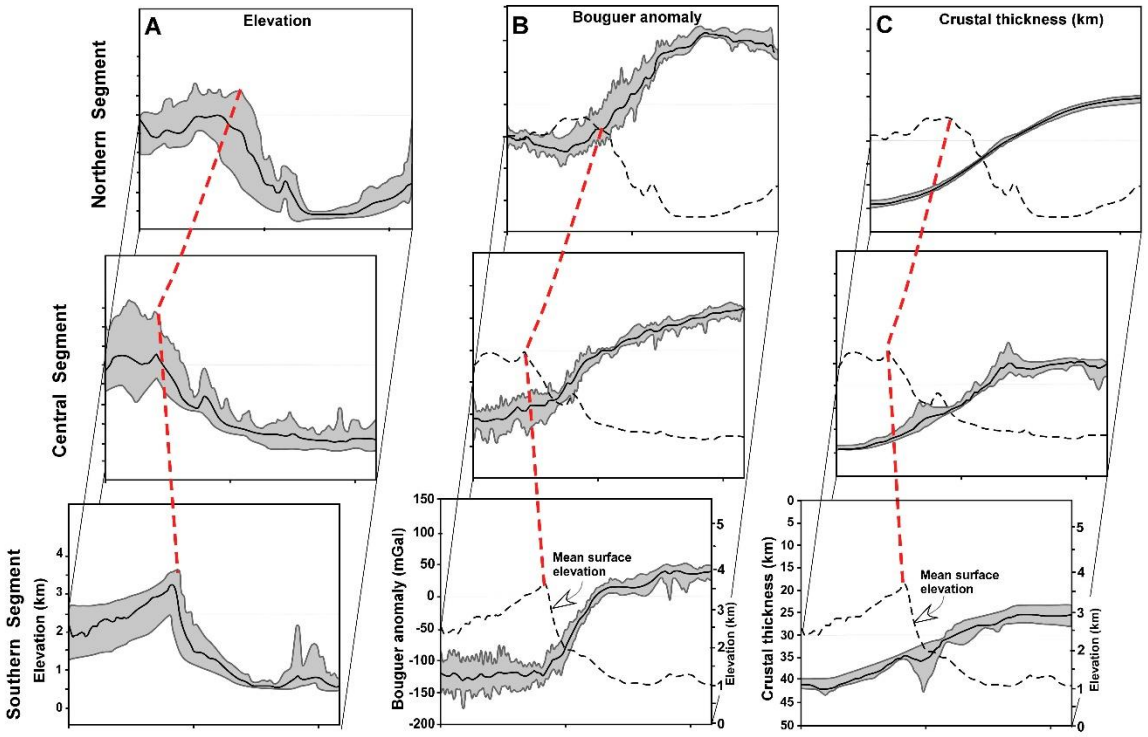

Figure 3.11: Summary of swath profiles of elevation, Bouguer gravity anomaly and crustal thickness variation across the three 50 km window in the north, central and southern segments. (A) Elevation – Red broken line showing the approximate location of the edge of the highest point in that specific segment. (B) Bouguer gravity anomaly and the mean surface elevation. (C) Crustal thickness and the mean surface elevation. The highest escarpment in the southern segment overlies a thicker, possibly underplated crust.

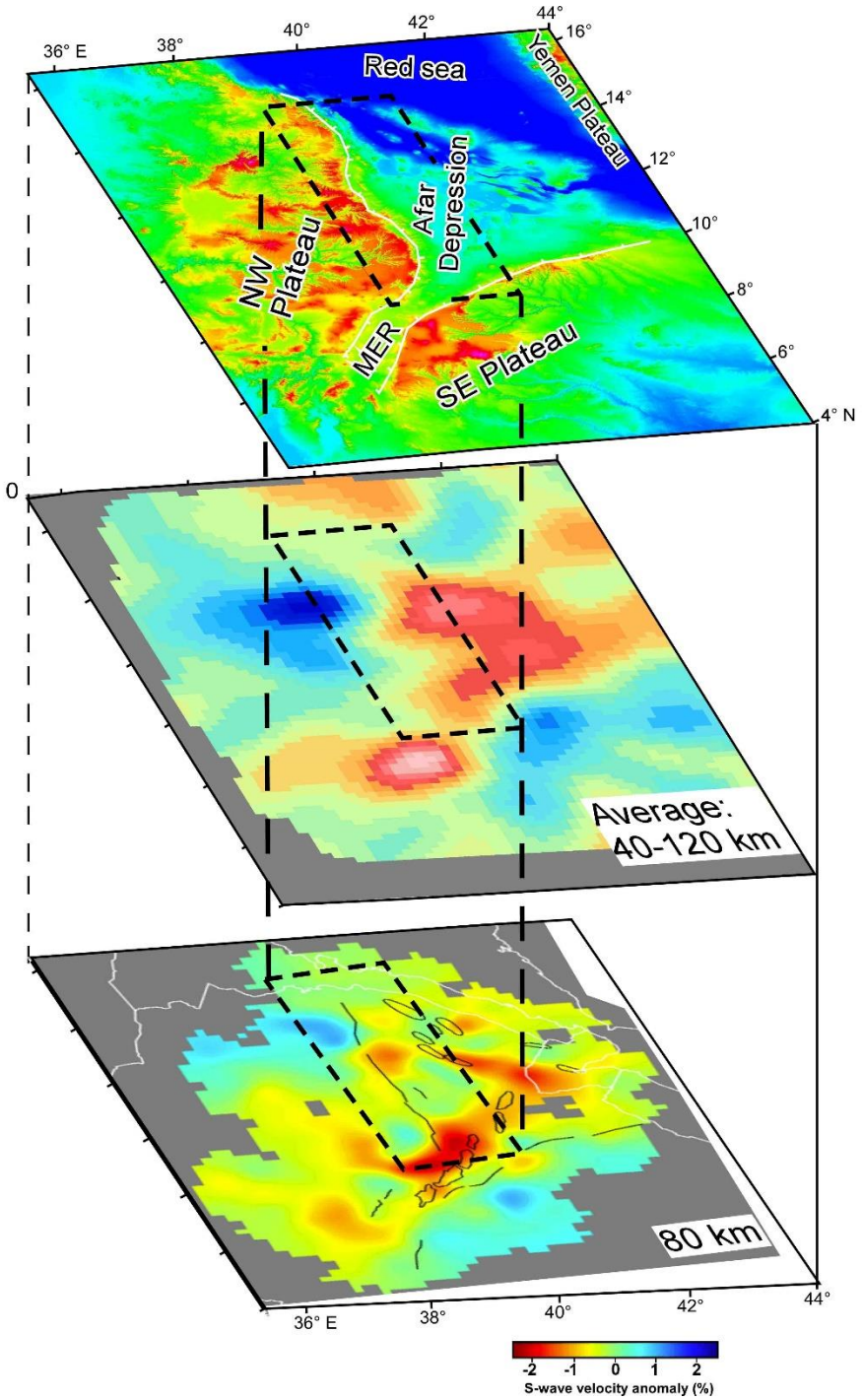

Figure 3.12: Shear-wave tomographic model of the Ethiopian plateau and rift region showing s-wave perturbations in the upper lithosphere at present (after Galacher et al 2016). (A) DEM of the Ethiopian plateau and surrounding region, rifts. (B) Tomography at an average depth of 40-120. (C) Tomography at depth of 80 Km.

3.8. CONCLUSION

We provided a comprehensive analysis of the topographic and tectono-magmatic features of the western escarpment using regional and semi-local topographic and geophysical data and parameters. We found a general correspondence between the various morphometric parameters along the escarpment. In addition, almost all parameters show distinct, maximum anomalous values in the north, central and southern sections of the escarpment. However, despite significant rifting and magmatism, and crustal thinning along the rift, we found a more or less similar mean topographic pattern. The integrated analysis of gravity and magnetic data, and associated derivative maps was able to show the location, geometry and orientation of the major tectono-magmatic boundaries previously mapped from field and other geophysical methods. Our geophysical results clearly show the along-strike segmentation of the escarpment, particularly within the transitional and rift floor transect.

The presence of small, yet notable topographic variation correlate-able with that of tectono-magmatic shows coupling between tectonic and surface processes. We interpret such correspondence as indicative of second order segmentation along the escarpment reflecting the local interplay between varying uplift and denudation. However, segmentation along the edge of the plateau transect is not as pervasive as one could assume given the drastic variation in crustal architecture from south to north. These implies topographic development is primarily controlled by a regional process. The interpretation of regional control in escarpment is in agreement with a hypothesis of dynamic topographic support substantiated by considerations of seismic tomography and gravity data, regional topographic doming, and geochemical data. Whereas variation in climate and the rate and extent of rifting, magmatism along the escarpment has been documented to have influence on topography, the combined analysis of morphometric and geophysical data shows that these later processes play a secondary role in the landscape evolution of the of the escarpment system.

3.9. ACKNOWLEDGMENT

We thank International Gravimetric Bureau for the gravity data. This is Oklahoma State University, Boone Pickens School of Geology contribution number 2019-xx.

3.10. REFERENCES

Abdelsalam, M. G., and Stern, R. J., 1996, Sutures and shear zones in the Arabian-Nubian Shield: Journal of African Earth Sciences, v. 23, no. 3, p. 289-310.

Alemu, T., Abdelsalam, M. G., Dawit, E. L., Atnafu, B., and Mickus, K. L., 2018, The Paleozoic–Mesozoic Mekele Sedimentary Basin in Ethiopia: An example of an exhumed IntraCONtinental Sag (ICONS) basin: Journal of African Earth Sciences, v. 143, p. 40-58.

Asrat, A., Barbey, P., and Gleizes, G., 2001, The Precambrian geology of Ethiopia: a review: Africa Geoscience Review, v. 8, p. 271-288.

Ayalew, D., and Gibson, S. A., 2009, Head-to-tail transition of the Afar mantle plume: Geochemical evidence from a Miocene bimodal basalt–rhyolite succession in the Ethiopian Large Igneous Province: Lithos, v. 112, p. 461-476.

Ayalew, D., Barbey, P., Marty, B., Reisberg, L., Yirgu, G., and Pik, R., 2002, Source, genesis, and timing of giant ignimbrite deposits associated with Ethiopian continental flood basalts: Geochimica et Cosmochimica Acta, v. 66, p. 1429-1448.

Balmino, G., Vales, N., Bonvalot, S., and Briais, A., 2012, Spherical harmonic modelling to ultra-high degree of Bouguer and isostatic anomalies: Journal of Geodesy, v. 86, p. 499-520.

Barberi, F., Ferrara, G., Santacroce, R., and Varet, J., 197, Structural evolution of the Afar triple junction, p. 38-54.

Barberi, F., Santacroce, R., and Varet, J., 1974, Silicic peralkaline volcanic rocks of the Afar depression (Ethiopia): Bulletin Volcanologique, v. 38, p. 755-790.

Bastow, I. D., Stuart, G. W., Kendall, J. M., and Ebinger, C. J., 2005, Upper-mantle seismic structure in a region of incipient continental breakup: northern Ethiopian rift: Geophysical Journal International, v. 162, p. 479-493.

Beyene, A., and Abdelsalam, M. G., 2005, Tectonics of the Afar Depression: A review and synthesis: Journal of African Earth Sciences, v. 41, p. 41-59.

Beyth, M., 1972, Paleozoic-Mesozoic sedimentary basin of Mekele outlier, northern Ethiopia: AAPG Bulletin, v. 56, p. 2426-2439.

Bonini, M., Corti, G., Innocenti, F., Manetti, P., Mazzarini, F., Abebe, T., and Pecskay, Z., 2005, Evolution of the Main Ethiopian Rift in the frame of Afar and Kenya rifts propagation: Tectonics, v. 24, p. 1-21.

Bonvalot, S., Balmino, G., Briais, A., Kuhn, M., Peyrefitte, A., Vales, N., Biancale, R., Gabalda, G., Moreaux, G. and Reinquin, F., 2012, World gravity map: Bureau Gravimetrique International (BGI), Map, CGMW-BGI-CNES728, IRD, Paris.

Bosellini, A., 1986, East Africa continental margins: Geology, v. 14, no. 1, p. 76-78.

Bosellini, A., Russo, A., Fantozzi, P. L., Assefa, G., and Solomon, T., 1997, The Mesozoic succession of the Mekele outlier (Tigre province, Ethiopia): Memorie di Scienze Geologiche, v. 49, p. 95-116.

Bosworth, W., 1992, Mesozoic and early Tertiary rift tectonics in East Africa: Tectonophysics, v. 209, p. 115-137.

Bridges, D. L., Mickus, K., Gao, S. S., Abdelsalam, M. G., and Alemu, A., 2012, Magnetic stripes of a transitional continental rift in Afar: Geology, v. 40, no. 3, p. 203-206.

Burov, E., and Cloetingh, S., 1997, Erosion and rift dynamics: new thermomechanical aspects of post-rift evolution of extensional basins: Earth and Planetary Science Letters, v. 150, p. 7-26.

Bussert, R., 2010, Exhumed erosional landforms of the Late Palaeozoic glaciation in northern Ethiopia: indicators of ice-flow direction, palaeolandscape and regional ice dynamics: Gondwana Research, v. 18, p. 356-369.

Chorowicz, J., 2005, The east African rift system: Journal of African Earth Sciences, v. 43, p. 379-410.

Chorowicz, J. Collet, B., Bonavia, F., and Korme, T., 1999, Left-lateral strike-slip tectonics and gravity induced individualisation of wide continental blocks in the western Afar margin: Eclogae Geologicae Helvetiae, v. 92, p. 149-158.

Collet, B., Taud, H., Parrot, J. F., Bonavia, F., and Chorowicz, J., 2000, A new kinematic approach for the Danakil block using a Digital Elevation Model representation: Tectonophysics, v. 316, p. 343-357.

Cornwell, D. G., Maguire, P. K., England, R. W., and Stuart, G. W., 2010, Imaging detailed crustal structure and magmatic intrusion across the Ethiopian Rift using a dense linear broadband array: Geochemistry, Geophysics, Geosystems, v. 11, p. 1-21.

Corti, G., Molin, P., Sembroni, A., Bastow, I. D., and Keir, D., 2018, Control of Pre-rift Lithospheric Structure on the Architecture and Evolution of Continental Rifts: Insights From the Main Ethiopian Rift, East Africa: Tectonics, v. 37, p. 477-496.

Coulié, E., Quidelleur, X., Gillot, P. Y., Courtillot, V., Lefèvre, J. C., and Chiesa, S., 2003, Comparative K–Ar and Ar/Ar dating of Ethiopian and Yemenite Oligocene volcanism: implications for timing and duration of the Ethiopian traps: Earth and Planetary Science Letters, v. 206, p. 477-492.

Courtillot, V., Achache, J., Landre, F., Bonhommet, N., Montigny, R., and Féraud, G., 1984, Episodic spreading and rift propagation: new paleomagnetic and geochronologic data from the Afar nascent passive margin: Journal of Geophysical Research: Solid Earth, v. 89, p. 3315-3333.

Cyr, A. J., Granger, D. E., Olivetti, V., and Molin, P., 2010, Quantifying rock uplift rates using channel steepness and cosmogenic nuclide–determined erosion rates: Examples from northern and southern Italy: Lithosphere, v. 2, p. 188-198.

Dainelli, G., 1943, Geologia dell'Africa Orientale (3 vols. text, 1 vol. maps). R: Accad. Ital., Roma.

Daly, M. C., Chorowicz, J., and Fairhead, J. D., 1989, Rift basin evolution in Africa: the influence of reactivated steep basement shear zones: Geological Society, London, Special Publications, v. 44, p. 309-334.

Davidson, A., and Rex, D. C., 1980, Age of volcanism and rifting in southwestern Ethiopia: Nature, v. 283, p. 657.

Dow, D., Beyth, M., and Hailu, T., 1971, Palaeozoic glacial rocks recently discovered in northern Ethiopia: Geological Magazine, v. 108, p. 53-60.

Dugda, M. T., Nyblade, A. A., Julia, J., Langston, C. A., Ammon, C. J., and Simiyu, S., 2005, Crustal structure in Ethiopia and Kenya from receiver function analysis: Implications for rift development in eastern Africa: Journal of Geophysical Research: Solid Earth, v. 110, p. 1-15.

Ebinger, C. J., 1989, Tectonic development of the western branch of the East African rift system: Geological Society of America Bulletin, v. 101, p. 885-903.

Ebinger, C. J., and Hayward, N. J., 1996, Soft plates and hot spots: Views from Afar: Journal of Geophysical Research: Solid Earth, v. 101, p. 21859-21876.

Ebinger, C. J., Yemane, T., Woldegabriel, G., Aronson, J. L., and Walter, R. C., 1993, Late Eocene–Recent volcanism and faulting in the southern main Ethiopian rift: Journal of the Geological Society, v. 50, p. 99-108.

Ebinger, C. J., and Sleep, N. H., 1998, Cenozoic magmatism throughout east Africa resulting from impact of a single plume: Nature, v. 395, p. 788.

England, P., and Molnar, P., 1990, Surface uplift, uplift of rocks, and exhumation of rocks: Geology, v. 18, p. 1173-1177.

Gani, N.D.S, Gani, M., and Abdelsalam, M.G., 2007, Blue Nile incision on the Ethiopian Plateau: pulsed plateau growth, Pliocene uplift and hominin evolution: GSA Today, v. 17, p. 4–11.

Gashawbeza, E. M., Klemperer, S. L., Nyblade, A. A., Walker, K. T., and Keranen, K. M., 2004, Shear-wave splitting in Ethiopia: Precambrian mantle anisotropy locally modified by Neogene rifting: Geophysical Research Letters, v. 31.

Garland, C.R., 1980, Geology of the Adigrat area: Geol. Surv. Ethiopia Mem. V. 1, p. 1–51.

George, R., Rogers, N., and Kelley, S., 1998, Earliest magmatism in Ethiopia: Evidence for two mantle plumes in one flood basalt province: Geology, v. 26, p. 923-926.

Geosoft inc., 2015, Magmap filtering how-to guide.

Gilchrist, A. R., and Summerfield, M. A., 1990, Differential denudation and flexural isostasy in formation of rifted-margin upwarps: Nature, v. 346, p. 739.

Gilchrist, A. R., and Summerfield, M. A., 1991, Denudation, isostasy and landscape evolution: Earth Surface Processes and Landforms, v. 16, p. 555-562.

Gunnell, Y., and Harbor, D., 2008, Structural underprint and tectonic overprint in the Angavo (Madagascar) and Western Ghats (India)-Implications for understanding scarp evolution at passive margins: Journal Geological Society of India, v. 71, p. 763.

Hammond, J. O., Kendall, J. M., Stuart, G. W., Keir, D., Ebinger, C., Ayele, A., and Belachew, M., 2011, The nature of the crust beneath the Afar triple junction: Evidence from receiver functions: Geochemistry, Geophysics, Geosystems, v. 12.

Hofmann, C., Courtillot, V., Feraud, G., Rochette, P., Yirgu, G., Ketefo, E., and Pik, R., 1997, Timing of the Ethiopian flood basalt event and implications for plume birth and global change: Nature, v. 389, p. 838–841.

Illsley-Kemp, F., Keir, D., Bull, J. M., Gernon, T. M., Ebinger, C., Ayele, A., ... and Belachew, M., 2018, Seismicity during continental breakup in the Red Sea rift of Northern Afar: Journal of Geophysical Research: Solid Earth, v. 123, p. 2345-2362.

Ismail, E. H., and Abdelsalam, M. G., 2012, Morpho-tectonic analysis of the Tekeze River and the Blue Nile drainage systems on the Northwestern Plateau, Ethiopia: Journal of African earth sciences, v. 69, p. 34-47.

Jenness, J., 2006, Topographic Position Index (tpi_jen. avx) Extension for ArcView 3.x, v. 1.3a. Jenness Enterprises.

Jacobsen, B. H., 1987, A case for upward continuation as a standard separation filter for potential-field maps: Geophysics, v. 52, p. 1138-1148.

Jain, S., 1986, Total magnetic field reduction – the pole or equator? A model study: Canadian Journal of exploration geophysics, v. 24, p. 185-192.

Jepsen, D. H., and Athearn, M. J., 1962, East-west geologic sections, Blue Nile river basin, Ethiopia: Water Resources Department Addis Abeba, drawing, 5.2.

Katumwehe, A. B., Abdelsalam, M. G., Atekwana, E. A., and Laó-Dávila, D. A., 2016, Extent, kinematics and tectonic origin of the Precambrian Aswa Shear Zone in eastern Africa: Gondwana Research, v. 34, p. 241-253.

Kazmin, V., 1971, Precambrian of Ethiopia: Nature Physical Science, v. 230, p. 176.

Kazmin, V., Shifferaw, A., and Balcha, T., 1978, The Ethiopian basement: stratigraphy and possible manner of evolution: Geologische Rundschau, v. 67, p. 531-546.

Keir, D., Bastow, I. D., Whaler, K. A., Daly, E., Cornwell, D. G., and Hautot, S., 2009, Lower crustal earthquakes near the Ethiopian rift induced by magmatic processes: Geochemistry, Geophysics, Geosystems, v. 10.

Keir, D., Hamling, I.J., Ayele, A., Calais, E., Ebinger, C., Wright, T.J., Jacques, E., Mohamed, K., Hammond, J.O., Belachew, M. and Baker, E., 2009, Evidence for focused magmatic

accretion at segment centers from lateral dike injections captured beneath the Red Sea rift in Afar: Geology, v. 37, p. 59-62.

Kieffer, B., Arndt, N., Lapierre, H., Bastien, F., Bosch, D., Pecher, A., Yirgu, G., Ayalew, D., Weis, D., Jerram, D.A., Keller, F., and Meugniot, C., 2004, Flood and shield basalts from Ethiopia: magmas from the African superswell: Journal of Petrology, v. 45, p. 793-834.

Kirby, E., and Whipple, K. X., 2012, Expression of active tectonics in erosional landscapes: Journal of Structural Geology, v. 44, p. 54-75.

Kirby, E., Whipple, K. X., Tang, W., and Chen, Z., 2003, Distribution of active rock uplift along the eastern margin of the Tibetan Plateau: Inferences from bedrock channel longitudinal profiles: Journal of Geophysical Research: Solid Earth, v. 108.

Korostelev, F., Weemstra, C., Leroy, S., Boschi, L., Keir, D., Ren, Y., Molinari, I., Ahmed, A., Stuart, G.W., Rolandone, F., and Khanbari, K., 2015, Magmatism on rift flanks: Insights from ambient noise phase velocity in Afar region: Geophysical Research Letters, v. 42, p. 2179-2188.

Kröner, A., 1985, Ophiolites and the evolution of tectonic boundaries in the late proterozoic Arabian—Nubian shield of northeast Africa and Arabia: Precambrian Research, v. 27, p. 277-300.

Kursten, M. O. C., 1975, Tectonic inventory of the Danakil Depression: in the Afar Depression of Ethiopia: Schweizerbart Stuttgart. p. 170-174.

Lahitte, P., Gillot, P. Y., and Courtillot, V., 2003, Silicic central volcanoes as precursors to rift propagation: the Afar case: Earth and Planetary Science Letters, v. 207, p. 103-116.

Laske, G., Masters, G., Ma, Z., and Pasyanos, M., 2013, Update on CRUST1. 0—A 1-degree global model of Earth's crust: in Geophys. Res. Abstr, v. 15, p. 2658: Vienna, Austria, EGU General Assembly.

Levitte, D., 1970, The Geology of Mekele (Report on the Geology of the central part of sheet ND 37-11): Geological Survey of Ethiopia, Addis Ababa.

Mackenzie, G. D., Thybo, H., and Maguire, P. K. H., 2005, Crustal velocity structure across the Main Ethiopian Rift: results from two-dimensional wide-angle seismic modelling: Geophysical Journal International, v. 162, p. 994-1006.

Makris, J., and Ginzburg, A., 1987, The Afar Depression: transition between continental rifting and sea-floor spreading: Tectonophysics, v. 141, p. 199-214.

Mammo, T., 2010, Delineation of sub-basalt sedimentary basins in hydrocarbon exploration in North Ethiopia: Marine and Petroleum Geology, v. 27, p. 895-908.

Mammo, T., 2013, Crustal structure of the flood basalt province of Ethiopia from constrained 3-D gravity inversion: Pure and Applied Geophysics, v. 170, p. 2185-2206.

Manighetti, I., Tapponnier, P., Courtillot, V., Gallet, Y., Jacques, E., and Gillot, P. Y., 2001, Strain transfer between disconnected, propagating rifts in Afar: Journal of Geophysical Research: Solid Earth, v. 106, p. 13613-13665.

Matmon, A., Bierman, P., and Enzel, Y., 2002, Pattern and tempo of great escarpment erosion: Geology, v. 30, p. 1135-1138.

McDougall, I., Morton, W. H., and Williams, M. A. J., 1975, Age and rates of denudation of Trap Series basalts at Blue Nile Gorge, Ethiopia: Nature, v. 254, p. 207.

Merla, G., Abbate, E., Azzaroli, A., Bruni, P., Fazzuoli, M., Sagri, M., and Tacconi, P., 1979, A geological map of Ethiopia and Somalia: Comment. Pergamon, Oxford, 95 pp.

Meyer, B., Chulliat, A., and Saltus, R., 2017, Derivation and error analysis of the earth magnetic anomaly grid at 2 arc min resolution version 3 (EMAG2v3): Geochemistry, Geophysics, Geosystems, v. 18, p. 4522-4537.

Miller, H. G., and Singh, V., 1994, Potential field tilt—a new concept for location of potential field sources: Journal of Applied Geophysics, v. 32, p. 213-217.

Mohr, P. A., 1972, Surface structure and plate tectonics of Afar: Tectonophysics, v. 15, p. 3-18.

Mohr, P., and Zanettin, B., 1988, The Ethiopian flood basalt province: in Continental flood basalts, p. 63-110. Springer, Dordrecht.

Mohr, P., 1974a, Mapping of the major structures of the African Rift System: Smithsonian Institution Astrophysical Observatory Special Report, 361, 70.

Mohr, P., 1974b, Structural elements of the Afar margins: Data from ERTS-1 imagery: Bulletin of the Geophysical Observatory, Haile Selassie I University, v. 15, p. 83–89.

Moucha, R., and Forte, A. M., 2011, Changes in African topography driven by mantle convection: Nature Geoscience, 4, p. 707.

Ndougsa-Mbarga, T., Feumoe, A. N. S., Manguelle-Dicoum, E., and Fairhead, J. D., 2012, Aeromagnetic data interpretation to locate buried faults in south-east Cameroon: Geophysica, v. 48, p. 49-63.

Nyblade, A. A., 2011, The upper-mantle low-velocity anomaly beneath Ethiopia, Kenya, and Tanzania: Constraints on the origin of the African superswell in eastern Africa and plate versus plume models of mantle dynamics: Geological Society of America Special Papers, v. 478, p. 37-50.

Nyblade, A. A., and Brazier, R. A., 2002, Precambrian lithospheric controls on the development of the East African rift system: Geology, v. 30, p. 755-758.

Osmundsen, P. T., and Redfield, T. F., 2011, Crustal taper and topography at passive continental margins: Terra Nova, v. 23, p. 349-361.

Pik, R., Deniel, C., Coulon, C., Yirgu, G., Hofmann, C., and Ayalew, D., 1998, The northwestern Ethiopian Plateau flood basalts: classification and spatial distribution of magma types: Journal of Volcanology and Geothermal Research, v. 81, p. 91-111.

Pik, R., Deniel, C., Coulon, C., Yirgu, G., and Marty, B., 1999, Isotopic and trace element signatures of Ethiopian flood basalts: evidence for plume–lithosphere interactions: Geochimica et Cosmochimica Acta, v. 63, p. 2263-2279.

Pik, R., Marty, B., Carignan, J., and Lavé, J., 2003, Stability of the Upper Nile drainage network (Ethiopia) deduced from (U–Th)/He thermochronometry: implications for uplift and erosion of the Afar plume dome: Earth and Planetary Science Letters, v. 215, p. 73-88.

Pik, R., Marty, B., Carignan, J., Yirgu, G., and Ayalew, T., 2008, Timing of East African Rift development in southern Ethiopia: Implication for mantle plume activity and evolution of topography: Geology, v. 36, p. 167-170.

Ring, U., 1994, The influence of preexisting structure on the evolution of the Cenozoic Malawi rift (East African rift system): Tectonics, v. 13, p. 313-326.

Rogers, N. W., 2006, Basaltic magmatism and the geodynamics of the East African Rift System: Geological Society, London, Special Publications, v. 259, p. 77-93.

Rogers, N., Macdonald, R., Fitton, J. G., George, R., Smith, M., and Barreiro, B., 2000, Two mantle plumes beneath the East African rift system: Sr, Nd and Pb isotope evidence from Kenya Rift basalts: Earth and Planetary Science Letters, v. 176, p. 387-400.

Rooney, T. O., Mohr, P., Dosso, L., and Hall, C., 2013, Geochemical evidence of mantle reservoir evolution during progressive rifting along the western Afar margin: Geochimica et Cosmochimica Acta, v. 102, p. 65-88.

Russo, A., Assefa, G., and Atnafu, B., 1994, Sedimentary evolution of the Abay River (Blue Nile) Basin, Ethiopia. With 4 figures in the text: Neues Jahrbuch Fur Geologie Und Palaontologie-Monatshefte, v. 5, p. 291-308.

Schilling, J. G., 1973, Afar mantle plume: rare earth evidence: Nature Physical Science, v. 242, p. 2-5.

Schwanghart, W., and Scherler, D., 2014, TopoToolbox 2–MATLAB-based software for topographic analysis and modeling in Earth surface sciences: Earth Surface Dynamics, v. 2, p. 1-7.

Seidl, M. A., Weissel, J. K., and Pratson, L. F., 1996, The kinematics and pattern of escarpment retreat across the rifted continental margin of SE Australia: Basin Research, v. 8, p. 301-316.

Sembroni, A., Faccenna, C., Becker, T. W., Molin, P., and Abebe, B., 2016a, Long-term, deep-mantle support of the Ethiopia-Yemen Plateau: Tectonics, v. 35, p. 469-488.

Sembroni, A., Molin, P., Pazzaglia, F. J., Faccenna, C., and Abebe, B., 2016, Evolution of continental-scale drainage in response to mantle dynamics and surface processes: An example from the Ethiopian Highlands: Geomorphology, v. 261, p. 12-29.

Şengör, A.M.C., 2001, Elevation as indicator of mantle-plume activity, in Ernst, R.E., and Buchan, K.L., eds., Mantle Plumes: Their identification through time: Geological Society of America Special Paper 352, p. 183–225.

Shackleton, R. M., 1986, Precambrian collision tectonics in Africa: Geological Society, London, Special Publications, v. 19, p. 329-349.

Smets, B., Delvaux, D., Ross, K. A., Poppe, S., Kervyn, M., d'Oreye, N., and Kervyn, F., 2016, The role of inherited crustal structures and magmatism in the development of rift segments: Insights from the Kivu basin, western branch of the East African Rift: Tectonophysics, v. 683, p. 62-76.

Stab, M., Bellahsen, N., Pik, R., Quidelleur, X., Ayalew, D., and Leroy, S., 2016, Modes of rifting in magma-rich settings: Tectono-magmatic evolution of Central Afar: Tectonics, v. 35, p. 2-38.

Stern, R. J., 1994, Arc assembly and continental collision in the Neoproterozoic East African Orogen: implications for the consolidation of Gondwanaland: Annual Review of Earth and Planetary Sciences, v. 22, p. 319-351.

Tadesse, T., 1996, Structure across a possible intra-oceanic suture zone in the low-grade Pan-African rocks of northern Ethiopia: Journal of African Earth Sciences, v. 23, p. 375-381.

Tagil, S., and Jenness, J., 2008, GIS-based automated landform classification and topographic, landcover and geologic attributes of landforms around the Yazoren Polje, Turkey: Journal of Applied Sciences, v. 8, p. 910-921.

Tefera, M., Chernet, T., Haro, W., 1996, Explanation of the Geological Map of Ethiopia: The Federal Democratic Republic of Ethiopia, Ministry of Mines and Energy, Bulletin 3, 79p.

Telbisz, T., Kovács, G., Székely, B., and Szabó, J., 2013, Topographic swath profile analysis: a generalization and sensitivity evaluation of a digital terrain analysis tool: Zeitschrift für Geomorphologie, v. 57, p. 485-513.

Tesfaye, S., Harding, D. J., and Kusky, T. M., 2003, Early continental breakup boundary and migration of the Afar triple junction, Ethiopia: GSA Bulletin, v. 115, p. 1053-1067.

Tiberi, C., Ebinger, C., Ballu, V., Stuart, G., and Oluma, B., 2005, Inverse models of gravity data from the Red Sea-Aden-East African rifts triple junction zone: Geophysical Journal International, v. 163, p. 775-787.

Tucker, G. E., and Slingerland, R. L., 1994, Erosional dynamics, flexural isostasy, and long-lived escarpments: A numerical modeling study: Journal of Geophysical Research: Solid Earth, v. 99, p. 12229-12243.

Ukstins, I. A., Renne, P. R., Wolfenden, E., Baker, J., Ayalew, D., and Menzies, M., 2002, Matching conjugate volcanic rifted margins: 40Ar/39Ar chrono-stratigraphy of pre-and syn-rift bimodal flood volcanism in Ethiopia and Yemen: Earth and Planetary Science Letters, v. 198, p. 289-306.

Vail, J. R., 1985, Pan-African (late Precambrian) tectonic terrains and the reconstruction of the Arabian-Nubian Shield: Geology, v. 13, p. 839-842.

van der Beek, P., Andriessen, P., and Cloetingh, S., 1995, Morphotectonic evolution of rifted continental margins: Inferences from a coupled tectonic-surface processes model and fission track thermochronology: Tectonics, v. 14, p. 406-421.

Varet, J., 2018, Southern Afar: The Main Ethiopian Rift (MER) Northern Extremity: in Geology of Afar (East Africa), p. 253-281. Springer, Cham.

Weissel, J. K., and Karner, G. D., 1989, Flexural uplift of rift flanks due to mechanical unloading of the lithosphere during extension: Journal of Geophysical Research: Solid Earth, v. 94, p. 13919-13950.

Weissel, J. K., Malinverno, A., Harding, D. J., and Karner, G. D., 1995, Erosional development of the Ethiopian Plateau of northeast Africa from a fractal analysis of topography: in Fractals in petroleum geology and earth processes, p. 127-142. Springer, Boston, MA.

Whipple, K. X., 2004, Bedrock rivers and the geomorphology of active orogens: Annu. Rev. Earth Planet. Sci., v. 32, p. 151-185.

Whipple, K. X., and Tucker, G. E., 1999, Dynamics of the stream-power river incision model: Implications for height limits of mountain ranges, landscape response timescales, and research needs: Journal of Geophysical Research: Solid Earth, v. 104, p. 17661-17674.

Wobus, C., Whipple, K.X., Kirby, E., Snyder, N., Johnson, J., Spyropolou, K., Crosby, B., Sheehan, D. and Willett, S.D., 2006, Tectonics from topography: Procedures, promise, and pitfalls: Special papers-geological society of America, v. 398, p. 1-55.

Woldegabriel, G., Aronson, J. L., and Walter, R. C., 1990, Geology, geochronology, and rift basin development in the central sector of the Main Ethiopia Rift: Geological Society of America Bulletin, v. 102, p. 439-458.

WoldeGabriel, G., Heiken, G., White, T. D., Asfaw, B., Hart, W. K., and Renne, P. R., 2000, Volcanism, tectonism, sedimentation, and the paleoanthropological record in the Ethiopian Rift System: Special papers-geological society of America, p. 83-99.

Wolela, A., 2007, Source rock potential of the Blue Nile (Abay) basin, Ethiopia: Journal of Petroleum Geology, v. 30, p. 389-402.

Wolfenden, E., Ebinger, C., Yirgu, G., Deino, A., and Ayalew, D., 2004, Evolution of the northern Main Ethiopian rift: birth of a triple junction: Earth and Planetary Science Letters, v. 224, p. 213-228.

Wolfenden, E., Ebinger, C., Yirgu, G., Renne, P. R., and Kelley, S. P., 2005, Evolution of a volcanic rifted margin: Southern Red Sea, Ethiopia: Geological Society of America Bulletin, v. 117, p. 846-864.

Xue, L., Alemu, T., Gani, N. D., and Abdelsalam, M. G., 2018, Spatial and temporal variation of tectonic uplift in the southeastern Ethiopian Plateau from morphotectonic analysis: Geomorphology, v. 309, p. 98-111.

Zanettin, B., and Justin-Visentin, E., 1975), Tectonical and volcanological evolution of the western Afar margin (Ethiopia): E. Schweizerb. Verlag., p. 300-309.

Zanettin, B., Justin-Visentin, E., and Piccirillo, E. M., 1978, Volcanic succession, tectonics and magmatology in central Ethiopia: Soc. cooper. tipogr..

CHAPTER IV

STRATIGRAPHIC CONTROLS ON THE MORPHO-TECTONIC EVOLUTION OF THE GORGE OF THE NILE, ETHIOPIA

4.1. ABSTRACT

We present new results of remote sensing and field studies aimed at understanding the evolution of the SW-flowing segment of the Gorge of the Nile in the NW Ethiopian Plateau and possible stratigraphic controls on its incision history. This ~1500 m deep canyon was carved on the NW Plateau by the Blue Nile River. The gorge exposes a ~1100 m thick Mesozoic sedimentary section overlain by ~400 m thick Cenozoic flood basalt. Previous studies have shown that the Blue Nile incision started ~30 Ma with significant increase in the incision rate at ~10 and ~6 Ma, possibly due to pulsed plateau uplift associated with the dynamics of the Afar mantle plume. We constructed a geologic cross-section using data from field observations, Digital Elevation Models (DEMs) extracted from the 30 m Shuttle Radar Topography Mission (SRTM), Landsat TM multi-spectral data and previously published stratigraphic documents. Subsequently, we measured the valley width and valley symmetry as a function of depth at 20 m intervals. Finally, we calculated the normalized valley width, and the amount of incision through time by converting the rate of incision into incision depth at 1 Ma interval starting at 30 Ma.

Our results show that the Blue Nile River, during its incision history to form the Gorge of the Nile: (1) maintained a uniform increase in width, except when it was incising through the upper part

of flood basalts and the lowermost part of Mesozoic sedimentary section (through a shale and sandstone units). Generally, the river widened by ~30 m per 1 m depth with the exceptions of an increase in the upper part of the flood basalt to 50 m per 1 m depth and the shale and sandstone unit to 70 m per 1 m depth. Conversely, the width decreased to 10 m per 1 m depth in sandstone unit; (2) maintained a NW asymmetrical valley throughout its incision history until it reached the sandstone unit where the river's valley became either symmetrical or slightly asymmetrical to the NW or SE. The NW asymmetry might be due to the pre-rift doming of the Ethiopian Plateau, and later rift-flank uplift. (3) incised for ~700 m through the flood basalt and the upper part of the Mesozoic sedimentary section between 30 and 10 Ma (slow incision rate), incised for an additional ~200 m through middle part of the Mesozoic sedimentary section between 10 and 6 Ma (moderate incision), and incised for ~600 m through lower part of the Mesozoic sedimentary section between 6 Ma and present (high incision rate).

4.2. INTRODUCTION

Increase in erosion activities of bedrock rivers is directly related to increase in their gradient due to tectonic uplift, increase in discharge driven by higher precipitation, or a combination of the two factors (e.g. Tucker and Slingerland, 1997). In turn, the increase of sediment flux driven by increase of precipitation is influenced by the erodibility of the lithology forming the bedrock (e.g. Sklar and Dietrich, 2001). Additionally, local structures play an important role in enhancing bedrock rivers incision (e.g. Cunha et al., 2005). Hence, understanding the geomorphological evolution of major bedrock rivers requires the understanding of the relative roles of tectonic uplift, climate change, bedrock lithology, and local structures in shaping the geometry of the river's valley. In this work, we focus in examining the role of bedrock lithology in controlling river incision using the spectacular southwest (henceforth referred to as SW)-flowing segment of the Blue Nile River at

the Gorge of the Nile in the northwestern (henceforth referred to as NW) Ethiopian Plateau as a site (Fig. 4.1A and B). Specifically, we use the Dejen-Gohatsion section, which is the most accessible segment of the Gorge of the Nile, to explore the combined influence of bedrock lithology and tectonic uplift in shaping the valleys of bedrock rivers.

The geomorphology of Ethiopia can be divided into the NW Plateau and the southeast (henceforth referred to as SE) Plateau separated by the Afar Depression in the northeast (henceforth referred to as NE) and the Main Ethiopian Rift to the SW (Fig. 4.1B). The NW Plateau is highly incised by the Tekeze River at its northern part, by the Blue Nile River at its central part, and the Omo River at its southern part (Fig. 4.1B). Dominating the central part of the NW Plateau through a ~200 degrees semi-circular loop of drainage, the Blue Nile River emerges from Lake Tana as a SE-flowing river, then turns South (henceforth referred to as S) and SW before turning NW to reach the lowlands of Sudan. The SW-flowing segment of the river is an ideal site for examining the influence of lithology and tectonic uplift on the incision history of bedrock rivers. This is because in this segment the river has incised for ~1500 m into the NW Plateau exposing over 250 millions of years (henceforth referred to as Ma) of geological history including Cenozoic flood basalt underlain by Mesozoic sedimentary rocks (Figs. 4.2 and 4.3). Here, the river has incised through a variety of lithological units with different rock strength. It is also where pulsed plateau uplift (possibly due to the uprising Afar mantle plume) and rift-flank uplift (related to the opening of the Afar Depression and the Main Ethiopian Rift) are shown to have influenced the incision history of the Blue Nile (Gani et al., 2007; Ismail and Abdelsalam, 2012).

In this study, we conducted field mapping of stratigraphic contacts and orientations of extensional structures, analysis of Digital Elevation Model (DEM) extracted from Shuttle Radar Topography Mission (SRTM) data, and analysis of Landsat Thematic Mapper (TM) data. We also used geological data from previous studies and information from the geological map of Debre Markos sheet compiled by the geological survey of Ethiopia (Mohr, 1963; Assefa, 1981; Russo et al., 1994;

Gani et al., 2009; Chumburo et al., 2009). We first establish the stratigraphic framework of the study area. Subsequently, we used these data to calculate the valley width, normalized valley width, and valley asymmetry. Additionally, we used the accelerated, three-phase incision curve of Gani et al. (2007) (started at ~30 Ma with increase in rate at ~10 and ~6 Ma) to calculate the amount of incision of the Blue Nile River into the NW Plateau as a function of time and stratigraphy. The main objective of this work is to quantitatively (using geomorphic parameters) examine the evolution of the SW-flowing segment of the Gorge of the Nile in the NW Plateau and possible stratigraphic controls on its incision history. We subsequently discuss our results within the framework of the tectonic uplift history of the NW Plateau and neighboring rift margins.

4.3. GEODYNAMIC EVOLUTION AND STRATIGRAPHY

4.3.1. THE BLUE NILE AND THE GORGE OF THE NILE

The Blue Nile River (also locally called Abay River) is one of the major tributaries of the River Nile (Fig. 4.1A). The river originates as a series of small springs called the Springs of Sakala and flows North (henceforth referred to as N) into the largest lake in Ethiopia, Lake Tana (Fig. 4.1B). Along its 900 km journey within Ethiopia, the river drains through the NW Plateau before arriving at the lowlands of Sudan. The NW Plateau is bounded in the East (henceforth referred to as E) by the western escarpment of the Afar Depression, in the SE by the northwestern escarpment of the Main Ethiopian Rift, and in the West (henceforth referred to as W) by the Tana erosional escarpment (Fig. 4.1B). The NW Plateau is covered with thick successions of Oligocene flood basalt with an average elevation of 2.5 km above sea level (asl) (Hofmann et al., 1997). The plateau is also characterized by the presence of many Miocene shield volcanoes such as Mount Gish, Choke, Guna and Guguftu (Fig. 4.1B). Some of these shield volcanoes reach elevations of up to 4 km asl., and have influenced the incision of the bedrock rivers into the NW Plateau (Gani and Abdelsalam, 2006; Ismail and Abdelsalam, 2012). The Blue Nile River forms a ~200 degrees semi-circular bend as it flows around the Choke shield volcano creating the Gorge of the Nile also known

as the Grand Canyon of Africa at the SW segment of the river (Fig. 4.1B). Buried beneath the Oligocene flood basalt is a thick section of Paleozoic - Mesozoic sedimentary rock which rests unconformably above Precambrian crystalline rock (Jespen and Athearn, 1961; Mohr, 1963; Assefa, 1981; 1991; Russo et al., 1994; Gani et al., 2009; Dawit, 2010). The regional geological map draped onto SRTM DEM is shown in Figure 4.2.

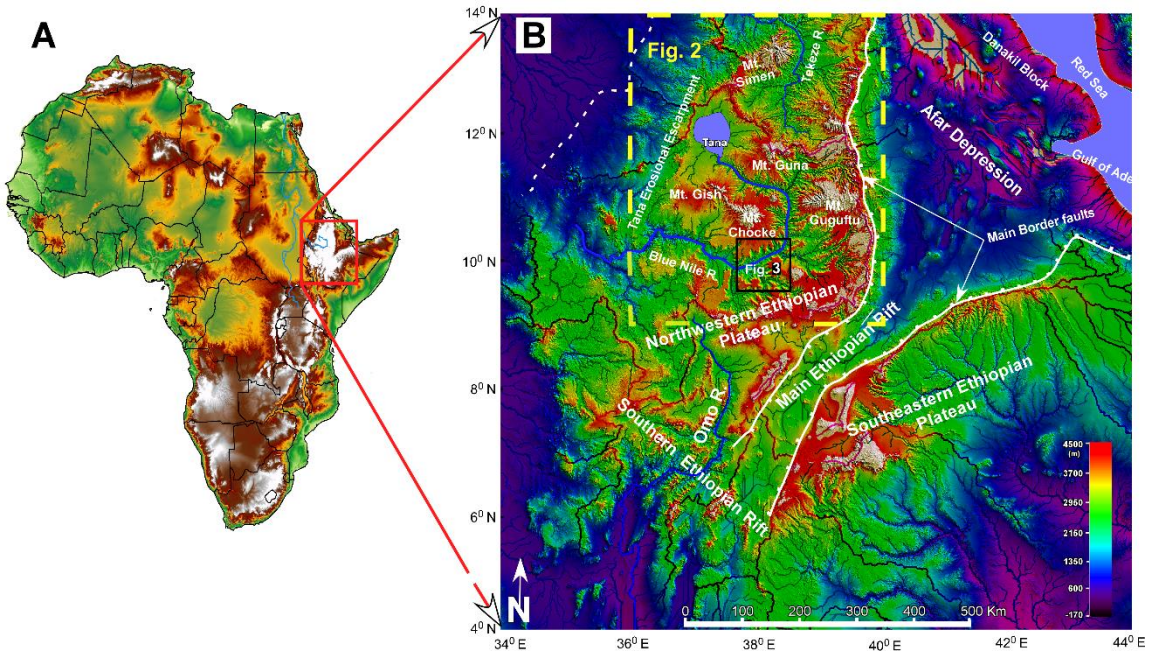

Figure 4.1: (A) Location of the Gorge of the Nile in Africa. The Gorge is located in the NW Plateau within the Blue Nile Basin. (B) Location of the study area within the SW-flowing segment of the Blue Nile. The Blue Nile River flows form Lake Tana southward over flood basalt and makes a semi-circular loop along the Chocke Mountain incising deeper into the sedimentary section and flows SW through the study area, where 1.5 km section is exposed.

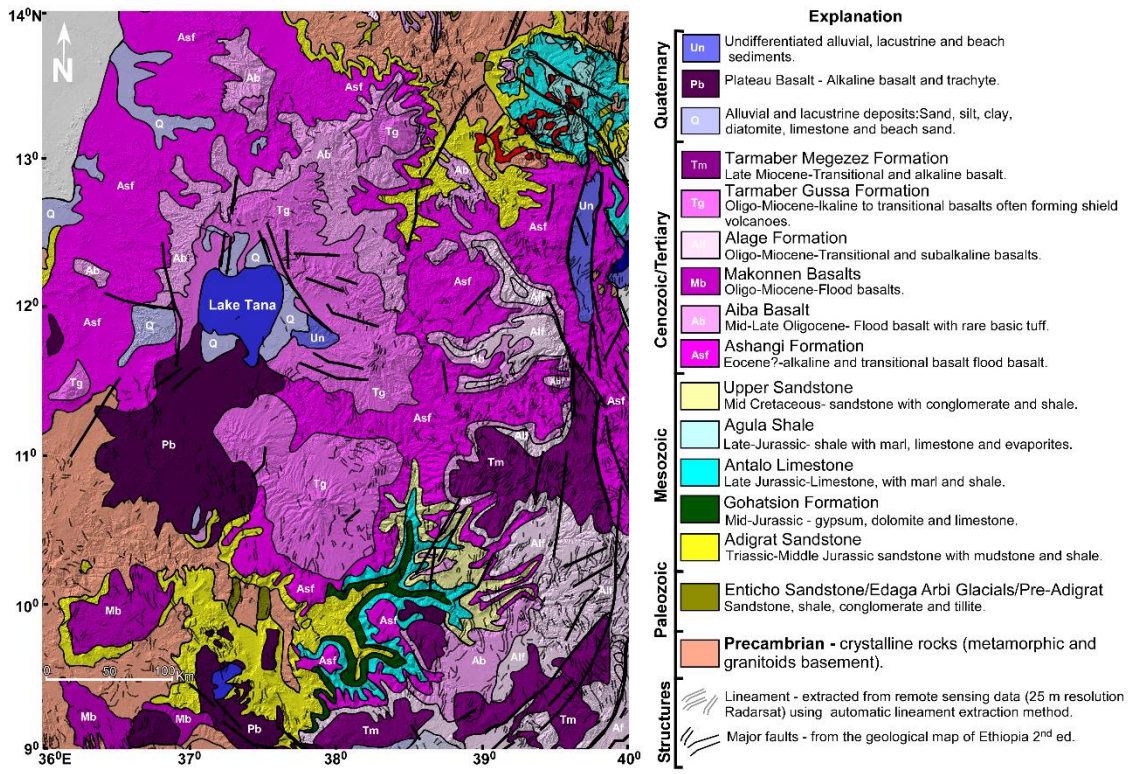

Figure 4.2: Geological map of the Northwestern Ethiopian Plateau modified from Tefera et al. (1996) draped over hill-shade Digital Elevation Model (DEM).

4.3.2. STRATIGRAPHY OF THE GORGE OF THE NILE

One of the places where an almost complete stratigraphic record of the Blue Nile sedimentary basin is exposed is the Gorge of the Nile (between the towns of Dejen and Gohatsion) at the SW-flowing segment of the Blue Nile River (Figs. 4.3). From bottom to top, the stratigraphy of the Gorge of the Nile overlying the Precambrian crystalline basement, can be summarized into five lithostratigraphic units including pre-Adigrat, Adigrat Sandstone, Gohatsion Formation, Antalo Limestone, and Oligocene flood basalt (Fig. 4.4).

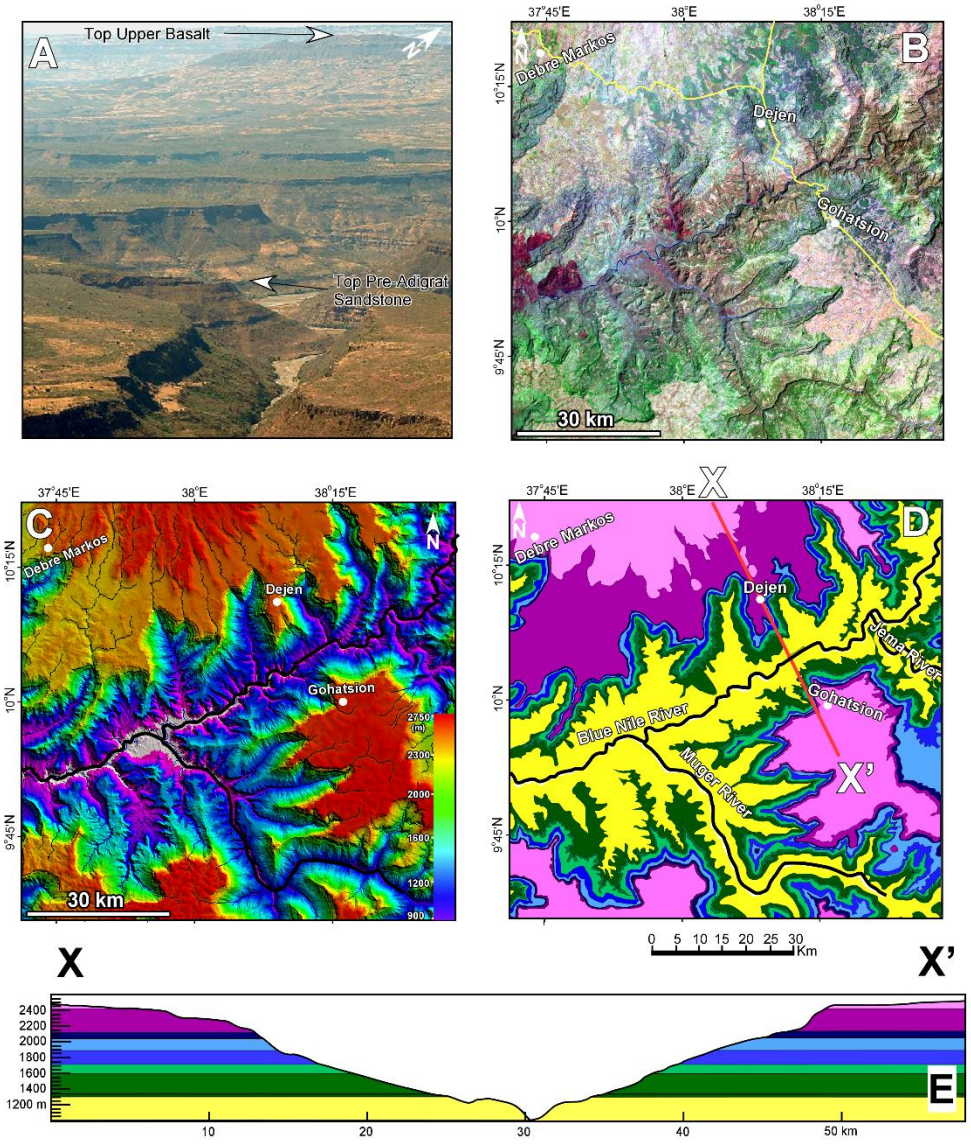

Figure 4.3: (A) Wide-angle field photograph (not to scale) of the SW-flowing segment of the Gorge of the Nile. The photo shows layer-cake stratigraphy of the Gorge where the pre-Adigrat Sandstone forms the base just above the river and the Upper Basalt forming the top surface. (B) 7-4-2 Landsat Thematic Mapper (TM) image of the study area. (C) Color-coded hill-shade Digital Elevation Model (DEM) of the study area extracted from the 30m spatial resolution Shuttle Radar Topography Mission (SRTM) data. (D) Geological map of the study area. Lithological units are as in the stratigraphic column in Figure 4.4. (E) Geological cross-section along baseline X-X' shown in Figure 4.3D. Vertical Exaggeration = 5.

The pre-Adigrat is possibly equivalent to Karoo sedimentary rocks indicating a latest Carboniferous to Permian age (Dawit, 2010). It is only locally exposed in the SW-flowing segment. It is predominantly composed of medium to fine grained sandstone deposited in an alluvial plains and/or lacustrine-deltaic environment (Dawit, 2010).

The Adigrat Sandstone is predominantly cross-bedded sandstone with occasional mudstone units deposited in environments ranging from continental to shallow marine setting, possibly during the Triassic to middle Jurassic (Russo et al., 1994; Wolela, 2008; Dawit and Bussert, 2009). It has a thickness of ~315 m in the SW-flowing segment of the Blue Nile River (Fig. 4.4).

The Gohatsion Formation is Jurassic in age and contains cyclic repetition of facies successions dominated by gypsum, shale, dolomite and sandstone containing hummocky cross stratification. This formation is possibly deposited in peritidal environment with associated lagoonal and pond water bodies (Assefa, 1981; Russo et al., 1994). In the study area, the Gohatsion Formation can be divided into Lower unit (~30 m thick dominated by greyish-greenish glauconitic shaley mudstone and sandstone), Middle unit (~260 m thick dominated by gypsum, dolostone, marl and shale) and Upper unit (~110 m thick dominated by variegated shale and mudstone).

Overlying the Gohatsion Formation is the Middle-Late Jurassic Antalo Limestone, a predominantly limestone and marly unit deposited in shallow marine environment (Russo et al., 1994; Atnafu, 2003). It can also be divided into Lower, Middle and Upper units composed of thinly bedded micritic limestone interbedded with shale with ~180 m thickness, marl and thinly bedded micritic limestone reaching a thickness of ~140 m and a cliff forming micritic limestone with interbedded grainstone thickness of ~60 m, respectively (Fig. 4.4).

The flood basalts at the SW-flowing segment, formally named the Ashangi Basalt (Zanettin et al., 1980), can be subdivided into an Upper and a Lower unit. The Upper and Lower Basalts are separated by an intertrappean thin and discontinuous sedimentary unit locally containing lignite;

but this unit also has an extensive occurrence throughout the NW Plateau (Abbate et al., 2014). The most characteristic feature of the Lower Basalt is the presence of meter-scale hexagonal columnar joints forming ~300 m thick basaltic section (Fig. 4.4). This is followed by the Upper Basalt with similar hexagonal columnar joints. It's flat top forms the top of the NW Plateau and is covered with residual soil (Fig. 4.3C). Almost all the ages obtained from different section of the flood basalt in the NW Plateau cluster around ~30 Ma (Hofmann et al., 1997; Rochette et al., 1998; Ayalew et al., 2002; Coulié et al., 2003). In addition, this basaltic unit is also mapped as the Oligocene Lumame basalt in the recent geological map of the Debre Markos Sheet, despite being reported as the Eocene Ashangi Formation (e.g. Zanettin et al., 1980) and on the geological map of Ethiopia (Fig. 4.2; Tefera et al., 1996). One important note pertaining to the volcanic history of the NW Plateau is that the studies indicating ages older than ~30 Ma are mostly from southern Ethiopia (Davidson and Rex, 1980; Ebinger et al., 1993; George et al., 1998). In the NW Plateau, geochronological data indicate a spatially widespread and fastly erupted volcanic episode considered to have been caused by the Afar mantle plume, which also resulted in a domal uplift of both the NW and SE plateaus (Ebinger and Sleep, 1998; Şengör, 2001; Pik et al., 2003; Rogers, 2006).

4.3.3. GEODYNAMIC EVOLUTION OF THE BLUE NILE SEDIMENTARY BASIN

Beneath the extensive volcanic pile, though predominantly exposed along the Blue Nile River and its tributaries, there lies a 1-2 km thick Mesozoic-Paleozoic sedimentary basin referred to as the Blue Nile sedimentary basin. Below, we summarize the geodynamic evolution of the basin based on two comprehensive stratigraphic and structural studies (Russo et al., 1994 and Gani et al., 2009).

Russo et al. (1994) introduced a five-stage geodynamic evolution of the Blue Nile sedimentary basin: (1) Peneplanation stage that resulted in the denudation of the Precambrian crystalline basement. Sedimentological and geomorphic (Coltorti et al., 2007; Bussert, 2010; Abbate et al.,

2015) and thermochronologic studies (Mock et al., 1999) have shown long term denudation and tectonic quiescence following the Neoproterozoic Pan-African orogenic event. It is also arguably marked by the deposition of Paleozoic clastic sedimentary rocks on top of a slowly subsiding Neoproterozoic crystalline basement, similar to the sag phase of the neighboring Mekele Sedimentary Basin (Alemu et al., 2018). (2) Intracontinental rift stage associated with the Late Paleozoic to middle Mesozoic fragmentation of Gondwana that resulted in the development of Karoo rifts and NW-trending interior rifts including the Blue Nile Basin. (3) Post-rift stage marked by the deposition of the Triassic-Jurassic basal clastic unit of the Adigrat Sandstone that overlies the Karoo rifts. (4) Early flooding, coeval rifting and subsidence followed by limited transgression and deposition of the Jurassic Gohatsion Formation. (5) Drowning stage with major transgression-regression event and deposition of the Late Jurassic-Cretaceous Antalo Limestone, Mugher Mudstone and Debre Libanos Sandstone.

Gani et al. (2009) introduced a three-stage evolutionary model for the formation of the Blue Nile sedimentary basin: (1) Pre-sedimentation phase, which resulted in the peneplanation of the Precambrian crystalline basement during the Paleozoic (corresponds to stage 1 of Russo et al. (1994)). (2) Sedimentation phase that resulted in the deposition of the bulk of the sedimentary section from Triassic to Middle Cretaceous (corresponds to stages from 2 to 5 of Russo et al. (1994)). (3) Post-sedimentation phase represented by extensive volcanism, uplift, denudation and intertrappean sedimentation from Oligocene to present time.

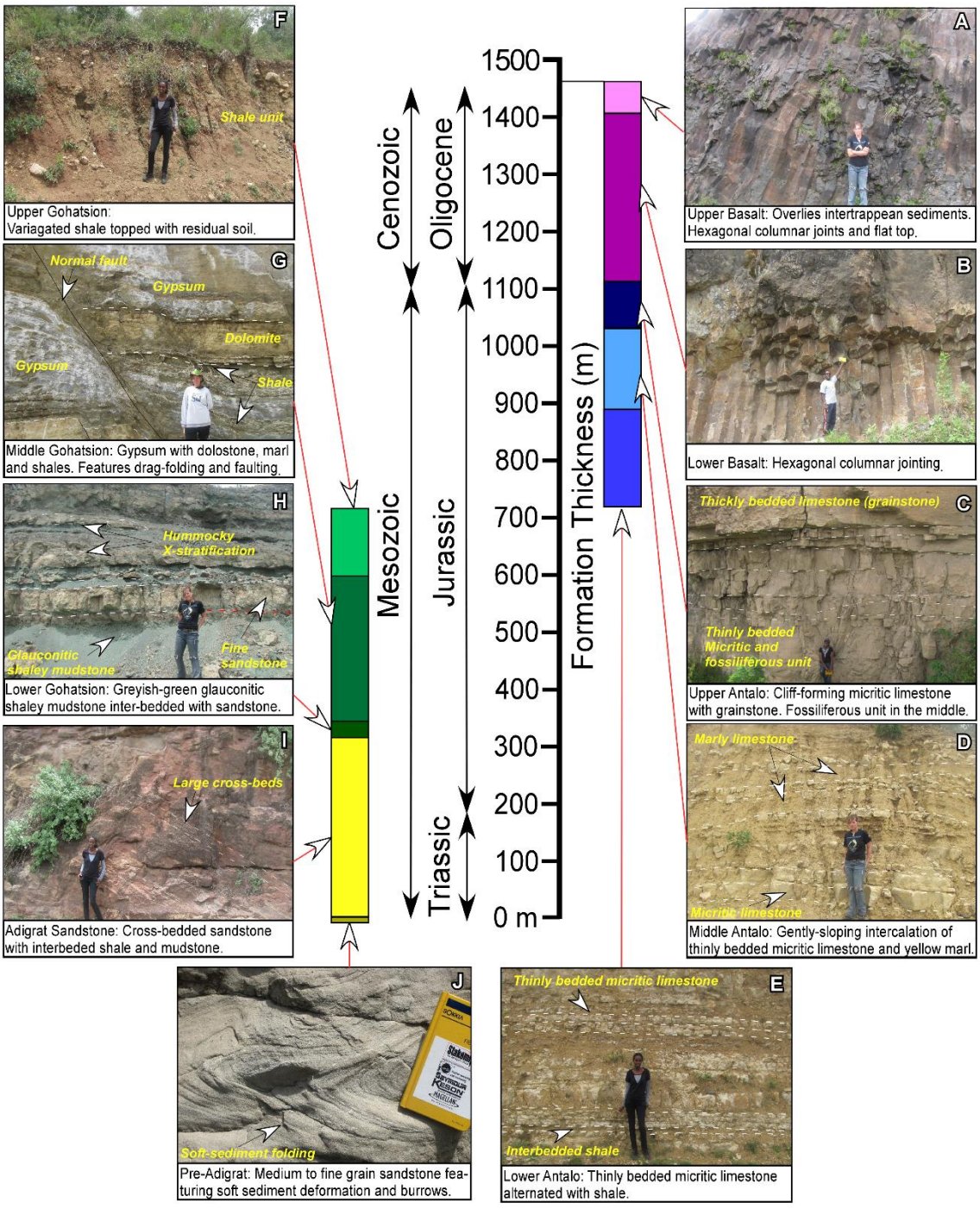

Figure 4.4: Stratigraphic column of the SW-flowing segment of the Blue Nile and the Gorge of the Nile established from field studies and information published in Gani et al. (2009). Photograph taken looking approximately south-southwest in A, B, C and D; East-northeast in E, South-southeast in F, G, H; East in I, and North in J. Person for scale.

4.4. GEOMORPHOLOGICAL EVOLUTION OF THE GORGE OF THE NILE

Studies of the incision of the Blue Nile River on the NW Plateau assume that the present-day drainage started developing following the Oligocene flood basalt, which erupted at ~30 Ma (Pik et al., 2003; Gani et al., 2007; Ismail and Abdelsalam, 2012; Sembroni et al., 2016 a and b). This is because the extrusion of the flood basalts must have buried any earlier drainage system. It is estimated that since ~30 Ma the Blue Nile drainage network has removed ~93,200 km3 of geological material from the NW Plateau (Gani et al., 2007). The geomorphologic setting is dominated by a series of deep gorges carved into the layer-cake stratigraphy of the NW Plateau (Fig. 4.3A). These steep gorges have formed as a result of multiple streams/tributaries flowing into the Blue Nile River that mostly originate in the surrounding elevated shield volcanoes (Fig. 4.2). In its SW-flowing segment the river has incised down close to the Precambrian crystalline basement exposing ~1.5 km of Paleozoic–Mesozoic sedimentary and Cenozoic volcanic rocks (Fig. 4.3).

Pik et al. (2003) provided the first combined (U-Th)/He thermochronologic and geomorphologic data from the NW Plateau, and advocated that the hydrological patterns of the plateau should have been acquired during the Oligocene, following immediately the extrusion of the flood basalt. Accordingly, Pik et al. (2003) proposed a steady-state incision model that assumes a steady, long-term plateau buildup and incision since ~25-29 Ma ago.

Using age of volcanoes and SRTM DEM data, Gani et al. (2007) proposed an accelerated three phase incision model for the NW Plateau. This is in contrast to the steady-state incision model of Pik et al. (2003) though both studies assume channel incision into the plateau to have started during early Oligocene and characterized by a slow early incision history. However, Gani et al. (2007) argues that the slow incision, which they considered to represent Phase I (30 Ma to 10 Ma) was followed by accelerated incision rates representing Phase II (10 Ma to 6 Ma) and Phase III (6 Ma to Present). Regional and local tectono-magmatic processes associated with the dynamics of the

Afar mantle plume are considered responsible for a pronounced and episodic plateau growth that may have resulted in the latest increase in incision of the Blue Nile River into the plateau.

Based off of morpho-tectonic study of the Tekeze and Blue Nile Basin, Ismail and Abdelsalam (2012) identified three major tectonic and volcanic episodes as being of a higher order control on river incision in the NW Plateau. The first major episode of regional uplift that commenced early in the Cenozoic possibly due to impingement of the Afar mantle plume beneath the lithosphere, has been considered as responsible for the formation of the longer wavelength, partially preserved dome-shaped topographic feature of the Ethiopian Plateau. Second, and probably with localized geomorphic effect, are the eruption of basaltic shield volcanoes such as Mount Choke and Guguftu around 22 Ma (Kieffer et al., 2004). The third and most recent episode involves accelerated plateau growth and river incision due to major rift flank uplift associated with the Afar Depresion and the Main Ethiopian Rift. The second and third episodes appear to coincide with eruptions of shield volcanoes such as the 10 Ma Mount Guna (Kieffer et al., 2004), and opening of the Afar Depression and Main Ethiopian Rift at ~11 Ma as suggested by Wolfenden et al. (2004) or at 6–5 Ma as suggested by Bonini et al. (2005). The uplift associated with the last episode is much more pronounced in areas close to the rift margin and decreases westward and northward from the Afar Depression and the Main Ethiopian Rift, respectively (Fig. 4.1B).

Dynamically supported plateau has been suggested for the NW Plateau based on the analysis of topographic and morpho-tectonic study (Sembroni et al., 2016a). This work implies long-term sustenance of the topography of the NW Plateau. Moreover, Sembroni et al. (2016b) proposed flexural uplift mechanism along both the flanks of the Afar Depression and the Main Ethiopian Rift as well as the Tana escarpment (Fig. 4.1B).

In summary, the geomorphologic setting of the NW Plateau provides a natural laboratory by which multiple geologic events, events with various spatial and temporal influence resulted in a landscape

sculpted by one of the biggest rivers in the world. In general, for areas at a distance from the margins of the Afar Depression and the Main Ethiopian Rift and shield volcanoes i.e. at the lower reaches of the Blue Nile River and Tekeze River, the steady-state model and the long-lived established hydrological stability of the drainage system is assumed to hold. Because these areas are more than 200 km away from the rifts flank, the flexural influence is assumed to be at a minimum, despite the reported occurrence of none-lithologic base level falls in the lower reaches of the Blue Nile Basin (Sembroni et al., 2016b).

4.5. METHODS

We conducted a detailed field measurement along the Dejen-Gohatsion transect (Fig. 4.3). The 30 m spatial resolution SRTM DEM and Landsat TM multi-spectral data combined with previously published stratigraphic data (e.g. Russo et al., 1994; Gani and Abdelsalam, 2006; Chumburo et al., 2009) was used to construct the geological map, cross-section and stratigraphic column (Figs. 4.3 and 4). We informally subdivided some of the stratigraphic units into upper, middle and lower units solely based on lithologic and morphologic appearance.

The cross-section was selected in this location and with this orientation (NNW-SSE) because, along this transect, the shape of this part of the valley has not been modified by any tributary draining into it. However, the influence of mass movement on valley parameters was only qualitatively assessed, and could therefore present a limitation. To minimize the uncertainty, we constructed the cross-section along the segment of the valley with a relatively low to moderate potential for susceptibility to landslide. We have also considered the possible influence of tectonic heterogeneity, especially the nature and orientation of major fractures (Fig. 4.5). The cross-section is shown to pass over areas with fewer tectonic heterogeneities. One other limitation of this study concerns the use of a single cross-section due to the fact that other part of the study area is

inaccessible to the type of detailed measurements we conducted. The nearest road crossing the Gorge of the Nile is tens of kilometers up and down stream of the river, and none in this particular segment of the Blue Nile River. This limitation is partly compensated by the simple layer-cake stratigraphic nature of the study area, which allows broad generalizations, at least for the SW-flowing segment. Thus, our approach is generally a lithostratigraphic one with little emphasis on small scale intra-formation variability within each formal and informal formations (Fig. 4.4).

One reasonable assumption we could make, an assumption based on multiple studies (e.g. Stock and Montgomery, 1999; Sklar and Dietrich, 2001; Forte et al., 2016), is that the stratigraphy plays significant role in shaping valley geometry. We then evaluated geomorphic anomalies with respect to assumed lithostratigraphic unit response. Subsequently, we used the cross-section to measure the valley width, calculate valley normalized width, and valley symmetry as a function of depth and in relation to different stratigraphic units. The Blue Nile incision rate curve constructed by Gani et al. (2007) was used to calculate the amount of incision through time. We have adopted this particular work because the proposed three stage accelerated uplift scenario appears to have been supported by geological and geochronological data. These includes geochronological data from southern Ethiopia, which suggests that exhumation of the Precambrian crystalline rocks and rifting occurred at ~12 and 8 Ma, respectively (Balestrieri et al., 2016). Moreover, Balestrieri et al. (2016) proposed using the same geochronological data that extension in the Main Ethiopian Rift is coeval and occurred at ~11 Ma. This is in agreement with the suggestion of Ismail and Abdelsalam (2012) that rift-flank uplift related to the Afar Depression and the Main Ethiopian Rift has modified the older uplift which occurred as a result of the rise of the Afar mantle plume. In addition, though still debatable, estimates of the age of appearance of the Ethiopian soil in Egypt are generally within the Pleistocene epoch (e.g. Issawi and McCauley, 1992; Talbot and Williams, 2009; Macgregor, 2012), suggesting a higher rate of influx of sediment from the NW Plateau, and hence rapid incision.

Table 4.1 (See Appendices) shows the valley width of the Blue Nile valley measured at 20 m depth interval. Using the same 20 m depth interval, we calculated the normalized valley width by subtracting the valley width in the specific depth interval from the valley width in the depth interval immediately above it (Fig. 4.6). Regardless of their amount, similar normalized valley width values indicate that the valley is approaching a perfect V-shape geometry. Higher normalized valley width values indicate that the valley has a wide V-shape geometry whereas lower values indicate narrow V-shape geometry. We calculated the asymmetry at 20 m depth interval by dividing the distance between the axis of the Blue Nile valley and the NW flank of the Gorge of the Nile by the distance between the axis of the Blue Nile valley and the SE flank of the Gorge of the Nile (Fig. 4.6 and Table 4.1). A value of 1 indicates perfect symmetry of the valley; a value less than 1 indicates SE asymmetry and a value greater than 1 indicates NW asymmetry.

We calculated the amount of incision through time of the Blue Nile River in the NW Plateau by converting the rate of incision of Gani et al. (2007) into incision depth at 1 Ma interval starting at 30 Ma (Table 4.2: See Appendices). The curve shows that the incision rate at 30 Ma is 55.42 m/Ma and it is 316.32 m/Ma at 1 Ma. In 30 Ma, this increase in the incision rate produces a total amount of incision of 3070.03 m. One other way of finding the total incision is by just calculating the integral of the curve, which also gave us a similar result. However, the total amount of incision of the SW-flowing segment of the Blue Nile is only ~1500 m. Hence, we adjusted the 1 Ma incremental amount of incision by using a ratio of ~0.49 (dividing 1500 m by 3070.03 m) (Table 4.2).

We also conducted lineament mapping using both field measurement and remote sensing data. We collected strike and dip of joints and fractures from five formations, namely the upper basalt, upper Antalo, middle Antalo, Gohatsion Formation (most of the measurement from the gypsum dominated middle Gohatsion), and Adigrat Sandstone. The structural data is plotted on a lower

hemisphere equal area projections (stereonets) and azimuth-frequency plot (rose) diagrams (Fig. 4.5).

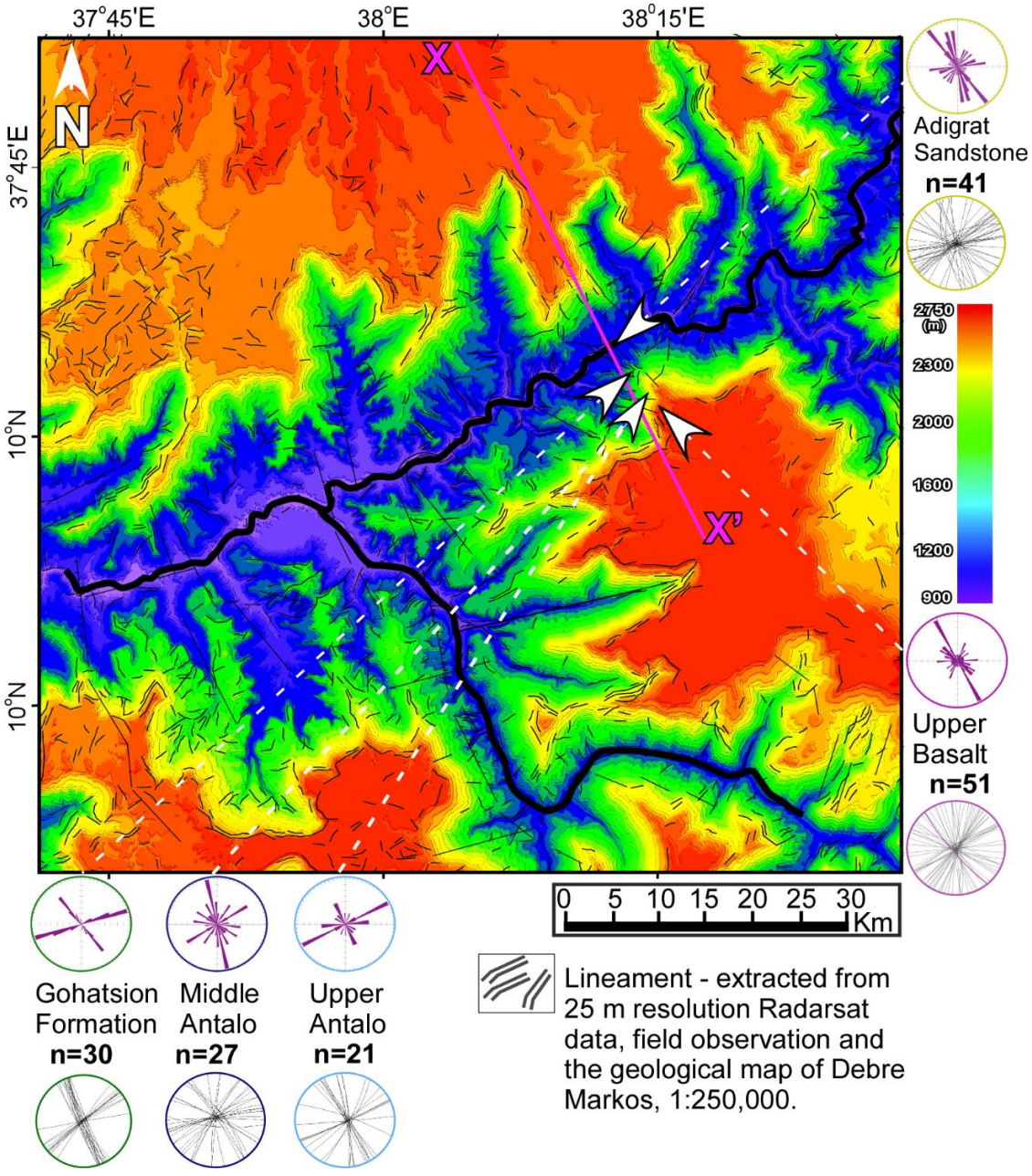

Figure 4.5: Structural lineament draped over color-coded hill-shade Digital Elevation Model (DEM), stereonets plot and rose diagrams of joint orientations. X-X' shows the location of the profile section in Figure 4.2E.

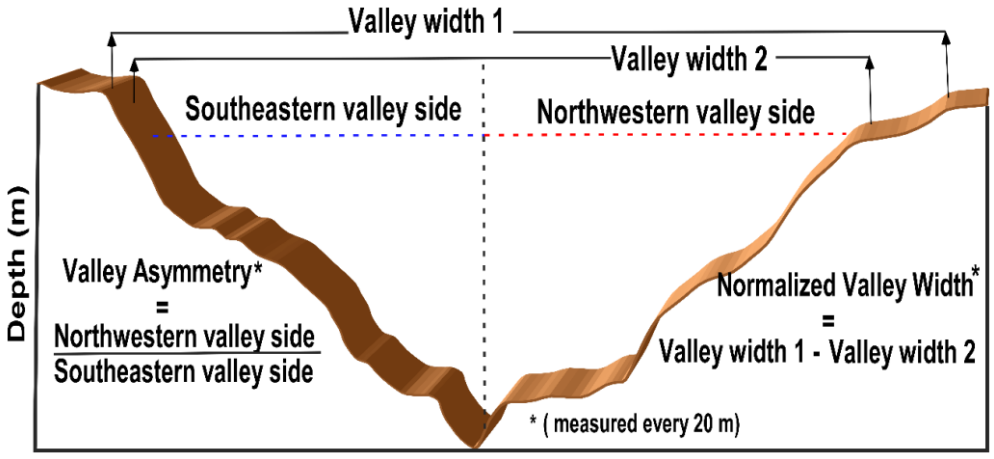

Figure 4.6: Conceptual sketch of measurement of valley parameters: valley width, normalized valley width and valley asymmetry. Valley width is measured wall to wall every 20 m depth interval. Then the subsequent width (e.g. width 2 in this figure) subtracted from the preceding width down 20 m (e.g. width1 in this figure) to get the normalized valley width for that interval and so on. For asymmetry, the northwestern side of the valley is subdivided by the southeastern side every 20 m interval.

4.6. RESULTS

4.6.1. VALLEY WIDTH

We plotted the valley width of the SW-flowing segment of the Blue Nile as a function of depth (Fig. 4.7). The plot shows that the Gorge of the Nile has four depth segments based on its widening as a function of depth. In its upper part at depth ranging between 0 m and 50 m (dominated by the Upper Basalt) the widening of the valley is high reaching ~50 m per 1 m depth. At 0 depth the width of the valley is ~47 km and it becomes ~42 km wide at 50 m depth. Between 50 m and 1050 m depth (dominated by the Lower Basalt, the Upper, Middle and Lower Antalo Limestone, and the Upper and Middle Gohatsion Formations) the valley generally maintains ~30 m per 1 m depth widening. The width of the Blue Nile valley is ~42 km at 50 m depth. The Gorge of the Nile exhibits the highest valley widening (~75 m per 1 m depth) between 1050 m and 1100 m depth. This depth

range is dominated by the Lower Gohatsion Formation were greyish-green glauconitic shaley mudstone inter-bedded with sandstone as well as the upper part of the Adigrat Sandstone. The valley width decreases from ~10 km at 1100 m depth to 3.5 m km at 1050 m depth. We attribute the higher widening rate to the high level of erodibility of the shaley mudstone. Below 1100 m (dominated by the lower part of the Adigrat Sandstone), the valley widening decreased to ~10 m per 1 m depth, documenting the lowest widening within the Blue Nile valley.

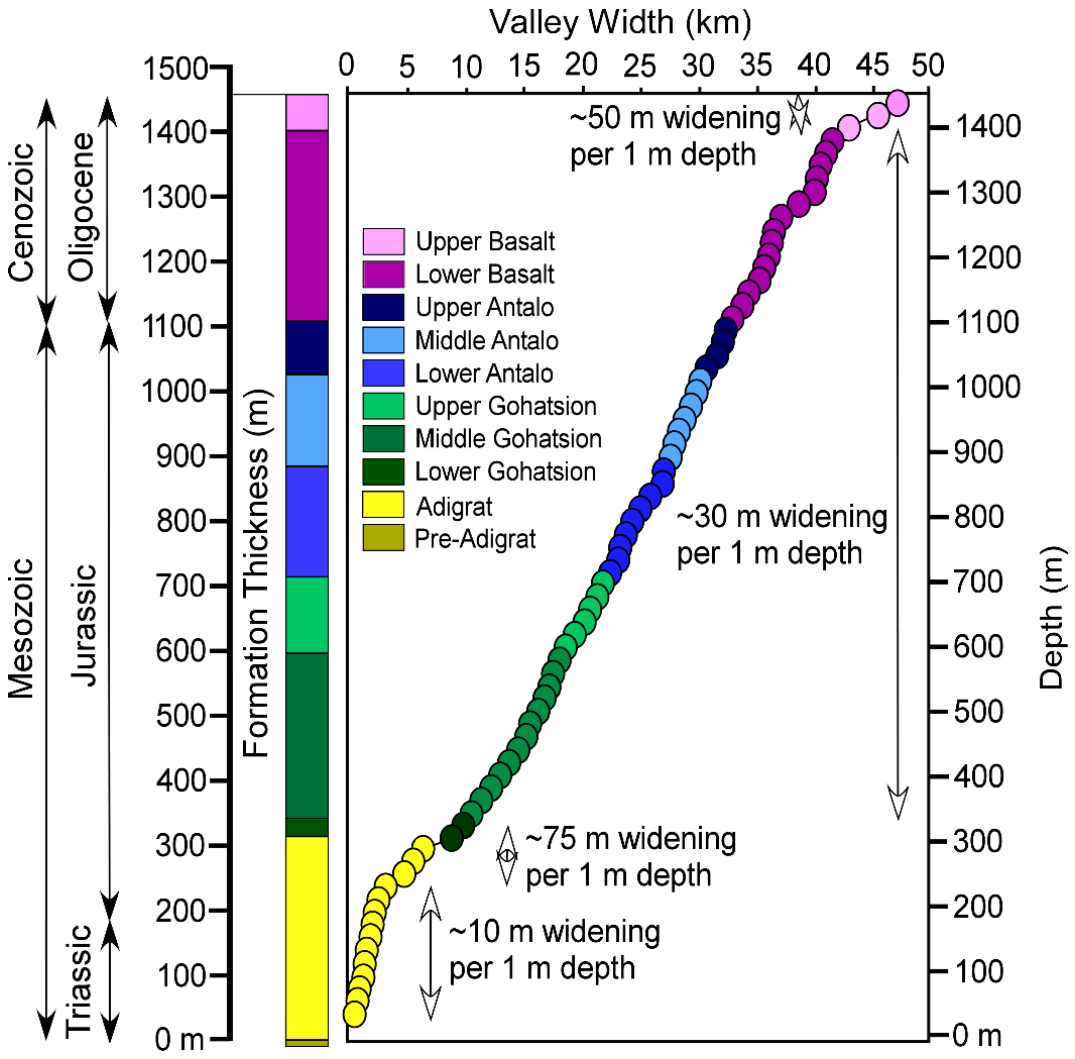

Figure 4.7: Plot of the width of the SW-flowing segment of the Gorge of the Nile as a function of depth.

4.6.2. NORMALIZED VALLEY WIDTH

We plotted the normalized valley width of the SW-flowing segment as a function of depth (Fig. 4.8). Here, we plot the differential value between two measurements, in-order to evaluate the presence of significant variation in width. Each measurement is normalized to show its difference from the preceding or subsequent measurement. For the most part, at depth between 100 m and 1050 m, the normalized valley width remained within 0.1 and 1 averaging 0.45. This depth is occupied by the Lower Basalt, the Upper, Middle and Lower Antalo Limestone, and Upper and Middle Gohatsion Formation. This suggests that the average geometry of the Gorge of the Nile at its SW-flowing segment is an open V-shape with an angle of ~170^{o} between its two walls. However, in the 0 m to 100 m and 1050 m 1100 m depth ranges where the Upper Basalt and the Lower Gohatsion Formation are exposed, the normalized valley width increases sharply reaching ~2.5. This indicates a gentle slope in these sections with the walls being nearly flat. Below 1100 depth, especially in the Middle and Lower part of the Adigrat Sandstone, the normalized valley width values are relatively low reaching ~0.1. This indicates that at this depth the Gorge of the Nile has an open V-shape with an angle of 160^{o} between its walls.

4.6.3. VALLEY SYMMETRY

We plotted the asymmetry of the SW-flowing segment as a function of depth (Fig. 4.9). The plot shows that the Gorge of the Nile has a NW asymmetry (values ranging between ~1.07 and ~1. 53) in the upper ~1200 m depth. The Upper and Lower Basalt, Upper, Middle and Lower Antalo Limestone, and the Upper and Middle Gohatsion formations, dominate this depth range. The Gorge of the Nile changes its asymmetry from NW to become SE or become symmetrical below ~1200 m depth. The Lower Gohatsion Formation (made-up of greyish-green glauconitic shaley mudstone inter-bedded with sandstone) and the upper part of the Adigrat Sandstone (cross-bedded sandstone with occasional mudstone units) dominate this depth. At ~1200 m depth, the asymmetry values

changed from ~1.50 to ~0.84. The Gorge of the Nile has a SE asymmetry (asymmetry value of 0.75) at ~1200 to ~1250 m depth (dominated by the middle part of the Adigrat Sandstone). At depths between ~1250 m and ~1400 m where the Adigrat Sandstone is exposed, the valley is mostly symmetrical. At depth between 1400 m and 1500 m where the lower part of the Adigrat Sandstone is exposed the valley has a NW asymmetry (asymmetry values between 1.25 and 1.5) then again a SE asymmetry (asymmetry values of 0.8).

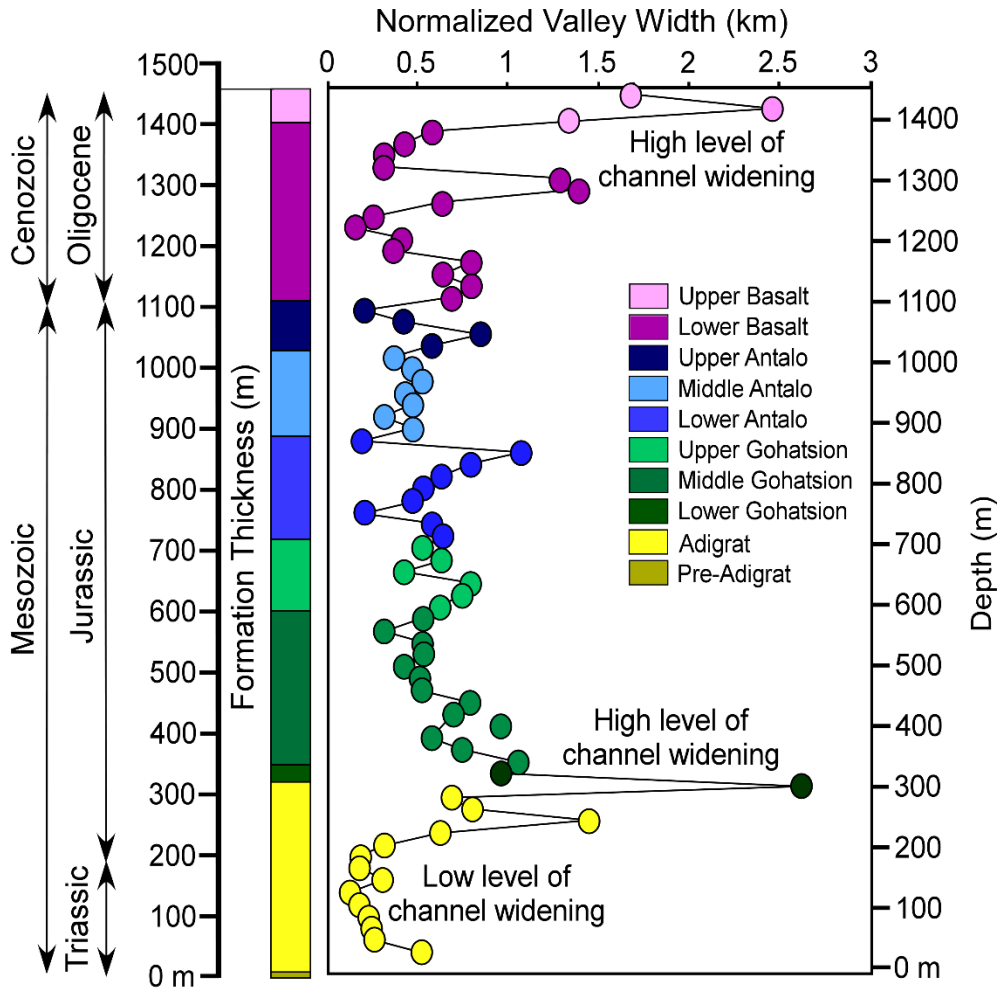

Figure 4.8: Plot of normalized valley width of the SW-flowing segment of the Gorge of the Nile as a function of depth. Similar normalized valley width values indicate ideal V-shape valley. High normalized valley width values indicate open V-shape geometry, whereas small normalized valley width values indicate a tight V-shape geometry.

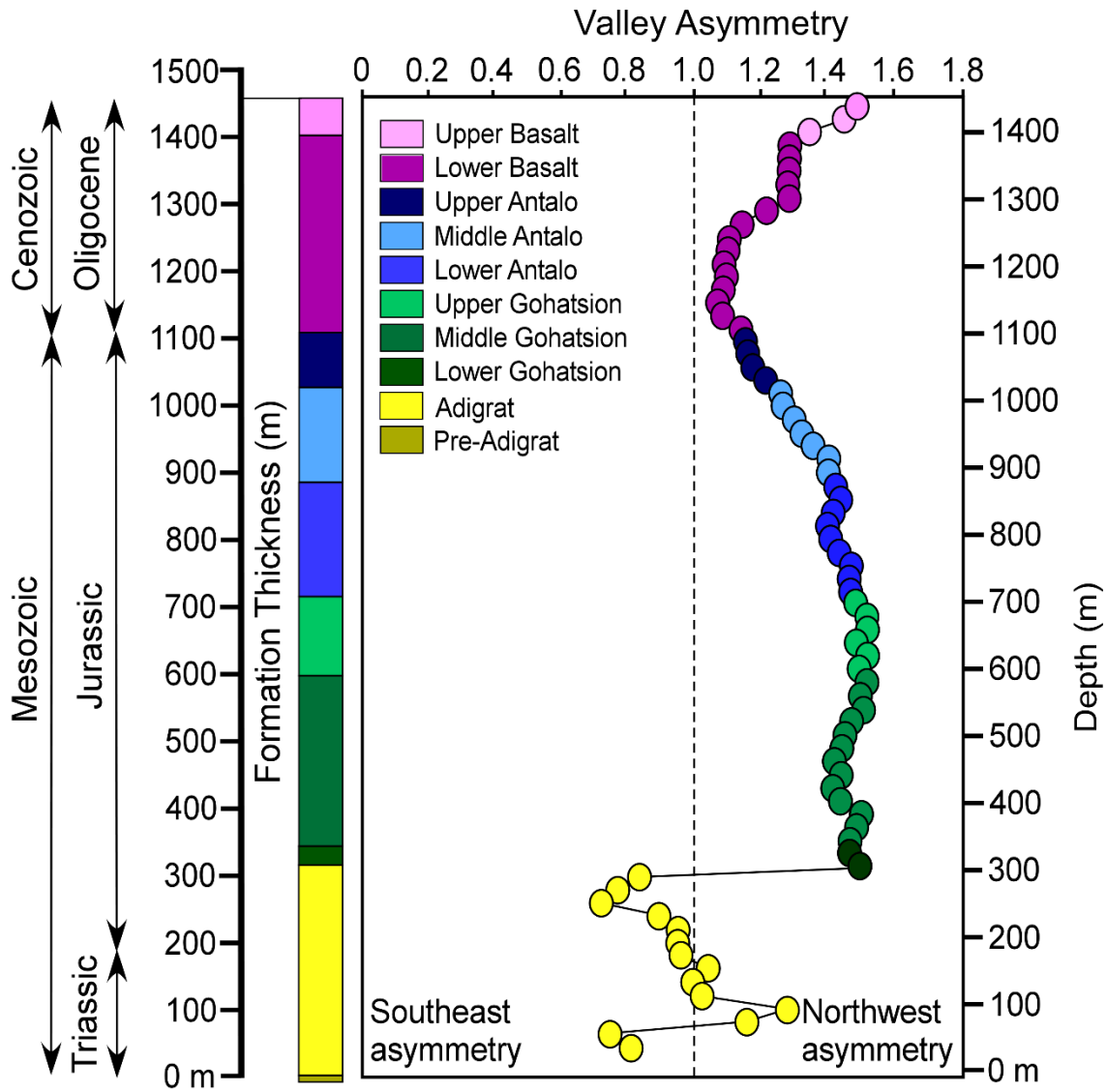

Figure 4.9: Plot of the asymmetry of the SW-flowing segment of the Blue Nile as a function of depth (distance between the axis of the Blue Nile and the NW flank of the Gorge of the Nile divided by the distance of between the axis of the Blue Nile and the SE flank of the Gorge of the Nile). A value of 1 indicates perfect symmetry of the valley; a value less than 1 indicates southeast asymmetry, and a value greater than 1 indicates northwest asymmetry.

4.6.4. INCISION DEPTH THROUGH TIME

We plotted the depth of the incision of the SW-flowing segment as a function of time (Fig. 10A). Following Gani et al. (2007) age brackets of the increased rate of incision at 30 Ma – 10 Ma, 10 Ma - 6 Ma, and 6 Ma – 0 Ma, the depth of the incision of the Blue Nile can be divided into three phases. We found that the Blue Nile incised ~700 m into the NW Plateau between 30 and 10 Ma. At the end of this phase, the incised river possibly reached the Lower Antalo Limestone, which is at present at an altitude of 1800 m above sea level (asl) at the SW-flowing segment of the Blue Nile River. Between 10 Ma and 6 Ma, ~200 m of incision was added allowing for Blue Nile valley to reach the upper part of the Gohatsion Formation, which is at ~1600 m asl at present elevation. From 6 Ma to present, another ~600 m of incision has been added and this corresponds to an accelerated incision rate compared to both previous phases.

4.7. DISCUSSION

An increasing number of studies have been conducted in the NW Ethiopian Plateau, where Blue Nile River has created a spectacular landscape and incised valleys (Pik et al., 2003; Gani et al., 2007; Ismail and Abdelsalam, 2012; Sembroni et al., 2016 a and b). These studies provide valuable data on the uplift history of the plateau, and significantly helped us to gain a new understanding of important aspects of the morpho-tectonic evolution of the region. Majority of the work broadly agree that the increase in incision has been being largely driven by tectonic uplift. These studies have also identified three base level falls that are not related to lithologic variation within the Blue Nile drainage basin (Gani et al., 2007; Ismail and Abdelsalam, 2012; Sembroni et al., 2016a), even though there seems to be disagreement about the scale with which the base level changes encapsulate uplift history of the plateau. Gani et al. (2007) argues, for example, that the geomorphology of the Blue Nile Basin may have been shaped by three phase accelerated plateau growth each followed by an increase in an incision rate, whereas Sembroni et al. (2016a) proposed

maintenance of long-term topography only slightly affected by these tectonic episodes. In the context of this discussion, may be tilting the balance in favor of three-phase accelerated incision, we recently reported similar three phase accelerated incision pattern in the SE Plateau (Xue et al., 2018).

Meanwhile, the influence of stratigraphy along with local structures and mass movement, even if previously been acknowledged (e.g. Gani and Abdelsalam, 2006), has not been thoroughly examined. Our lineament map shows no significant coincident between the dominant joint and fracture network and the river profile (Fig. 4.5). Most faults trend NW and assume the predominant Mesozoic sedimentary basin fabric while others are oriented parallel to the river, and were suggested as being related to the southwest oriented Main Ethiopian Rift (Russo et al., 1994; Gani et a., 2007; Azagegn et al., 2015). However, although some faults are traced across the trend of the river (Gani and Abdelsalam, 2006; Chumburo et al., 2009), there is no observable stratigraphic mismatch or any other evidence of apparent faulting that shows a clear influence of structural control, at least in this segment of the Blue Nile River.

From our analysis, it appears that the valley width normalized against the width at a preceding interval (Fig. 4.8), better describes the general trend of the stratigraphic response. Although there are observable anomalies associated with each stratigraphic unit, both valley width (Fig. 4.7) and normalized valley width (Fig. 4.8) do not show a clear-cut relationship to the variation in stratigraphy, and sometimes deviates from expected response based on previously conducted rock strength measurements from the same area (Ayalew and Yamagishi, 2004). One of the significant anomalous increase in valley width per depth (widening of ~50 m per 1 m depth or normalized valley width of ~2.5) is observed in the Upper Basalt (Fig. 4.8), a rock unit that is shown to have a relatively high strength. This basaltic unit was also incised during the slow phase 1 (30 Ma to 10 Ma) incision period (Fig. 4.10B). We attribute this to the fact that, at shallow depth, rivers have less-defined, and hence wider valley. This is because during the Oligocene, following the flood

basalt event, it is believed that any prior drainage system was buried, and incision started anew (Pik et al., 2003). The largest increase in valley width per depth (widening of ~75 m per 1 m depth or normalized valley width of ~2.5), however, is observed in the Lower Gohatsion, a shaley mudstone interbedded with fine grained sandstone unit (Figs. 4.7 and 4.8). Here, both tensile strength measurement and geomorphic data show a weak layer, and near flat gentle topography (Fig. 4.10B).

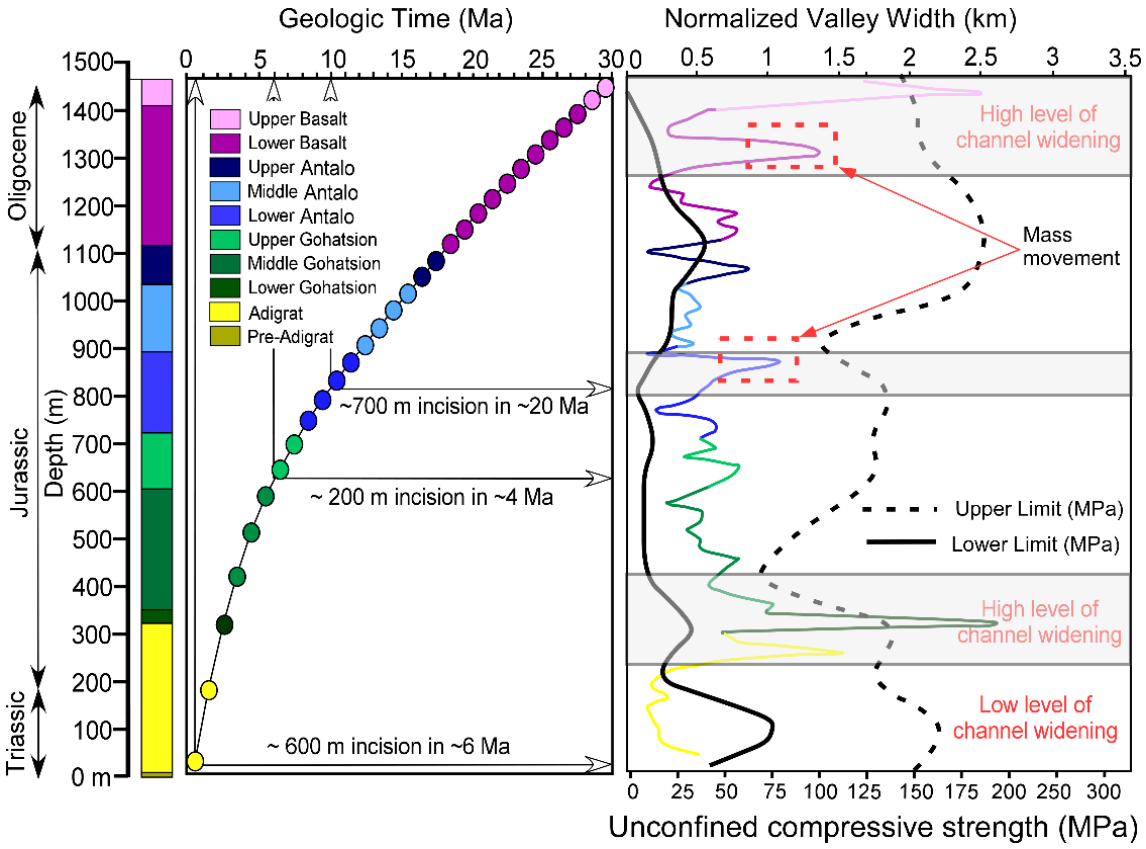

Figure 4.10: (A) Plot of depth of incision of the Blue Nile on the NW Plateau through time established from the inversion of the rate of incision through time curve of the Blue Nile published in Gani et al. (2007). The curve shows that the Blue Nile incised ~700 m into the Ethiopian Plateau between 30 and 10 Ma, ~200 m of incision between 10 and 6 Ma, and ~600 m of incision between 6 and 0 Ma. (B) Comparison of rock strength data from Ayalew and Yamagishi (2004) to calculated normalized valley width and major uplift episodes. Shaded region indicates coincident of relatively

weak strength layers with the change in incision pattern showing a moderate to high valley widening values.

In the rest of the stratigraphic column, despite lithologic difference between the various units (Lower Basalt, Upper Antalo, Middle Antalo, Lower Antalo, Upper Gohatsion, and Middle Gohatsion), the valley width maintains a uniform widening of 30 m per 1 m depth (and normalized valley width between 0.1 and 1), except in the lowermost portion of the gorge (Fig. 4.8). In addition, one may assume similar response from similar stratigraphic units throughout the section. For example, the Lower Gohatsion unit contains similar lithology, but strikingly higher valley widening value compared to the Upper Gohatsion unit. We speculate, such discrepancy may have been due to; (a) the contrast in erodibility between what lies above and below each unit, and whether or not there is a sharp or transitional boundary, (b) the topographic appearance (steepness) of the overlying and underlying units, and (c) the internal architecture of the stratigraphic units. To further explain this point, let's consider the Lower Gohatsion unit, which overlies the cliff forming relatively strong Adigrat Sandstone (a unit with the lowest valley widening per depth observed in the area). It is also overlain by the low-strength to moderate-strength gypsum dominated, gentler Middle Gohatsion unit. Here, the Lower Gohatsion is preferentially eroded, and widens almost approaching a flat surface over a lower, strong sandstone unit, and under a weaker upper boundary-layer (the Middle Gohatsion unit; Fig. 4.8). Meanwhile, the Upper Gohatsion unit, sandwiched between moderate-strength Lower Antalo and Middle Gohatsion, i.e. no significant contrast between upper and lower units, doesn't display as apparent preferential widening as the Lower Gohatsion unit.

Apart from the possible valley widening influences of upper and lower, weak and strong layers, we do have evidence that shows an increase in incision rate that was due to the anomalous uplift that commenced around 6 Ma (Gani et al., 2007). This was well before the Blue Nile River started

incising the Lower Gohatsion unit, but just after the Upper Gohatsion unit (Figs. 4.10 A and B). Hence, one would argue that the discrepancy in the valley widening between the Lower and Upper Gohatsion units could also be explained by the accelerated plateau growth forcing faster incision. Accordingly, we interpret the anomalous widening in the Lower Gohatsion unit as being due to the overlapping of enhanced incision caused by accelerated plateau growth and high erodibility of the lithology. The other small, but recognizable normalized valley widening anomaly within the generally uniform pattern is observed in the Lower Antalo unit, and in the middle of the basaltic unit, which are areas generally known for mass movements (Fig. 4.10B).

Such observations are perhaps in slight, yet significant contrast to the theoretical and few experimental studies that suggest disproportionate control of lithologic variation on landscape evolution in actively uplifting regions (e.g. Sklar and Dietrich, 2001; Forte et al., 2016). While we also have documented the effect of lithologic variation, and/ rock strength, e.g. softer rock eroding faster, and resulting gentler and wider valley, the extent with which the stratigraphic heterogeneity controlling the overall landscape evolution is difficult to ascertain. In addition, it is assumed that for lithological variations to significantly shape landscape, it generally requires a relatively long-term steady conditions (Whipple and Tucker, 1999; Sklar and Dietrich, 2001), which arguably is not the scenario in the study area. This has important implications for understanding the controls on uplift history, and whether the pulsed increase in incision is a response to the river incising through different rock types or tectonically forced plateau growth.

Numerical models have also shown the influence of variable rock strength stratigraphy on differential erosion, and their subsequent control on hillslope expression (Pederson and Tressler, 2012; Bursztyn et al., 2015; Forte et al., 2016). Nevertheless, such modelling is more complex in areas where the geology is fairly simple layer cake stratigraphic setting, which is the case at the Gorge of the Nile. This is because, in settings where the contact between rock units is horizontal, the lithology changes vertically and incision into the deep canyon interacts with variable rock.

Some similar observation could be made at our study area in which the hard sandy and limestone units with basalt often form cliff while the shaly and evaporate and muddy rock units form gentler slope (Fig. 4.3). However, only the normalized valley widening results in the Lower Gohatsion unit could possibly be explained by the nature of the hill slope expression i.e. a unit with gentle topographic expression showing anomalously higher widening per depth compared to the relatively stronger underlying and moderate overlying unit. In other cases, results of valley widening per depth are barely a reflection of the stratigraphy. This again shows that topographic expressions (such as alternating gentle and steep hillslope) in actively incising regions, is only partly controlled by the variation in lithologic type and on the strength of the stratigraphic units (e.g. Stock and Montgomery, 1999; Sklar and Dietrich, 2001; Forte et al., 2016). In addition, given most modeling studies only consider a constant uplift and simple two-layered stratigraphy and do not cover the full spectrum of possible scenarios, the extent to which stratigraphic variation significantly controls incision is quantitatively not reliable. Therefore, the long-term relationship between rock strength, hillslope expression and valley widening, and its control on overall valley geometry at least from our analysis and in our study area (Fig. 4.8), is not as forthright.

4.8. IMPLICATIONS

An important issue that has challenged scientists studying the East African Rift System is the relative timing of uplift, volcanism and extension (Ebinger and Sleep, 1998; Courtillot et al., 1999; Şengör, 2001; Pik et al., 2003). We know how to determine the age of volcanic rocks, especially through 40Ar/39Ar. However, it is difficult to determine the age of uplift through both fission-track and apatite/He methods in magma-rich rift system. This is because the Precambrian crystalline basement rocks needed for such measurement are thermally affected by the overlying volcanic pile, and thus, is challenging to deduce timing and extent of uplift.

Therefore, in such cases, morpho-tectonic analysis becomes important for providing relative chronology of events leading to development of rift systems. The substantial interest in the uplift history of the NW Plateau is motivated by its complex tectono-magmatic evolution. This includes impingement of the Afar mantle plume, formation of shield volcanoes and rift-flank uplift. For example, shield volcanoes such as the 24 million-year-old Choke has forced the Blue Nile River to make the 200 km semi-circular loop around the mountain and the river might as well be forced southwest by the Degem volcano south of the Gorge of the Nile (Fig. 4.1B).

There are few studies that have focused on the rift flank uplift, and specifically on its effect on drainage pattern (e.g. Weissel et al., 1995; Ebinger and Hayward, 1996; Sembroni et al., 2016b). We found in this study that the top 1200 m section of the Gorge of the Nile (for the first 20 Ma based on the inversion of the rate of incision through time curve of Gani et al., 2007; Fig. 4.10A), the average asymmetry index is 1.35, indicating that the NW portion of the Gorge of the Nile is around 35% wider on average than its SE side (Fig. 4.9). We interpreted this consistent NW asymmetry of the Gorge of the Nile that we found in the first 20 Ma of its incision as probably related to the pre-rift doming of the Ethiopian Plateau, and rift-flank uplift of the Afar Depression and the Main Ethiopian Rift. Although the timing of the opening of the Main Ethiopian Rift is not well constrained, it is generally agreed that it started during late Miocene, and was assumed that it may have resulted in considerable rift-flank uplift with a potential influence on the Blue Nile drainage system (Wolfenden et al, 2004; Bonini et al., 2005; Gani et al, 2007; Balestrieri et al., 2016; Sembroni et al., 2016b).

Thus, one would assume the NW asymmetry to continue throughout the section, in fact more pronounced by the effect of the rift-flank uplift from the late Miocene opening of the Main Ethiopia Rift. However, as we have observed from results of the valley widening, the valley asymmetry index also shows an anomalous shift at the Lower Gohatsion unit (Fig. 4.9). In this case, for a reason that we do not know yet, the asymmetry shifted towards the SE. Yet, despite this discrepancy

at the lower most section of the Gorge of the Nile, the overall average asymmetry index for this segment of the river at this particular section is around 1.28 or about 28% wider valley on the NW side, which is consistent with rift flank uplift of the Afar Depression and the Main Ethiopian Rift.

Understanding at what time different levels of the Cenozoic flood basalt and the Mesozoic sedimentary sections were exposed by the Blue Nile River also greatly benefits sediment budget studies. Principal areas of research such as timing of the Nile appearance in the Nile delta are issues in which disagreement still persists (Garzanti et al., 2006; Talbot and Williams, 2009; Macgregor, 2012; Abdelsalam, 2018). Equally important is, constraining erosional tendencies of the different rock types of the Blue Nile drainage system, a major source of sediment for downstream basins that have served as sinks. For instance, sedimentological estimations show that the Gezira Formation in eastern Sudan is built from ~7000 km3 of sediment, mostly clay (Williams, 1969). Williams (1969) suggested that the source of much of the Gezira Formation sediment is the weathering of the upper basaltic units that tops the NW Plateau. Hence, analysis of the stratigraphy and sedimentology of the Gezira Formation will benefit from understanding at what time the Blue Nile River exposed the different levels of the Cenozoic flood basalt and the Mesozoic sedimentary sections. Moreover, the timing of connection between the Blue Nile River and the White Nile at Khartoum is, at best, poorly constrained (e.g. Abdelsalam, 2018). After their connection at Khartoum, the two rivers become the River Nile, which continues north into Egypt to deposit its sediment in the Nile submerged cone. Nonetheless, estimates of the age of appearance of the weathering products of the NW Plateau in the Nile submerged cone are highly variable. Early works suggested that this connection occurred during the Pleistocene epoch (Rossignol, 1961, 1962; Emel'yanov, 1972; Issawi and McCauley, 1992; Talbot and Williams, 2009). However, recently from detrital zircon analysis of the Nile Basin, Garzanti et al. (2018) found the presence of Oligocene zircons in the Nile tributaries in Sudan and Egypt and attributed this to the connection of these segments of the Nile to the Ethiopian Nile since Oligocene. In addition, a U-Pb zircon ages

and Sr-Nd isotopic data from the sediment of the Nile submerged delta also shows that the River Nile was connected to its sources within the Cenozoic Continental Flood Basalts in Ethiopia since the Oligocene (Fielding et al., 2018).

4.9. CONCLUSIONS

There is a general consensus in that the NW Plateau contains a dynamically evolving landscape captured in the incision history of the Blue Nile River. The first order plateau-building process include the impingement of the Afar mantle plume beneath the lithosphere, however, the extent with which subsequent tectono-magmatic processes altered the regional landscape evolution is debatable. Superimposed on these processes are the effect of stratigraphy on morpho-tectonics evolution. Here, we utilized remote sensing analysis, field observation, and a previously published incision rate to understand the incision history of the Gorge of the Nile in the NW Plateau, and assess the role of the stratigraphy using geomorphic parameters that were previously unexplored.

Results from measured valley width and calculated normalized valley width showed a uniform valley widening for most part of the Gorge of the Nile except an anomalously wider valley in the Lower Gohatsion and the Upper Basalt unit. We interpreted the widening in the Lower Gohatsion unit as being due to the coincident of accelerated incision rate caused by plateau uplift and high erodibility of the lithologies constituting the unit. Additionally, we explain the widening in the Upper Basalt as due to the poorly defined nature of the valley when the river started incision ~30 Ma ago. The valley symmetry calculation on the other hand, showed that the valley of the Blue Nile has a NW asymmetry that we attributed as being due to the rift-flank uplift of the western margin of the Afar Depression and the northwestern margin of the Main Ethiopian Rift. Calculation of incision depth through time showed that the Blue Nile total amount of incision in the NW Plateau (~1500 m) was higher between 6 Ma and present compared to that between 6 Ma and 10 Ma and

10 Ma and 30 Ma. Our results have implications for understanding the sediment budget of the Nile system, and the sediment provenance of downstream sedimentary basins, which served as sinks for the sediment flux coming for the NW Plateau. Another implication relates to the tectonics of the East African Rift System in terms of establishing relative chronology of tectonic events such as volcanism, uplift and extension.

4.10. ACKNOWLEDGEMENTS

This work was supported by National Science Foundation – Office of International Science and Engineering – International Research Experience for Students (NSF-OISE-IRES) program Grant Number 0927906. We thank Addis Ababa University, Ethiopia for logistical support. This is Oklahoma State University, Boone Pickens School of Geology contribution number 2019-xx.

4.11. REFERENCES

Abbate, E., Bruni, P., Ferretti, M.P., Delmer, C., Laurenzi, M.A., Hagos, M., Bedri, O., Rook, L., Sagri, M., and Libsekal, Y., 2014, The East Africa Oligocene intertrappean beds: regional distribution, depositional environments and Afro/Arabian mammal dispersals: Journal of African Earth Sciences, v. 99, p. 463–489.

Abbate, E., Bruni, P., and Sagri, M., 2015, Geology of Ethiopia: A review and geomorphological perspectives, in Billi, P., eds., Landscapes and Landforms of Ethiopia, World Geomorphological Landscapes: Springer Science, Dordrecht, p. 33–64.

Abdelsalam, M. G., 2018, The Nile's journey through space and time: A geological perspective: Earth-Science Reviews, v. 177, p. 742-773.

Alemu, T., Abdelsalam, M. G., Dawit, E. L., Atnafu, B., and Mickus, K. L., 2018, The Paleozoic–Mesozoic Mekele Sedimentary Basin in Ethiopia: An Example of an Exhumed IntraCONtinental Sag (ICONS) Basin: Journal of African Earth Sciences, v. 143, p. 40-58.

Assefa, G., 1981, Gohatsion Formation: a new Lias-Malm lithostragraphic unit from the Abby River basin, Ethiopia: Geoscience Journal, v. 2, p. 63–88.

Assefa, G., 1991, Lithostratigraphy and environment of deposition of the Late Jurassic–Early Cretaceous sequence of the central part of Northwestern Plateau, Ethiopia: Neues Jahrbuch fur Geologie und Paleontologie Abhandunglen, v. 182, p. 255–284.

Atnafu, B., 2003, Facies and diagenetic development of Jurassic in the Abay River Basin, Ph.D. thesis, Friedrich Alexander Universität Erlangen, Nürnberg.

Ayalew, D., Barbey, P., Marty, B., Reisberg, L., Yirgu, G., and Pik, R., 2002, Source, genesis, and timing of giant ignimbrite deposits associated with Ethiopian continental flood basalts: Geochimica et Cosmochimica Acta, v. 66, p. 1429-1448.

Ayalew, L., and Yamagishi, H., 2004, Slope failures in the Blue Nile basin, as seen from landscape evolution perspective: Geomorphology, v. 57, p. 95-116.

Azagegn, T., Asrat, A., Ayenew, T., and Kebede, S., 2015, Litho-structural control on interbasin groundwater transfer in central Ethiopia: Journal of African Earth Sciences, v. 101, p. 383-395.

Balestrieri, M.L., Bonini, M., Corti, G., Sani, F., and Philippon, M., 2016, A refinement of the chronology of rift-related faulting in the Broadly Rifted Zone, southern Ethiopia, through apatite fission-track analysis: Tectonophysics, v. 671, p. 42-55.

Bonini, M., Corti, G., Innocenti, F., Manetti, P., Mazzarini, F., Abebe, T., and Pecskay, Z., 2005, Evolution of the Main Ethiopian Rift in the frame of Afar and Kenya rifts propagation: Tectonics, v. 24, TC1007.

Bursztyn, N., Pederson, J. L., Tressler, C., Mackley, R. D., and Mitchell, K. J., 2015, Rock strength along a fluvial transect of the Colorado Plateau–quantifying a fundamental control on geomorphology: Earth and Planetary Science Letters, v. 429, p. 90-100.

Bussert, R., 2010, Exhumed erosional landforms of the Late Palaeozoic glaciation in northern Ethiopia: indicators of ice-flow direction, palaeolandscape and regional ice dynamics: Gondwana Research, v. 18, p. 356–369.

Chumburo, F., Ayalew, A., H/ Mariam, D., Hailu, F., H/ Mariam, M., and Alemayehu, T., 2009, Geological map of Debre Markos, Sheet NC 37-6, 1:250,000: Geological Survey of Ethiopia, Addis Ababa.

Coltorti, M., Dramis, F., and Ollier, C.D., 2007, Planation surfaces in Northern Ethiopia: Geomorphology, v. 89, p. 287–296.

Coulié, E., Quidelleur, X., Gillot, P. Y., Courtillot, V., Lefèvre, J. C., and Chiesa, S., 2003, Comparative K–Ar and Ar/Ar dating of Ethiopian and Yemenite Oligocene volcanism: implications for timing and duration of the Ethiopian traps: Earth and Planetary Science Letters, v. 206, p. 477-492.

Courtillot, V., Jaupart, C., Manighetti, I., Tapponnier, P., and Besse, J., 1999, On causal links between flood basalts and continental breakup: Earth and Planetary Science Letters, v. 166, p. 177–195.

Cunha, P.P., Martins, A.A., Daveauc, S., and Friend, P.F., 2005, Tectonic control of the Tejo river fluvial incision during the late Cenozoic, in Ro´da˜o—central Portugal (Atlantic Iberian border): Geomorphology, v. 64, p. 271-298.

Davidson, A., and Rex, D. C., 1980, Age of volcanism and rifting in southwestern Ethiopia: Nature, v. 283, p. 657-658. Dawit, E., and Bussert, R., 2009, Stratigraphy and facies architecture of Adigrat Sandstone, Blue Nile Basin, Central Ethiopia: Zentral Blatt Geol. Paläonttol., v. 1, p. 217–232.

Dawit, L.E., 2010, Adigrat Sandstone in Northern and Central Ethiopia: Stratigraphy, Facies, Depositional Environments and Palynology: Ph.D. Thesis, Technische Universität Berlin, p. 166 p.

Ebinger, C. J., Yemane, T., Woldegabriel, G., Aronson, J. L., and Walter, R. C., 1993, Late Eocene–Recent volcanism and faulting in the southern main Ethiopian rift: Journal of the Geological Society, v. 150, p.99-108.

Ebinger, C. J., and Hayward, N. J., 1996, Soft plates and hot spots: Views from Afar: Journal of Geophysical Research: Solid Earth, v. 101, p. 21859-21876.

Ebinger, C.J., and Sleep, N.H., 1998, Cenozoic magmatism throughout east Africa resulting from impact of a single plume: Nature, v. 395, p. 788–791.

Emel'yanov, E. M., 1972, Principal types of recent bottom sediments in the Mediterranean Sea: their mineralogy and geochemistry, in Stanley, D. J., eds., The Mediterranean Sea: A Natural Sedimentation Laboratory: Dowden, Hutchinson and Ross, p. 355–386.

Fielding, L., Najman, Y., Millar, I., Butterworth, P., Garzanti, E., Vezzoli, G., Barfod, D. and Kneller, B., 2018, The initiation and evolution of the River Nile: Earth and Planetary Science Letters, v. 489, p. 166-178.

Forte, A. M., Yanites, B. J., and Whipple, K. X., 2016, Complexities of landscape evolution during incision through layered stratigraphy with contrasts in rock strength: Earth Surface Processes and Landforms, v. 41, p. 1736-1757.

Gani, N.D., and Abdelsalam, M.G., 2006, Remote sensing analysis of the Gorge of the Nile, Ethiopia with emphasis on Dejen–Gohatsion region: Journal of African Earth Sciences, v. 44, p. 135–150.

Gani, N.D.S, Gani, M., and Abdelsalam, M.G., 2007, Blue Nile incision on the Ethiopian Plateau: pulsed plateau growth, Pliocene uplift and hominin evolution: GSA Today, v. 17, p. 4–11.

Gani, N.D.S, Abdelsalam, M.G., Gera, S., and Gani, M., 2009, Stratigraphic and structural evolution of the Blue Nile Basin, Northwestern Ethiopian Plateau: Geological Journal, v. 44, p. 30–56.

Garzanti, E., Andò, S., Vezzoli, G., Megid, A. A. A., and El Kammar, A., 2006, Petrology of Nile River sands (Ethiopia and Sudan): sediment budgets and erosion patterns: Earth and Planetary Science Letters, v. 252, p. 327-341.

Garzanti, E., Vermeesch, P., Rittner, M., and Simmons, M., 2018, The zircon story of the Nile: Time-structure maps of source rocks and discontinuous propagation of detrital signals: Basin Research, p. 1-20.

George, R., Rogers, N., and Kelley, S., 1998, Earliest magmatism in Ethiopia: Evidence for two mantle plumes in one flood basalt province: Geology, v. 26, p. 923-926.

Hofmann, C., Courtillot, V., Feraud, G., Rochette, P., Yirgu, G., Ketefo, E., and Pik, R., 1997, Timing of the Ethiopian flood basalt event and implications of Plume birth and global change: Nature, v. 389, p. 838–841.

Ismail, E.H., and Abdelsalam, M.G., 2012, Morpho-tectonic analysis of the Tekeze River and the Blue Nile drainage systems on the Northwestern Plateau, Ethiopia: Journal of African Earth Sciences, v. 69, p. 34–47.

Issawi, B., and McCauley, J. F., 1992, The Cenozoic rivers of Egypt: the Nile problem, in Adams, B., and Friedman, R., eds., The Followers of Horus: Oxbow Press, Oxford, p. 1–18.

Jespen, D.H., and Athearn, M.J., 1961, Geologic plan and section of the left bank of the Blue Nile canyon near crossing of Addis Ababa-Debre Markos road: U.S. Dept. Interior: Addis Ababa Ethiopia's Water Resources Department, p. 35 p.

Kieffer, B., Arndt, N., Lapierre, H., Bastien, F., Bosch, D., Pecher, A., Yirgu, G., Ayalew, D., Weis, D., Jerram, D.A., Keller, F., and Meugniot, C., 2004, Flood and shield basalts from Ethiopia: magmas from the African Superswell: Journal of Petrology, v. 45, p. 793–834.

Macgregor, D. S., 2012, The development of the Nile drainage system: integration of onshore and offshore evidence: Petroleum Geoscience, v. 18, p. 417-431.

Mock, C., Arnaud, N.O., Cantagrel, J.-M., and Yirgu, G., 1999, 40Ar/39Ar thermochronology of the Ethiopian and Yemeni basements: reheating related to the Afar plume?: Tectonophysics, v. 314, p. 351–372.

Mohr, P.A., 1963, Occurrence of Karoo System sediments in Ethiopia: Nature, v. 199, p. 1086.

Pederson, J. L., and Tressler, C., 2012, Colorado River long-profile metrics, knickzones and their meaning: Earth and Planetary Science Letters, v. 345, p. 171-179.

Pik, R., Marty, B., Carignan, J., and Lave, J., 2003, Stability of Upper Nile drainage network (Ethiopia) deduces from (U–Th)/He thermochronometry: Implication of uplift and erosion of the Afar plume dome: Earth and Planetary Science Letters, v. 215, p. 73–88.

Rochette, P., Tamrat, E., Féraud, G., Pik, R., Courtillot, V., Ketefo, E., and Yirgu, G., 1998, Magnetostratigraphy and timing of the Oligocene Ethiopian traps: Earth and Planetary Science Letters, v. 164, p. 497-510.

Rogers, N. W., 2006, Basaltic magmatism and the geodynamics of the East African Rift System: Geological Society, London, Special Publications, v. 259, p. 77-93.

Rossignol, M., 1961, Analyses polliniques de sédiments marins quaternaires en Israel, I, Sédiments récents: Pollens et Spores, v. 3, p. 303–324.

Rossignol, M., 1962, Analyses polliniques de sédiments marins quaternaires en Israel, II, Sédiments pléistocènes: Pollens et Spores, v. 4, p. 121–148.

Russo, A., Assefa, G., and Atnafu, B., 1994, Sedimentary evolution of the Abby River (Blue Nile) Basin, Ethiopia: Neues Jahrbuch fu¨r Geologie und Palae¨ontologie Monatshefte, v. 5, p. 291–308.

Sembroni, A., Faccenna, C., Becker, T.W., Molin, P., and Abebe, B., 2016a, Long-term, deep-mantle support of the Ethiopia-Yemen Plateau: Tectonics, v.35, p. 469-488.

Sembroni, A., Molin, P., Pazzaglia, F.J., Faccenna, C., and Abebe, B., 2016b, Evolution of continental-scale drainage in response to mantle dynamics and surface processes: An example from the Ethiopian Highlands: Geomorphology, v. 261, p. 12-29.

Şengör, A.M.C., 2001, Elevation as indicator of mantle-plume activity, in Ernst, R.E., and Buchan, K.L., eds., Mantle Plumes: Their identification through time: Geological Society of America Special Paper 352, p. 183–225.

Sklar, L.S., and Dietrich, W.E., 2001, Sediment and rock strength controls on river incision into bedrock: Geology, v. 29, p. 1087–1090.

Stock, J. D., and Montgomery, D. R., 1999, Geologic constraints on bedrock river incision using the stream power law: Journal of Geophysical Research: Solid Earth, v. 104, p. 4983-4993.

Talbot, M.R., and Williams, M.A., 2009, Cenozoic evolution of the Nile basin, in Dumont H.J., eds., The Nile, Monographiae Biologicae: Springer, Dordrecht, v. 89, p. 37–60.

Tefera, M., Chernet, T., Haro, W., 1996, Geological Map of Ethiopia (1: 2,000,000), Second ed. Regional Mapping Department of the Ethiopian Geological Survey, Addis Ababa.

Tucker, G.E., and Slingerland, R., 1997, Drainage basin responses to climate change: Water Resources Research, v. 33, no. 8, p. 2031–2047.

Weissel, J. K., Malinverno, A., Harding, D. J., and Karner, G. D., 1995, Erosional development of the ethiopian Plateau of northeast Africa from a fractal analysis of topography: In Fractals in petroleum geology and earth processes, p. 127-142. Springer, Boston, MA.

Whipple, K. X., and Tucker, G. E., 1999, Dynamics of the stream-power river incision model: Implications for height limits of mountain ranges, landscape response timescales, and research needs: Journal of Geophysical Research: Solid Earth, v. 104, p. 17661-17674.

Williams, M. A. J., 1969, The Nile in the Sudan: The Geographical Journal, v. 135, no. 3, p. 489-491.

Wolela, A., 2008, Sedimentation of the Triassic-Jurassic Adigrat Sandstone Formation, Blue Nile Basin, Ethiopia: Journal of African Earth Sciences, v. 52, p. 30–42.

Wolfenden, E., Yirgu, G., Ebinger, C., Deino, A., and Ayalew, D., 2004, Evolution of the northern Main Ethiopian Rift: birth of a triple junction: Earth and Planetary Science Letters, p. 24, p. 213–228.

Xue, L., Alemu, T.B., Gani, N.D., and Abdelsalam, M.G., Spatial and temporal variation of tectonic uplift in the southeastern Ethiopian Plateau from morphotectonic analysis: Geomorphology, v. 309, p. 98-111.

Zanettin, B., Justin, V.E., Nicoletti, M., Piccirillo, E.M., 1980, Correlations among Ethiopian volcanic formations with special references to the chronological and stratigraphical problems of the “Trap Series”: Atti Convegni Acc Lincei Roma, v. 47, p. 231–252.

APPENDICES

TABLE 4.1

Present Elevation (m)	Distance from NW flank of the Gorge to the river axis (Km)	Distance from SE flank of the Gorge to the river axis (Km)	Total Valley Width (Km)	Asymmetry	Normalized Valley Width
2480	30.48012	23.11164	53.59176	1.318821165	
2460	28.22004	18.8856	47.10564	1.494262295	1.68732
2440	26.92746	18.49086	45.41832	1.456257848	2.46906
2420	24.67512	18.27414	42.94926	1.350275307	1.34676
2400	23.43672	18.16578	41.6025	1.290157648	0.58824
2380	23.11164	17.90262	41.01426	1.290964116	0.43344
2360	22.84074	17.74008	40.58082	1.287521815	0.31734
2340	22.63176	17.63172	40.26348	1.28358209	0.32508
2320	22.5234	17.415	39.9384	1.293333333	1.29258
2300	21.23082	17.415	38.64582	1.219111111	1.40094
2280	19.88406	17.36082	37.24488	1.145341061	0.64242
2260	19.29582	17.30664	36.60246	1.114937388	0.2709
2240	19.0791	17.25246	36.33156	1.105877075	0.16254
2220	18.91656	17.25246	36.16902	1.09645581	0.4257
2200	18.76176	16.98156	35.74332	1.104831358	0.37152
2180	18.49086	16.88094	35.3718	1.095369097	0.80496
2160	17.90262	16.66422	34.56684	1.074314909	0.65016
2140	17.6859	16.23078	33.91668	1.089651884	0.80496
2120	17.6859	15.42582	33.11172	1.146512795	0.6966
2100	17.415	15.00012	32.41512	1.160990712	0.21672
2080	17.36082	14.83758	32.1984	1.170057381	0.43344
2060	17.19828	14.56668	31.76496	1.180658874	0.85914
2040	16.98156	13.92426	30.90582	1.219566426	0.58824
2020	16.93512	13.38246	30.31758	1.265471371	0.37926

2000	16.77258	13.16574	29.93832	1.273956496	0.47988
1980	16.7184	12.74004	29.45844	1.312272175	0.5418
1960	16.50168	12.41496	28.91664	1.329177057	0.43344
1940	16.4475	12.0357	28.4832	1.366559486	0.47988
1920	16.39332	11.61	28.00332	1.412	0.32508
1900	16.1766	11.50164	27.67824	1.406460296	0.48762
1880	16.01406	11.17656	27.19062	1.432825485	0.20124
1860	15.96762	11.02176	26.98938	1.448735955	1.0836
1840	15.2091	10.69668	25.90578	1.421852388	0.80496
1820	14.67504	10.42578	25.10082	1.407572383	0.64242
1800	14.34996	10.10844	24.4584	1.419601838	0.5418
1780	14.13324	9.78336	23.9166	1.444620253	0.47988
1760	13.97844	9.45828	23.43672	1.477905074	0.21672
1740	13.8159	9.4041	23.22	1.469135802	0.58824
1720	13.49082	9.14094	22.63176	1.475867909	0.65016
1700	13.16574	8.81586	21.9816	1.493415277	0.53406
1680	12.95676	8.49078	21.44754	1.525979945	0.64242
1660	12.5775	8.22762	20.80512	1.52869238	0.43344
1640	12.19824	8.17344	20.37168	1.492424242	0.80496
1620	11.82672	7.74	19.56672	1.528	0.75852
1600	11.28492	7.52328	18.8082	1.5	0.63468
1580	10.96758	7.20594	18.17352	1.522019334	0.5418
1560	10.58832	7.0434	17.63172	1.503296703	0.32508
1540	10.42578	6.88086	17.30664	1.515185602	0.53406
1520	10.00008	6.7725	16.77258	1.476571429	0.5418
1500	9.62082	6.60996	16.23078	1.455503513	0.43344
1480	9.34992	6.44742	15.79734	1.450180072	0.52632
1460	8.9784	6.29262	15.27102	1.426814268	0.5418
1440	8.7075	6.02172	14.72922	1.446015424	0.80496
1420	8.17344	5.75082	13.92426	1.421265141	0.70434
1400	7.79418	5.42574	13.21992	1.436519258	0.9675
1380	7.36074	4.89168	12.25242	1.504746835	0.58824
1360	6.98922	4.67496	11.66418	1.495033113	0.75852
1340	6.5016	4.40406	10.90566	1.476274165	1.06812
1320	5.85918	3.97836	9.83754	1.472762646	0.9675
1300	5.32512	3.54492	8.87004	1.502183406	2.6316
1280	2.84832	3.39012	6.23844	0.840182648	0.6966
1260	2.42262	3.11922	5.54184	0.776674938	0.8127
1240	1.98918	2.73996	4.72914	0.725988701	1.45512
1220	1.55574	1.71828	3.27402	0.905405405	0.63468
1200	1.29258	1.34676	2.63934	0.959770115	0.32508
1180	1.13004	1.18422	2.31426	0.954248366	0.1935

1160	1.0449	1.07586	2.12076	0.971223022	0.18576
1140	0.99072	0.94428	1.935	1.049180328	0.32508
1120	0.80496	0.80496	1.60992	1	0.13158
1100	0.75078	0.72756	1.47834	1.031914894	0.18576
1080	0.72756	0.56502	1.29258	1.287671233	0.23994
1060	0.56502	0.48762	1.05264	1.158730159	0.24768
1040	0.3483	0.45666	0.80496	0.762711864	0.2709
1020	0.23994	0.29412	0.53406	0.815789474	0.53406

Table 4.1: Valley width, Asymmetry and Normalized Valley Width as calculated from DEM and field measurements.

TABLE 4.2

Age (Ma)	Incision (m)
	0
30	27.07649789
29	54.98219359
28	83.71708711
27	113.0579329
26	142.8133775
25	173.5893734
24	204.7799681
23	236.5765151
22	269.2022599
21	302.2426036
20	336.1121452
19	370.5876389
18	405.8923305
17	441.3883755
16	477.5222649
15	514.4534599
14	552.0224993
13	590.3888444
12	629.1697884
11	668.3653312
10	710.4311743

9	756.8024675
8	807.5111031
7	861.8873444
6	920.9836349
5	999.1833673
4	1094.828146
3	1210.182319
2	1345.43724
1	1499.986955

Table 4.2: Amount of incision through time as calculated from rate of incision of Gani et al. (2007).

VITA

Tadesse B Alemu

Candidate for the Degree of

DOCTOR OF PHILOSOPHY

Dissertation: INTRACONTINENTAL SAGS (ICONS) FORMATION, EXHUMATION AND LANDSCAPE EVOLUTION: THE ETHIOPIAN TESTIMONY

Major Field: GEOLOGY

Biographical

Education:

Completed the requirements for the Doctor of Philosophy in Geology at Oklahoma State University, Stillwater, Oklahoma in July, 2019.

Completed the requirements for the Master of Science in Earth Sciences (Fossil Fuel Exploration) at Addis Ababa University, Addis Ababa, Ethiopia in 2012.

Completed the requirements for the Bachelor of Science in Earth Sciences at Addis Ababa University, Addis Ababa, Ethiopia in 2009.

Experience:

Research and Teaching assistant, Boone Pickens School of Geology August 2014 – May 2019. UNAVCO USIP intern – summer 2018. Lecturer at Addis Ababa University, Ethiopia 2012-2013.

Field Experience

- Geologist, the Blue Nile Project, Ethiopia 2012-2018.
- Field assistant to Physical geology and structural geology field trips at OSU, 2016-2018
- Participant and logistics coordinator for the "Modeling Drainage Incision on the Ethiopian Plateau" project, 2009-2011.
- Led/co-led student field trips at Addis Ababa University, Ethiopia, 2010-2013.

Professional Memberships:

- Geological Society of America (GSA).
- National Association of Black Geologists (NABG).
- Society of Sedimentary Geology (SEPM).
- The National Association of Geoscience Teachers (NAGT).